JOURNAL OF
HAZARDOUS
MATERIALS

Management — Handling — Disposal — Risk Assessment

Review papers, normal papers, project reports and short communications are published dealing with all aspects of hazardous materials arising from their inherent chemical or physical properties. The scope of the journal is wide, ranging from basic aspects of preparation and handling to risk assessment and the presentation of case histories of incidents involving real hazards to employees or the public.

The following list, though not exhaustive, gives a general outline of the scope:

Properties: toxicity, corrosiveness, flammability, explosiveness, radioactivity, information data banks, dose–response relationships

Safety and health hazards: manufacturing, processing, transport, storage, disposal, major hazards and hazardous installations

Legislation: international, national and local codes of practice, threshold values, standards

Incidents: prevention, control, clean-up, communication, labelling, sources of information and assistance, case histories

Assessment: economic and general risk assessment, insurance, test methods, technical aspects of risk assessment of industrial hazards, reliability and consequence modelling, decision-making in risk management

Announcement from the Publisher

Elsevier Science Publishers encourages submission of articles on floppy disk.

All manuscripts may now be submitted on computer disk, with the eventual aim of reducing production times still further.

The preferred storage medium is a 5¼ or 3½ inch disk in MS-DOS format, although other systems are welcome, e.g. Macintosh.

After **final acceptance**, your disk plus one final, printed and exactly matching version (as a printout) should be submitted together to the editor. **It is important that the file on disk and the printout are identical**. Both will then be forwarded by the editor to Elsevier.

Illustrations should be provided in the usual manner.

Please follow the general instructions on style/arrangement and, in particular, the reference style of this journal as given in 'Instructions to Authors'.

Please label the disk with your name, the software & hardware used and the name of the file to be processed.

Contact the Publisher for further information:

Elsevier Science Publishers
Journal of Hazardous Materials
P.O. Box 330
1000 AH Amsterdam, The Netherlands
Phone: (+31-20) 5862 821   Fax: (+31-20) 5862 845

ELSEVIER SCIENCE PUBLISHERS

Editorial

Three papers on vapour cloud explosions

Three papers are presented in the first part of this issue, to illustrate the state of the art in predicting the effects of vapour cloud explosions. They were commissioned by the OECD/IGUS Working Group on Hazards and Mitigation of Industrial Explosions (IGUS = International Group of experts on Unstable Substances). The Working Group meets once per annum to discuss progress in the study of industrial explosions. Its members are drawn from Government bodies and from those organisations who advise Government bodies.

The papers reflect the three distinct stages in the study of vapour cloud explosions. Leyer writes about the unconfined explosion. Numerous experiments by several research organisations have demonstrated the difficulty in obtaining a blast wave sufficiently strong to damage buildings from an unconfined explosion with a low energy ignition. Van den Berg and Lannoy, amongst others, demonstrated that to obtain that strong, damaging, blast wave some means of accelerating the flame is needed. Partial confinement of the explosion and obstruction by items of the chemical plant can provide that acceleration mechanism. In The Netherlands the Multi-Energy method for predicting the blast overpressure from an accidental explosion makes use of the concept of flame acceleration by obstructions, and uses correlations based on simple numerical computations to guide the reader in making predictions. The authors suggest the use of more sophisticated computer codes to calculate the progress and acceleration of flame in the obstructed region. The paper by Hjertager describes one such code developed in Norway. Hjertager's computer model has been successful in predicting explosion pressures in simple situations and for the very congested situation on off-shore oil and gas rigs and it could be used to predict the pressure to be used as source for the Multi-Energy method.

The IGUS Working Group has been a focus for discussing the progress of this work, and for the interchange of ideas on an informal basis without the constraints of publication or commercial interests. I hope that it will continue to work in this way in future meetings.

REX E. BRITTER

Unconfined deflagrative explosion without turbulence: Experiment and model

J.C. Leyer[a,*], D. Desbordes[a], J.P. Saint-Cloud[a] and A. Lannoy[b]

[a] *Laboratoire d'Energétique et de Détonique (URA 193 CNRS) ENSMA — Université de Poitiers, Rue Guillaume VII, 86034 Poitiers (France)*
[b] *EDF — Direction des Etudes et Recherches, 25, Allée Privée, Carrefour Pleyel, 93206 Saint-Denis Cedex 1 (France)*

Abstract

This paper reviews laboratory, balloon and open-field experiments, which have been performed to study the deflagration regime in free air. In the first part, the paper considers briefly the different models available to estimate deflagrative unconfined explosion effects, without turbulence. Then a description is given of the known tests conducted, which indicates the effective scale of the various experiments, their operating conditions and the kind of the measurements done. The main results are presented and discussed in some detail to assess the role on the explosion yields of important parameters such as the fuel concentration gradients, the shape and size of the inflammable mixture, and the ignition energy. The overall conclusion of this survey is that inflammable mixtures drifting over open field and ignited, will burn with a low flame speed and consequently will generate very weak pressure effects.

1. Introduction

In the design and construction of industrial installations, it is necessary, for safety purposes, to take into account the potential explosion hazards resulting from accidental spills. These take the form of a massive release of a dangerous product, generally a hydrocarbon, followed by the formation in the atmosphere of an inflammable cloud. Depending on the weather conditions and topography, such a cloud may drift, and if it is ignited, the pressure wave created by the explosion may cause serious damage, even at considerable distances. In order to protect the safety functions of a plant, where large quantities of inflammable materials are processed, stored or transported, it appears necessary to assess the overloads that must be built in to the structures.

Analysis of vapour cloud explosions which have actually occurred [1] has proved that blast effects are potentially devastating up to large distances from

---

*To whom correspondence should be addressed.

the centre of explosion. Significant blast effects are generated only if the energy is released in a short period of time, which means that the flame speed must be high.

One of the explosion regimes which could occur, is the detonation of the inflammable part of the unconfined cloud. Detonation is the most severe explosion regime, producing high velocity up to 1900 m/s and pressures up to 17 bars. But in view of the very large ignition energies required to directly initiate the detonation of a fuel-air mixture [2], near an optimum concentration, this detonation regime can be ruled out in practical conditions.

The other explosion regime is deflagration, which is more likely and which can also explain damage observed in all past accidents [3]. To judge the severity of such an explosion regime, an important research effort has been done to characterize the nature and the effects of deflagrations. A wide variety of tests, from small scale tests (at laboratory scale) to large scale (on open field) have been performed, so that there is now a considerable data base available on fuel-air deflagrations and pressure effects due to deflagrative explosions.

The present chapter is concerned with deflagration tests of unconfined inflammable fuel-air mixtures, without turbulence. We review field and laboratory experiments which may provide information on the deflagration of an unconfined vapour cloud. The objectives are as follows:

(a) a very short description of deflagration modellings used for analyzing and interpreting deflagration tests;

(b) a list of deflagration experiments whose data are presently available, including their conditions and configurations,

(c) a study and discussion of the main factors which may influence the combustion regime:
- effects of the concentration (homogeneous and heterogeneous media),
- effects of the cloud shape,
- effects of the energy released by ignition,
- effects of the size of the cloud.

2. Deflagrative explosion models: A brief survey

The simplest way to simulate an unconfined fuel-air mixture deflagrative explosion and to measure the blast generated, is to enclose into a slight confinement a uniform well-monitored composition of the inflammable mixture. Usually, the confinements are of spherical, hemispherical on the ground, pancake, cubic or rectangular shapes. The mixture boundary is formed by a soap film in laboratory scale experiments, and a rubber or plastic sheet in field experiments. When ignited at the center of symmetry, the mixture supports, in the absence of any obstacle or partial confinement, the propagation of a diverging spherical flame front. Furthermore, if pressure wave reflections, due to impedance mismatching on the interface at the sheet are ignored (an assumption which will be shown not strictly valid in the next items), the flame

expansion, free of any turbulence, occurs as in an infinite homogeneous medium. In such a situation, the flame history being known, the generated flow field can be calculated as described in the present item.

2.1 The spherical expanding flame model

All the above described conditions being fulfilled, the spherical expanding flame front may be thought as a thin discontinuity (compared to any characteristic observation length in the hydrodynamic field generated by the flame) which confines the burnt gases in a state of zero velocity. The spatial velocity (or speed) V_F of the front is therefore given by:

$$V_F = \beta S_u \tag{1}$$

where S_u is the apparent burning velocity which can be estimated from laminar burning velocity value S_u^o (if the front instability is taken into account for correction) for most of hydrocarbon and hydrogen–air mixtures. The expansion ratio β is the density ratio of fresh to burnt gases calculated at the front discontinuity which supports a very small pressure drop for moderate flame velocities V_F. Consequently β is quite well estimated by the ratio of the adiabatic flame temperature (at ambient pressure) of the mixture to the ambient temperature (perfect gas assumption). If R_o is the radius of the initial unburnt mixture (initial radius of the spherical balloon), mass conservation implies that the final flame radius R_m (maximum radius of the flame ball) be given by:

$$R_m = \beta^{1/3} R_o \tag{2}$$

Experiments [4] with hydrocarbon–air mixtures of nearly stoichiometric composition – equivalence ratio ϕ roughly in the range 0.9 (lean) to 1.2 (rich) – show that a good estimate of β is around 8. This experimental value is smaller than the calculated adiabatic one [5]. Proofs of the existence of radiative losses from burnt gas to the surroundings were observed with large balloons [4] which could explain the β deficit. Notice, for $\beta \sim 6$, relation (2) gives

$$R_m \sim 1.8 R_o \tag{3}$$

To estimate the flame velocity from relation (1), care must be taken to select an appropriate value of the apparent burning velocity S_u. Numerous experiments (see, for instance Refs. [6, 7]) demonstrated that a cellular structure appears for most fuel–air mixtures (hydrocarbon, hydrogen) when the flame radius r_F reaches about 5 to 10 cm, and the actual flame front surface is augmented compared to the smooth spherical flame surface having the same mean radius. Large balloon experiments [8] and analytical treatment [9] are in agreement to estimate surface increase by a factor k of the order of 1.5 to 2.5. This factor must be included in relation (1) to get the actual value of V_F for large flame radius, multiplying the laminar value S_u^o by the factor k. Even at very large flame radius r_F ($r_F > 5$ m in Ref. [8]), self-generated turbulence effects

do not appear. Only obstacles, like grids as in the experiments by Wagner et al. [10], are able to acceleratre sufficiently the flame front to give an apparent burning velocity to be included in relation (1), up to eight times the laminar value S_u^o.

2.2 Calculation of the hydrodynamic field

For moderate flame speed (compared to the sound velocity in burnt gases) the assumption of gas at rest in the flame ball is valid. Therefore, the flow field generated by the expanding spherical flame may be thought of as the field created by an equivalent spherical piston. For constant flame speed, this approach has been pioneered by Taylor [11], solved numerically by Kuhl et al. [12] as a limiting case of blast wave, and more recently, described analytically by Deshaies and co-workers [13–15].

For faster flames and detonative explosions, a number of numerical codes are now available (see, for instance, Refs. [16, 17]) for computation of blast pressure. As they are discussed in a separate chapter of this issue, only the model by Deshaies [7, 18] will be discussed here in more detail, because it is very appropriate to flow field calculations in the case of balloon experiments.

In this model [7] the flow is divided into three consecutive zones: (i) near the flame front an incompressible source flow; (ii) for distance $r > 2r_F$, r_F denoting the flame radius, the incompressible zone matches with an acoustic source flow; (iii) the acoustic zone is fitted to the leading zone entering the undisturbed medium at rest. The leading zone consists in an acoustic wave, unless the flame speed exceeds about 130 m/s. In this latter case, the leading pressure wave becomes a shock wave whose amplitude increases with the flame speed. Adopting this division of the flow into three zones, a complete field solution was found for a constant velocity flame of any speed [14]. The solution allows the pressure and velocity profiles versus time t at a given distance r (or versus distance r at a given time t) as shown on the schematic representation of Fig. 1, to be drawn as soon as the constant value of V_F is known.

The interesting fact, with respect to the interpretation of balloon experiments, is that the first order of the solution corresponding to constant velocity flames, can be extended to the case of variable flame velocity, provided that the flame accelerations remain moderate to prevent the formation of shock waves in the flow field. For clarity, the relationships giving the pressure and velocity fields generated by the expanding spherical flame whose path is given by the function $r_F(t)$, are reproduced here from Ref. [18]. The overpressure $\Delta p(r, t) = p(r, t) - p_0$ and velocity $u(r, t)$ in the environment of density ρ_0 at pressure p_0, are given at the first order and at distance r respectively by:

$$\Delta p = \frac{\rho_0(1 - \beta^{-1})}{r}\left(2r_F\left(\frac{dr_F}{dt}\right)^2 + r_F^2\left(\frac{d^2 r_F}{dt^2}\right) - \frac{1 - \beta^{-1}}{2}\frac{r_F^4}{r^3}\left(\frac{dr_F}{dt}\right)^2\right) \tag{4}$$

$$u = (1 - \beta^{-1})\frac{r_F^2}{r^2}\left(\frac{dr_F}{dt}\right) \tag{5}$$
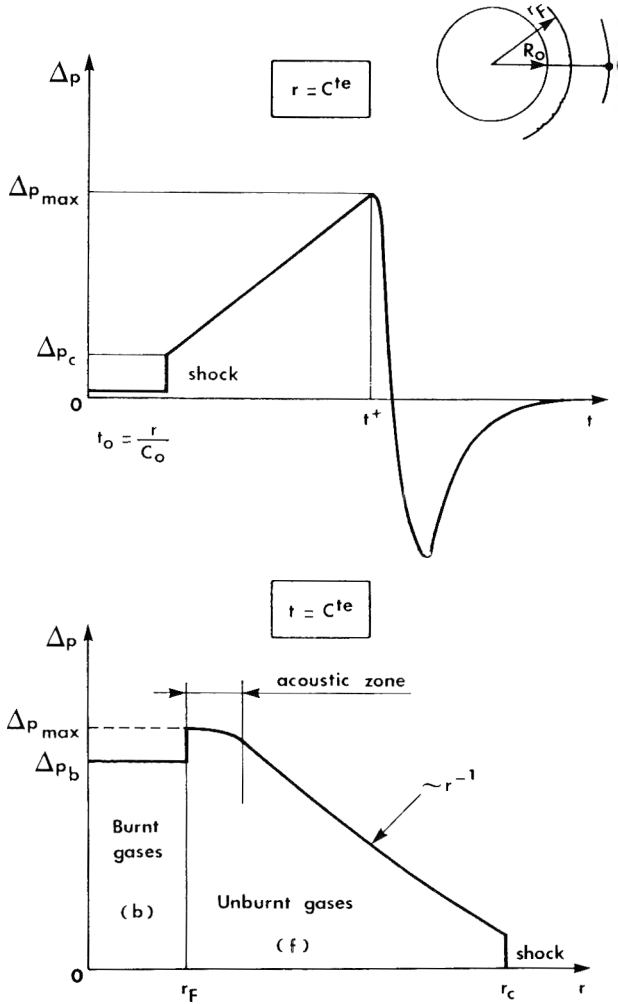
Fig. 1. Typical overpressure records by a spherical flame expanding at constant velocity: (a) versus time at a fixed distance r from the ignition point; (b) versus distance at a fixed time t. Notice that the shock wave indicated is an acoustic wave for flame speed V_F below 130 m/s.

near the front ($r \sim r_F$), and by

$$\Delta p = \frac{\rho_0(1-\beta^{-1})}{r}\left(2r_F(\tau)\left(\frac{\mathrm{d}r_F(\tau)}{\mathrm{d}\tau}\right)^2 + r_F^2\left(\frac{\mathrm{d}^2 r_F(\tau)}{\mathrm{d}\tau^2}\right)\right) \qquad (6)$$

$$u = (1-\beta^{-1})\left\{\frac{r_F^2(\tau)}{r^2}\left(\frac{\mathrm{d}r_F(\tau)}{\mathrm{d}\tau}\right) + \frac{1}{rc_0}\left[2r_F(\tau)\left(\frac{\mathrm{d}r_F(\tau)}{\mathrm{d}\tau}\right)^2 + r_F^2(\tau)\left(\frac{\mathrm{d}^2 r_F(\tau)}{\mathrm{d}\tau^2}\right)\right]\right\} \qquad (7)$$

in the acoustic zone ($r_F > 2R_o$). R_o designs the initial radius of the inflammable volume and in relations (6) and (7), $\tau = t - r/c_o$, is the time variable, c_o the sound velocity in the undisturbed medium.

Relationship (6) can be rewritten in the following form:

$$p(r, t) - p_o = \frac{\rho_o(1 - \beta^{-1})}{4\pi r} \frac{d^2 V}{d\tau^2} \tag{8}$$

which contains explicitly the acoustic source volume V whose variations versus time defines completely the monopole acoustic source strength, provided the expansion ratio β of the mixture may be considered as a constant.

The acoustic approach has been followed by several authors. Strehlow [19] used it to characterize the maximum peak overpressure generated by a pancake- or cigar-shaped cloud with central or edge ignition. A more sophisticated model, involving a distribution of simple sources successively activated according to the law of flame development, was proposed by Auton and Pickles [20] to exhibit the asymmetry of the pressure field in case of a cigar-shaped cloud ignited from the center. A similar model has been developed by Catlin [21] for non-spherical clouds lying on the ground with different aspect ratios. These latter calculations were found to agree fairly well with the results of experiments at small scale carried out with cylindrical clouds, point ignited on ground at the centre [22].

In the frame of acoustic models, it should be noticed that the pressure field depends not only on the flame speed V_F, but also on its variations (see relation (6)). Moreover the contribution of flame acceleration (or slowing down) to the pressure field is proportional to the squared flame radius. This important fact should not be ignored in practical situations of very large cloud: A final flame acceleration may lead to severe peak overpressures, although the flame speed be moderate during the main part of its travel across the cloud. One should say, however, that numerical blast calculations [17, 23] demonstrate that this effect is less and less pronounced as the mean flame speed is increased.

To conclude this brief review of the deflagrative explosion models, we will retain, for the next, the following statements:

1. The flow field generated by an unconfined constant velocity spherical flame is completely known.

2. A first order solution is available to describe the near field and the acoustic field taking into account the flame speed variations provided that the front mean velocity remains moderate (below about 130 m/s). The flame accelerations should be also sufficiently moderate to prevent shock-wave formation in the field.

3. Acoustic simple source models can be extended using an appropriate source array to take into account non-spherical shape and edge ignition. In that case, directional effects appear in the hydrodynamic field of the unconfined explosion.

3. The review of experiments on deflagrative unconfined explosion

A great need exists for data for the estimation of blast yields by accidental explosions and also for validation of the theoretical predictions. This is the main objective of laboratory and field experiments on unconfined deflagrative combustion without turbulence.

All the models just reviewed demonstrate that the pressure field depends not only on the flame speed but also on its time variations. Moreover, models show that the overpressure can be determined only in the case where the complete flame history is known in detail. These predictions can be accepted for practical use if there are reliable experimental results with which they can be compared.

The test programs conducted up to now cover generally four distinct topics whose objectives are as follows:

(1) *The concentration effect*: tests with homogeneous mixtures have been performed to study the influence of spontaneous acceleration of the deflagration and to validate models of the pressure field generated by a deflagration; Similarly, tests in non-uniform composition mixtures have been carried out to observe the flame acceleration effects produced by fuel concentration gradients which would occur in a real explosive cloud.

(2) *The shape effect*: to study the influence of the initial shape of the inflammable volume on the pressure field produced, a number of tests with various geometries (spherical, cylindrical, pancake and very complex shape of a real drifting cloud) have been run.

(3) *The size effect*: tests have been performed to characterize the effects of the explosion scale, when the volume of the inflammable charge is increased in a wide range from a volume of some liters up to several thousands of cubic meters.

(4) *The ignition effect*: the effect of energy released by ignition on the explosion regime obtained and on consequent flame speeds has been experimentally determined.

The influence of these four parameters is discussed in some detail in the following section. It is clear that all the experiments have a direct relevance to accidental explosions which have actually occurred as well as theoretical interest.

A complete list of the experiments, of which we are aware, on unconfined deflagration without turbulence is given in Table 1.

The expression "without turbulence" means that the flame trajectory is not affected by semi-confinements, by hot gases turbulent jet ignition, by crossing obstacles like grids, and the like, that is, in short, not affected by any cause liable for producing turbulences in the flow of unburnt gases and, as a result, forced accelerations of the flame.

TABLE 1

List of experimental conditions of the main balloon type experiments reported in the literature

No.	Tests	Year	Principal reference	Fuel	Volume	Geometry	Number of tests
1	Shell	1965	[27]	Ethylene Propane Methane Hydrogen	Small	Spherical (soap bubble)	A number
2	Nantes	1970	[28]	Natural gas	• Instantaneous $3\,m^3$ liquid • Continuous $0.17\,m^3/min$	Real cloud	40
3	China Lake	1975	[8]	Methane	$262\,m^3$	Hemispherical	3
		1977		Propane Ethylene Ethylene oxide	$2095\,m^3$		6 1 2
4	ENSMA	1979	[18]	Hydrogen Methane Propane Ethylene (+ oxygen argon)	$30\,dm^3$	Spherical or hemispherical (soap bubble)	A number
5	ENSMA	1980	[22]	Ethylene	$17\,dm^3$	Cylindrical (soap bubble)	A number
6	Shell-- Maplin Sand	1980	[29]	Natural gas	Spills • Continuous $2.8\,5.8\,m^3/mm$	Real cloud	7 4
				Propane	• Instantaneous $5-12\,m^3$		
7	Charles 1	1981	[4]	Ethylene Acetylene	$12\,m^3$	Spherical	12

Objective	Destruction of the enclosure	Topography	Concentration	Measures		Ignition
				Pressure	Flame trajectory	
Study of the noise produced by a flame		Laboratory	—	1 Acoustic microph.	High-speed camera	Electrical spark
Extent of a cloud	No confinement	Open field	A number	—	Photography	Torch
Flame propagation and flame acceleration process Unconfined or partially confined medium	No	Open field	—	10	High-speed camera	Weak source
Spontaneously accelerating flames	Yes	Laboratory	1 partial pressure	1	High-speed camera	Discharge of a capacitor or low energy spark
Effects of the deflagration of a pancake-shaped cloud	No confinement	Laboratory	1 partial pressure	1	High-speed camera	Low energy spark
Measurement of flame propagation and pressure waves generated by the deflagration of a real cloud (after a liquified gas spill on water)		Open field	200	24	Video	Spark ignition (number = 10)
Homogeneous medium–Influence of spontaneous acceleration on pressure	Yes and no	Open field	1	8	High-speed camera	Low energy electric ignition

TABLE 1. Continued

No.	Tests	Year	Principal reference	Fuel	Volume	Geometry	Number of tests
8	KWU	1981	[24]	Hydrogen	$7.5\,m^3$ $50\,m^3$ $260\,m^3$ $2100\,m^3$	Hemispherical	7 3 2 1
9	Coyote (3, 5, 6, 7)	1981	[30]	Natural gas	LNG spill $14.6\,m^3$ $28.0\,m^3$ $22.8\,m^3$ $26.0\,m^3$	Real cloud	4
10	TNO	1982	[31]	Propane	Up to $1000\,kg$ between flammability limits	Real cloud	10
11	Charles 2	1982 1983	[8]	Ethylene	$12\,m^3$	Spherical	11
12	Charles 3	1983	[4]	Ethylene	$12\,m^3$	Spherical	11
13	Shell	1983 1984	[32]	Natural gas Propane	$3700\,m^3$	Cylindrical (segment of a pancake–shaped cloud)	15
14	Charles 4	1984	[4]	Ethylene	$125\,m^3$	Half cubical $(6.3 \times 6.3 \times 3.15)$	3

Objective	Destruction of the enclosure	Topography	Concen-tration	Measures		Ignition
				Pressure	Flame trajectory	
Influence of cloud extension and ignition energy on flame speed	No	Open field	—	10	High-speed camera	Highly variable up to 1000 J (exploding wires)
Vapour burn experiments after liquified natural gas flame propogation	No confinement	Open field	89	2	Flame velocity sensors and photography	Flames or jet ignition
Effect of obstacles, but some unobstructed tests have been carried out (vaporization from a pond)	No confinement	Open field	—	A number	Video flame	Pyrotechnic ignition
Acceleration effects produced by fuel concentration gradients	Yes	Open field	2	8	High-speed camera	Low energy electric ignition
Effects of energy released by ignition	Yes	Open field	1	8	High-speed camera	Low energy electric ignition + plastic charge
Effects of obstacles and jet ignition: Unobstructed tests with natural gas Unobstructed tests with propane Unobstructed tests with jet ignition	Yes	Open field	7	9	Flame dectors and high-speed camera and video	Low energy or jet ignition
Effects of the size of the flammable cloud	Yes	Open field	3	8	High-speed camera	Low energy electric ignition

In Table 1, the principal features of the experimental campaigns are specified and in columns, one can find successively:
- the principal reference where the tests concerned are described extensively;
- the fuels used, which involve a large scale of reactivity, ranging from methane (the less reactive fuel) to very reactive fuels such as acetylene or hydrogen,
- the volume experimented;
- the configuration and geometry;
- the purpose cf the tests and the phenomena studied;
- the surrounding topography;
- the extent of measurements: concentration, pressure, time of arrival of the flame, etc.;
- the type of ignition device.

Note that three different types of experiments are quoted in the table:

1. *Laboratory-scale experiments* which are very useful. Generally, the inflammable mixture is contained in a soap bubble and is ignited at its centre of symmetry or at the edge, the confinement by the bubble wall does not affect the flame developmert. Such small scale tests allow isolation of some process occurring in the deflagration and they can easily be multiplied.

2. *Enclosure-type experiments* (intermediate or large scale) which include balloon or pancake experiments. The simulated inflammable cloud is held in a thin bag, as shown on the typical arrangement of Fig. 2, and the mixture burns when ignited. In some tests, the balloon skin is destroyed before ignition,
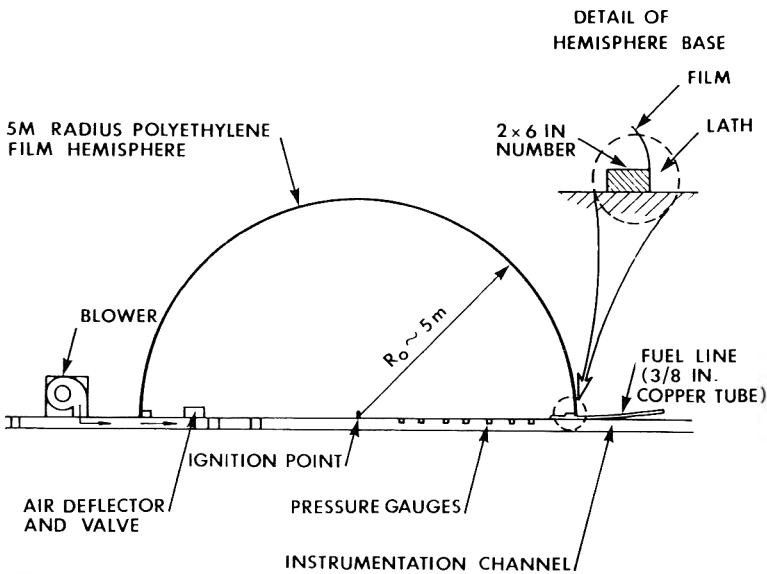

Fig. 2. Typical experimental arrangement for balloon-type experiments in medium-size scale (from Ref. [8]).

and the combustible mixture is in contact with the atmosphere as the flame front travels across the volume. In other tests, on the other hand, the destruction of the initial thin confinement is not operated. Particular attention is paid to this experimental procedure: indeed, a comparison between completely unconfined tests and other ones with a latex confinement of the charge (see, for instance, Ref. [4]) has shown that flame speeds are virtually the same during the first period of the propagation in the inflammable mixture and therefore the pressure field is unaffected; by contrast, the presence of a skin may have an effect on the final acceleration of the flame and the pressure signals may be different. Consequently, the overpressure values may be overestimated when the confinement is not removed before ignition (see also Section 4.1, below);

3. *Real cloud experiments* (at large scale) which allow the shape and the scale parameters to be investigated. Large quantities of inflammable materials are released, vaporized in the environment where an inflammable drifting cloud is formed, whose combustion is closely monitored. Flame speeds and overpressures are measured. The size of these tests is such that they represent a full-scale test for accident scenarios in an open space.

The influence on the unconfined deflagrative combustion of the principal parameters investigated is analyzed in more detail in the following paragraphs, on the basis of the experiments listed in the Table 1.

4. The main results

The flame speed and maximum overpressure ranges, observed in the different tests retained in the Table 1, are listed in Table 2. The analysis of this set of results allow the effects of fuel concentration (uniform or not), and of the cloud shape and size to be separated.

4.1 Effect of fuel concentration

4.1.1 The uniform composition mixtures
Results for uniform composition mixtures of common hydrocarbons and hydrogen with air are available (tests 1, 3, 7, 8, 14 in Table 2) in a large volume range: 10^{-5} to 4×10^3 m^3 approximately. The common feature to all these tests, is that the observed overpressures are always found between about 1 and 60 millibars, amplitudes which are unable to cause severe damage to the environment.

Generally speaking, the measured flame spatial velocity is well estimated by relation (1) in which the multiplying factor k is included to take into account the flame front folding. Three was found to be a rather conservative value for k. The expansion ratio β can be estimated from the maximum radius of the front and S_u^o taken as the classical laminar burning velocity of the fuel-air mixture for the given composition.

TABLE 2

Summary of results obtained from the experiments listed in Table 1

No.	Tests	Fuel	Concentration or equivalence ratio
1	Shell (1965)	Hydrocarbons and Hydrogen	CH_4 C_2H_4 (9%) C_3H_8 H_2
2	Nantes	Natural gas	Real cloud
3	China Lake	Methane Propane Ethylene Ethylene oxide	10% 5% 6.5% 7.7%
4	ENSMA (1979)	H_2 CH_4 C_3H_8 C_2H_4	Superoxygenated air, stoichiometry relative to O_2
	(Spherical)		
5	ENSMA (1980) (cylindrical)	C_2H_4	Superoxygenated air, stoichiometry relative to O_2
6	Shell–Maplin Sand	Natural gas Propane	Real cloud
7	Charles 1	Ethylene Acetylene	1 1.3 1 1.8

Flame speed (m/s)	Overpressure (mbar) ($r \sim 2R_o$)	Comments
3–20	0–0.6 (distance r ?)	Various compositions of superoxygenated air mixtures giving burning velocities as $0.4 < S^\circ_u < 1.9$ m/s
5–15	Not measured	Real cloud
5.2–8.9	—	Balloon experiments
6.1–12.6	—	
17.3	—	
13.4–22.5	—	
3–100	1–350	Soap bubbles $2 < \phi < 40$ cm experiments with mixtures of volumetric composition as: $C_nH_m + YO_2 + ZN_2$ Y stoichiometry $0 < Z < Z_{air}$
3–50	1–150	
<10	<0.8	
<28	<0.4	
8.5 11	3.3–5	Homogeneous
11 17	6.4–21.6	
20 32		
17 38		

8	KWU	Hydrogen	Stoichiometry
9	Coyote	Natural gas	Real cloud
10	TNO	Propane	Real cloud
11	Charles 2	Ethylene	Concentration gradients
12	Charles 3	Ethylene	1.1
13	Shell	Natural gas	1.1
		Propane	1.1
		Natural gas	1.1
14	Charles 4	Ethylene	6.7%

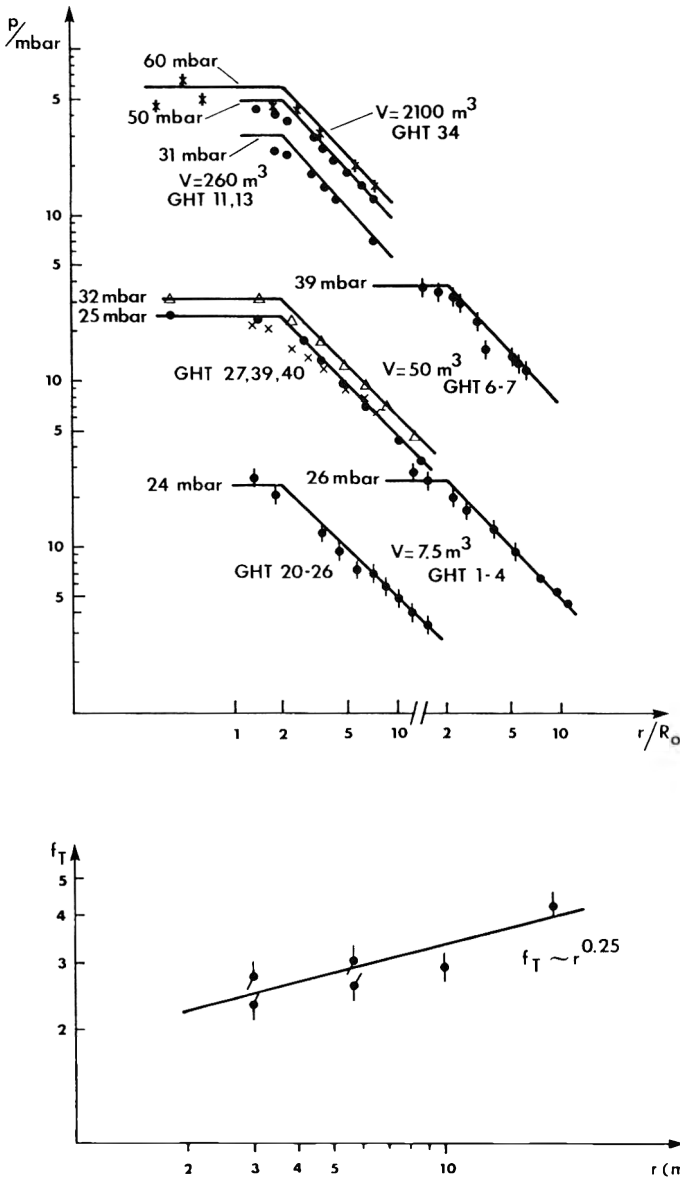|		
<83.6	<60	Volume effect
1–15	A few mbars	Real cloud
100		Jet ignition
3–10 (in one test, 32 m/s)	0.3 (calculated)	
18–29	3.4–8.5	
<32	<12	
10	4–5	
30–40	10–15	
90–145	83–222	Jet ignition
11–20	12	

Fig. 3. Variations of overpressures versus distance (a), and flame velocity versus distance (b). Spherical explosion of H_2-air stoichiometric mixtures (from Ref. [24]).

The pressure field calculated from relations (4) to (7), or from analogous acoustic models. is in most cases in good agreement with the measurements. Figure 3 from Ref. [24] is an example of such an agreement for H_2-air mixtures at stoichiometry over a large volume interval: the peak overpressures exhibit

an acoustic behavior, decreasing outside the flame ball with the inverse of the distance r. Moreover, the constant pressure inside is related to the constant velocity spherical flame model (see Ref. [7] and Fig. 1) which can predict fairly correct values of the pressure signals.

Actually, even with uniform composition mixtures, the flame propagation velocity V_F is not a constant. Smooth successive spontaneous accelerations due to changes in the front structure are reported in Ref. [18] for small flames. Woolfolk and Ablow [25] noticed that the radius r_F of the fast spherical deflagration in H_2–O_2 stoichiometric mixtures ($R_o = 0.455$ and 0.8 m) varies with time as:

$$r_F \sim t^{1.36} \tag{9}$$

that means a flame speed V_F increasing with time t as $t^{0.36}$. A similar behavior is reported in Ref. [24] for H_2–air mixtures for which the ratio of the actual flame speed to its laminar value increases with flame radius as $r^{0.25}$ (Fig. 3(b)). The flame front accelerates during the end of the propagating phase, several causes being involved in this behavior: (a) the balloon sheet is often maintained by a supporting device, acting as an obstacle (grids or so); (b) when the wall is destroyed before ignition — as in Charles 1 test — a perturbed, rippled interface is left between the mixture and the ambient air leading to a flame acceleration. This phenomenon is even observed (but slightly) with the light confinement offered by the soap film in bubbles experiments [5].

Pressure wave shape and amplitudes (see Fig. 1) and flame speed variations have been correlated in the acoustic region for some tests: starting from the recorded pressure signal versus time at a given distance r, the flame speed and flame path are reconstructed by two successive integrations of relation (6). This method, used in the Charles 1 test set [4] and in other tests has confirmed that the flame speed V_F was effectively increased (as clearly seen on the example of Fig. 4) at the moment when the flame radius became larger than approximately 1.5 m (the initial radius of the charge was $R_o = 1.4$ m).

The consequence of the occurrence of an accelerated end phase is to yield peak overpressures higher (multiplied by a factor of 2 in some cases) than the peak pressure which would be observed at a constant flame speed (from ignition time to end of combustion) evaluated on the theoretical basis of relation (1).

4.1.2 Mixtures exhibiting a fuel concentration discontinuity

With the objective of assessing the influence of more severe accelerations of the flame, some experiments were performed at a laboratory scale [18] or at a medium scale (in Charles 2 tests [4] involving 12 m^3 of several ethylene–air mixtures), where a fuel concentration discontinuity was displayed along the flame path. Rich or poor compositions were associated to nearly stoichiometric ones to provoke noticeable variations in the flame speed. In the example of Fig. 5, the mixtures, initially confined within two concentric latex balloons of radii $R_i = 0.9$ and $R_e = 1.4$ m respectively, are ignited at the centre, and the flame propagates from rich (13% C_2H_4) to stoichiometric (8.5% C_2H_4)
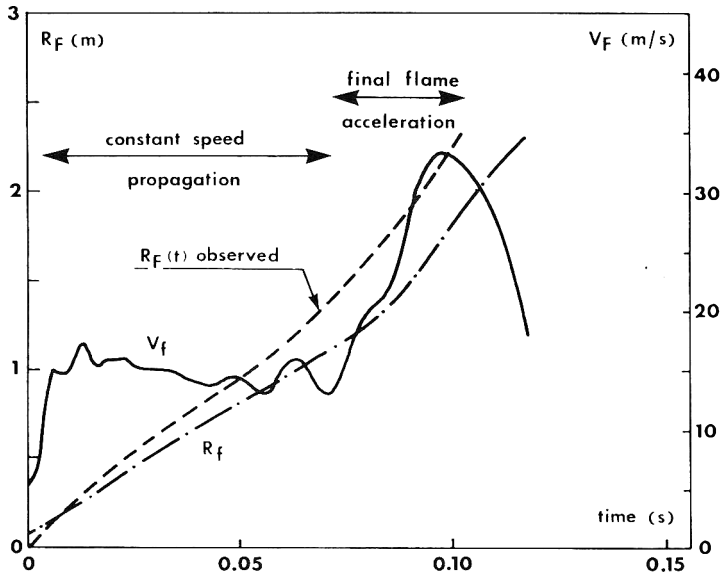
Fig. 4. Flame trajectory $r_F(t)$ and flame velocity $V_F(t)$ versus time in the case of a 12 m^3 deflagrative explosion of acetylene–air mixture (Charles 1 tests, Ref. [4]). Notice the flame acceleration in the final period of the propagation.

compositions. Instead of the expected flame acceleration at radius $r_F \sim 2R_i$, an oscillatory propagation was observed in the rich mixture ($0 < t < 90$ ms), followed by a constant speed travel at the transition between the two mixtures ($t \sim 100$ ms) and, curiously, the flame slowed down abruptly when burning the stoichiometric composition. Such behavior could probably be explained by the destruction of the balloon skins before ignition, allowing turbulences to be induced, and interdiffusion between the two mixtures and between the external mixture and air, to occur. Actually, in some Charles 2 tests where the balloons were not destroyed, normal behavior was observed: acceleration (or slowing down owing to fuel percentage) of the flame occurred at the interface of the inner balloon, and the peak pressure (enhanced by the confinement) corresponded to the end of burning of the fastest composition.

Generally speaking, the balloons were either destroyed or not before ignition and whatever the adjoining compositions, the maximum flame speeds were found to be larger by a factor of about 1.5 compared to the value observed with the fastest uniform composition (8.5% C_2H_4) experimented in Charles 1 tests. Consequently, the overpressure peaks found in Charles 1 tests, were multiplied by a factor of 2 to 3 by the influence of the composition discontinuity. Moreover, the pressure signals displayed severe oscillations, which could reinforce damages in real accidents as far as resonant effects on the structure are concerned in actual hazards.

Finally, the acoustic correlation (relation (7)) gave satisfactory results in the interpretation of the experiments as for the uniform compositions.
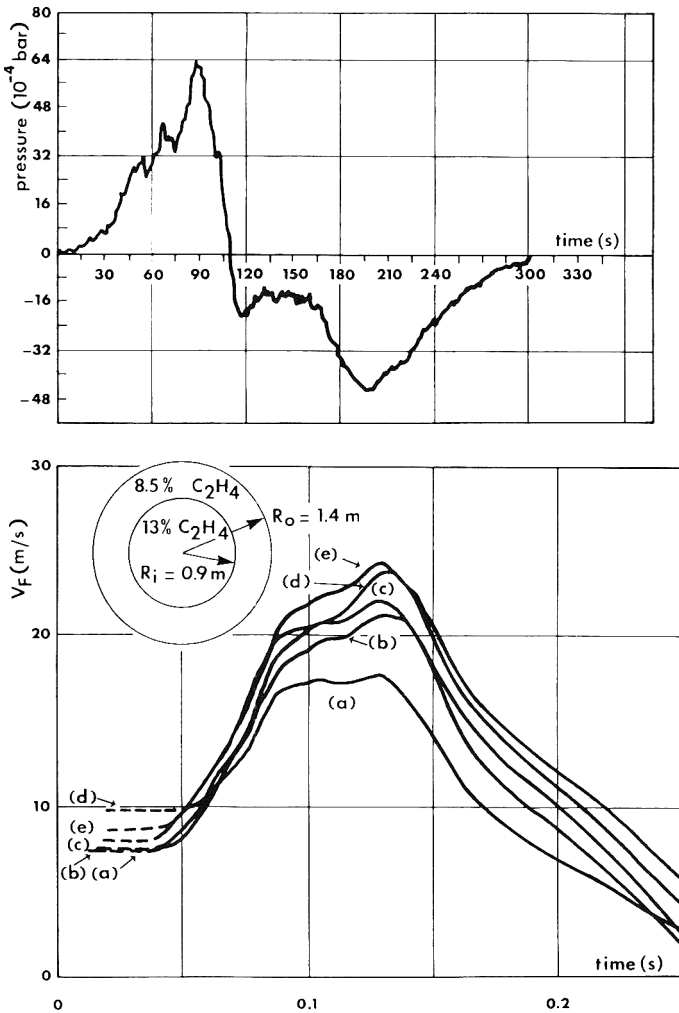
Fig. 5. Typical measured pressure record (a) and calculated flame velocity (b) in the case of deflagrative explosion of a 12 m³ volume of ethylene–air mixtures with a concentration step on the flame path (Charles 2 tests, Ref. [4]).

The largest peak overpressure was actually observed when the flame acceleration was rejected at the end of the propagation (large flame radius). It was particularly the case if the richest mixture (13% C_2H_4) was set at the outer boundary, allowing after-burning with the surrounding air to occur in the last phase.

4.2 Influence of the shape of the charges

Up to now, spherical charges ignited at the center have been discussed. To simulate the most probable real situation of a flat unconfined cloud, experiments

with cylinders [22] or fuel spreading on the ground are more realistic. Clearly, depending on the height to length ratio (aspect ratio ε) of the mixture volume, and/or on the location of the ignition point relative to the volume boundary, only the initial period of the flame propagation can be spherical. This phase ends as part of the flame front contacts the air boundary allowing the burnt gases to be released to the surroundings. The flame speed V_F and front surface A_F decrease, and consequently the strength of the equivalent acoustic source is reduced (see eq. (8)).
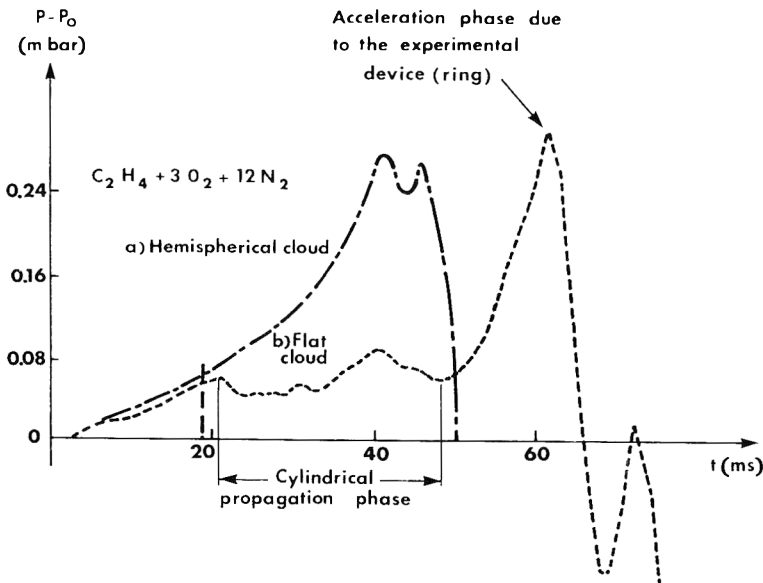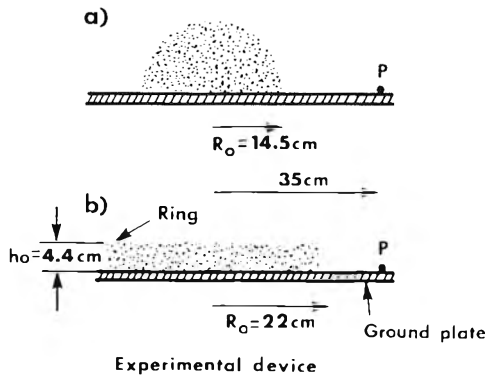

Fig. 6. Comparison of pressure signals versus time at a fixed distance observed in the case of spherical and cylindrical ethylene–air clouds (from Ref. [22]).

This behavior is illustrated in Fig. 6 where typical pressure signals from the deflagration of a hemisphere and of a cylinder of the same volume (C_2H_4–air stoichiometric) are compared. The flame speed, $V_F = 6$ m/s during the spherical phase, decreases to $V_F = 3.5$ m/s, for the cylindrical propagation which generates a nearly constant overpressure (the final peak due to the particular experimental arrangment of Ref. [22] should be ignored when there are no obstacles).

Typically, peak overpressure generated by the deflagration of flat volumes are significantly smaller than in the spherical case, and become very weak when the aspect ratio ε is reduced. This general conclusion is confirmed by larger scale experiments as shown on Fig. 7 and also by real cloud experiments

Combustion in segment represents that in full cloud

Large pancake-shaped gas cloud

Expanding flame

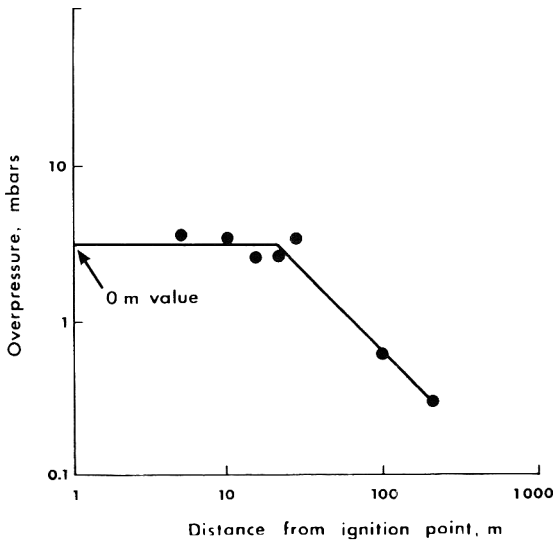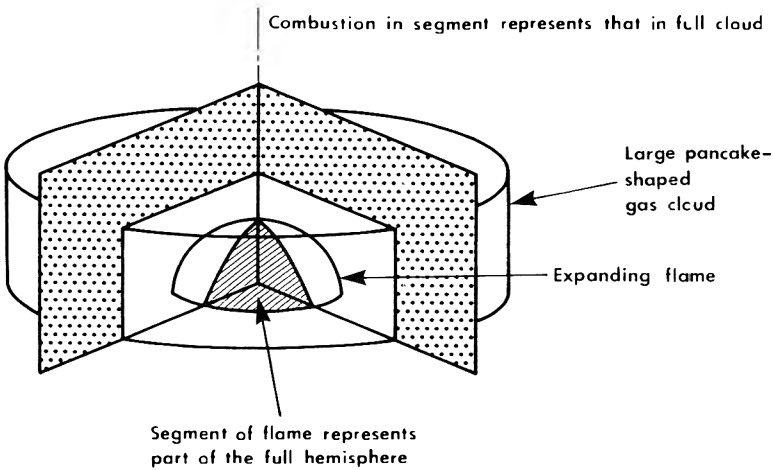Segment of flame represents part of the full hemisphere

Fig. 7. Peak overpressure registered in large scale cylindrical unconfined explosions (from Ref. [32]).

such as 9, 6, 13 in Table 2. Even with fast flames ($V_F \sim 100$ m/s) observed with turbulent jet ignition, overpressures remain always in the range of a few millibars. Acoustic models (Refs. [18–22]) are very useful to explain the far field pressure, at least qualitatively. Near the exploding cloud, the pressure field may exhibit asymmetry [21] and non-acoustic decay of the wave.

4.3 Influence of the volume of the explosive mixture
As already mentioned in the above items, hemispherical balloons have been used to experiment up to about 2100 m^3. With central weak ignition and in the case of uniform mixture composition, there is a tendency for the spherical flame to accelerate continuously with increasing radius (see Refs. [24, 25] and Fig. 3). But the acceleration remains moderate, as evidenced by the results of Lind [8] given in Fig. 8 relative to propane and methane–air mixtures. So, one may expect more pronounced blast effects with large sized flames, but without any obstacles or turbulence the velocities are much lower than observed during a predetonation period or in confinements. The overpressures observed are far below 100 mbars, and then are non-catastrophic for the environment.

It should be noticed that buoyancy effects are observed for a spherical flame whose radius exceeds about one meter for hydrocarbon–air mixtures. As a consequence, the flame speed in the vertical direction is larger than in the horizontal one (see Fig. 8). This effect was also observed in Charles experiments with 125 m^3 of ethylene–air (6.7% C_2H_4) contained in a retractable rectangular box [4]. In this case, the measured pressure field was comparable to the calculated field taking into account the flame speed observed in the 45° direction. So buoyancy effects are certainly responsible for the asymmetry in the generated field but are of negligible influence on the overpressure values.

The negligible influence of the size of the mixture volumes on unconfined deflagrative explosion yields is further confirmed by large scale trials simulating real clouds. For instance, in tests 6, 9, 10 on Table 2, measured overpressure did not exceed a few millibars and flame velocities were lower than 15 m/s, as shown in Fig. 9.

4.4 Strong ignition energy
For the most part of the experiments performed, ignition energy was low (spark or fuse composition). If one expects ignition by hot jets, which involves turbulent propagation and for that reason is discussed elsewhere, strong ignition was studied in Charles 3 (see Table 2) only. Twelve cubic meters of ethylene–air mixtures (8.5%) were fired using the detonation of 5–8 g of a solid explosive and a deflagration was observed to propagate behind a decaying spherical shock wave. In the initial phase, the flame boosted by the shock was accelerated up to about 100 m/s, but the flame speed suddenly decreases around $r_F \sim 1$ m, and, completely decoupled from the shock wave, recovered an almost constant velocity of the order of 30 m/s (compared to about 12 m/s for weak ignition of the same mixture). As a consequence, in the far field, the leading shock wave generated by the solid explosive detonation having completely
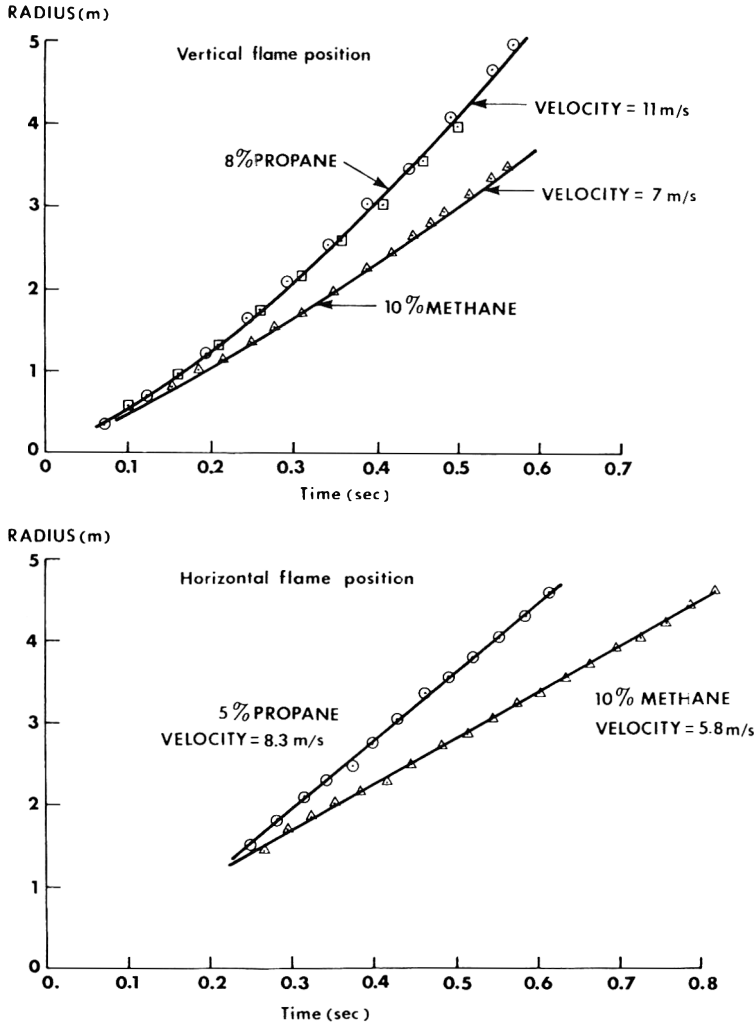
Fig. 8. Large scale balloon experiments. Illustration of buoyancy effects on the flame propagation (from Ref. [8]).

decayed, the peak overpressure observed was at most 10 mbars, as shown on Fig. 10, and thus was relevant for acoustic interpretation. It should be noticed that previous tests [26] demonstrated that 10–12 g of the same explosive were able to initiate the detonation of the ethylene–air mixture; but intermediate regimes of fast deflagration could never be generated even with accurate weighting of the explosive mass between 8 and 10 grams.

So it could be concluded that, even with sensitive mixtures, strong ignition without turbulence lead either to detonation or to slow deflagration. In the last case, fast deflagration at a speed of several hundred meters per second is restricted to the very beginning of the propagation which is not self-sustained.
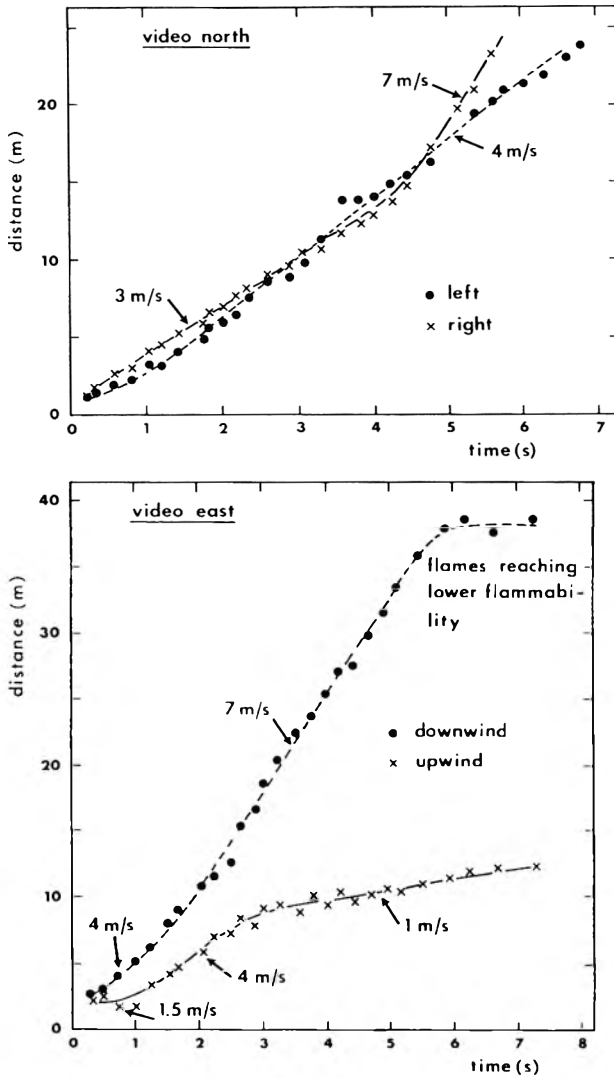
Fig. 9. Flame trajectories in real cloud explosion (from Ref. [31]). Propane–air cloud without obstacles.

5. Conclusion

The present chapter reviews several sets of experiments, at small, intermediate and large scale, which have been performed because of the lack of knowledge to predict the yields of unconfined deflagrative combustion.

The results of all these tests, without any source of turbulence generation, confirm the low values of the flame speed even for the more reactive fuels.
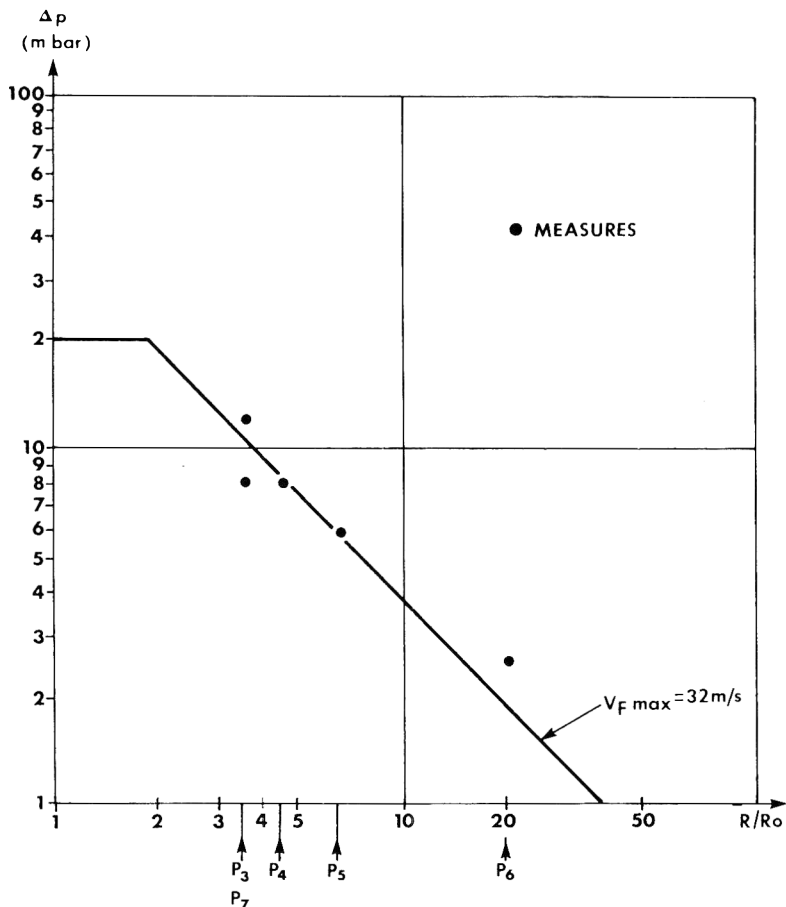
Fig. 10. Maximum peak overpressures versus distance observed with ethylene–air mixture in the case of strong ignition energy (Charles 3 tests Ref. [4]).

Experimental values of flame speed are of the order of 15 m/s, for an equivalence ratio of 1, except for hydrogen and acetylene which have had values of 30 m/s reported. As a result, truly unconfined fuel–air explosions produces very weak pressure effects, of the order of few millibars near the edge of the inflammable charge. No important scale effects have been observed.

The pressure field has been found to be highly dependent on the acceleration of the flame which could be generated either by the experimental device itself (especially at the boundary of the charge) or by fuel concentration gradients in the inflammable mixture. But they never cause an important increase in the peak overpressure to be observed, even if the cloud is ignited by a strong ignition source such as a solid explosive mass. However, ignition by hot turbulent jet issuing from a confinement should be treated with care.

In the light of pressure levels recorded in a completely open space, such conditions of explosion do not appear to be a major risk. The only causes of greater overpressures, capable of inflicting severe damage on structures, would be high energy ignition combined with semi-confinement effects, obstacles effects and hot jet ignition, able to create turbulences on the flame path. These effects are discussed in some detail in separate chapters of this issue.

Considering as well established by now, the fact that truly unconfined deflagrative explosions are not very powerful and are easily supported by the conventional structures of most of the industrial plants, one may doubt the interest in future balloon experiments. Obviously, they should be restricted to cases where primary information is needed on the reactivity of new fuels, or on mixtures of several conventional fuels. Indeed, balloon experiments without turbulences are easy to perform rapidly and at relatively low cost. However, in no case can such types of experiments simulate actual large scale deflagrative explosion hazards in which obstacles and partial confinements are of drastic influence.

References

1   W.E. Baker, P.S. Cox, P.S. Westine, J.J. Kulesz and R.A. Strehlow, Explosion Hazards and Evaluation, Fundamental Studies in Engineering 5, Elsevier, Amsterdam, 1983.
2   D.C. Bull, J.E. Elsworth and P.J. Shuff, Detonation cell structures in fuel/air mixtures, Combust. Flame, 45 (1982) 7.
3   A. Lannoy, Analyse des explosions air–hydrocarbure en milieu libre – Etudes déterministe et probabiliste du scénario d'accident – Prévision des effets de surpression, Bulletin de la Direction des Etudes et Recherches d'Electricité de France, Série A, no. 4, 1984.
4   J. Brossard, D. Desbordes, N. Di Fabio, J.L. Garnier, A. Lannoy, J.C. Leyer, J. Perrot and J.P. Saint-Cloud, Caractérisation du champ de pression induit par l'explosion aérienne d'un mélange air–hydrocarbure, déflagration lente, déflagration rapide, Rapport EUR 9679 FR, Commission des Communautés européennes, Brussels, 1985. See also, from the same authors, Truly unconfined deflagrations of ethylene–air mixtures, in M. Summerfield (Ed.), Progress in Astronautics and Aeronautics, Vol. 106, Am. Inst. Aeronaut. Astronaut., Washington, DC, 1986, pp. 90–106.
5   J.C. Leyer, C. Guerraud and N. Manson, Flame propagation in small spheres of unconfined or slightly confined inflammable mixtures. 15th Int Symp. on Comb., The Combustion Institute Publ., Pittsburgh, PA, 1975, pp. 645–653.
6   A.G. Istratov and V.B. Librovich, On the stability of gas dynamic discontinuities associated with chemical reactions: the case of a spherical flame, Acta Astronautica, 14 (1969) 453–467.
7   B. Deshaies, Les flammes sphériques: Propagation divergente et combustion stationnaire, Thèse de Doctorat ès Sciences, no. 329, University of Poitiers, Poitiers, France, 1981.
8   C.D. Lind, Explosion hazards associated with spills of large quantities of hazardous materials, Phase 1, Final Report No. CG-D-30-75, Department of Transportation, U.S. Coast Guard, 1974.
9   G.I. Sivashinsky, Non-linear analysis of hydrodynamic instabilities in laminar flames, Parts I and II, Acta Astronautica, 4 (1977) 1177–1206 and 1207–1221.
10 K.J. Dörge, D. Pangritz and H.G. Wagner, Experiments on velocity augmentation of spherical flames by grids, Acta Astronautica, 3 (1976) 1067–1076.
11 G.I. Taylor, Proc. R. Soc. A 186 (1946) 273–292.

12   A.L. Kuhl, M.M. Kamel and A.K. Oppenheim, On flame generated self similar blast waves, 14th Symp. Int. on Comb., The Combustion Institute Publ., Pittsburgh, PA, 1973, pp. 1201–1214.

13   B. Deshaies and P. Clavin, Effets dynamiques engendrés par une flamme sphérique à vitesse constante, J. Mécanique, 18(2) (1979) 213–223.

14   P. Cambray and B. Deshaies, Ecoulement engendré par un piston sphérique: solution analytique approchée, Acta Astronautica, 5 (1978) 611–617.

15   P. Cambray, B. Deshaies and P. Clavin, Solution des équations d'Euler associée à l'explosion d'une sphère à vitesse constante, J. Phys., Colloq. C8, 40 (1979) 11.

16   A.K. Oppenheim, J. Kurylo, L.M. Cohen and M.M. Kamel, Shock Tube Symp., 1979.

17   C.J.M. van Wingerden, A.C. van Den Berg and J.P. Zeeuwen, Validation of numerical codes for the simulation of blast generated by vapor cloud explosions, In: M. Summerfield (Ed.), Prog. Astronaut. Aeronaut., 106 (1986) 422–435.

18   B. Deshaies and J.C. Leyer, Flow field induced by unconfined spherical accelerating flames, Combustion Flame, 40 (1981) 141–153.

19   R.A. Strehlow, The blast wave from deflagrative explosions: an acoustic approach, In: 13th Loss Prevention Symp. AIChE, Philadelphia, PA, 1980. (Abstract book).

20   T.R. Auton and J.H. Pickles, The calculation of blast waves from the explosions of pancake shaped vapour clouds, Central Electricity Research Laboratories RD/L/N210/78, 1978, p. 17.

21   C.A. Catlin, An acoustic model for predicting the overpressure caused by the deflagration of a ground lying vapour cloud, British Gas R & D Report, MRS E443, 1985.

22   J.C. Leyer, An experimental study of the pressure fields by exploding cylindrical clouds, Combustion Flame, 48 (1982) 251–263.

23   A.C. Van Den Berg, Computational investigation of blast due to spherical non steady deflagrative flames using low flame speed explosion simulation model, Report No. PML 1982–107, Prins Maurits Laboratorium, Rijswijk, The Netherlands, 1982.

24   W. Drenckhahn and C. Koch, Transition from slow deflagration to detonation, Seminar on the Results of the European Committees Indirect Action Research Program on Safety of Thermal Water Reactors, CEC Meeting, Brussels, 1985, In: Safety of Thermal Water Reactors, Graham and Trotman, London, 1985, pp. 223–240.

25   R.W. Woolfolk and C.M. Ablow, Blast waves from non ideal explosions, Proc. of Conf. Mechanisms of Explosion and Blast Waves, Feltman Research Laboratory, Picatinny Arsenal, Dover, 1973, p. 42.

26   J. Brossard, J.C. Leyer, D. Desbordes, J.P. Saint-Cloud, S. Hendricks, J.L. Garnier, A. Lannoy and J. Perrot, Air blast from unconfined gaseous detonations, in: M. Summerfield (Ed.), Progress in Astronautics and Aeronautics, Vol. 94, 1984, pp. 556–566.

27. A. Thomas and G.T. Williams, Flame noise: sound emission from spark ignited bubbles of combustion gas, Proc. R. Soc. A 294 (1966) 449–446.

28   R. Humbert-Basset and A. Montet, Dispersion dans l'atmosphère d'un nuage gazeux formé par épandage de GNL sur le sol, GNL3 Congress, Washington, 1972. (Abstract book).

29   W.J.S. Hirst and J.A. Eyre, Maplin Sands Experiments 1980: Combustion of large LNG and refrigerated liquid propane yields on the sea, Second Symposium on Heavy Gases and Risk Assessment, Frankfurt-am-Main, Germany, 25–26 May, 1982. In: S. Hartwig (Ed.), Batelle Inst./D. Reidel, Colombus, OH/Dordrecht, 1983

30   H.C. Rodean, W.J. Hogan, P.A. Urtiew, H.C. Goldwire, T.G. McRae and D.L. Morgan, Vapor burn analysis for the Coyote Series LNG Spill Experiments, Lawrence Livermore National Laboratory, Report UCRL 53530, Berkeley, CA, April 1984.

31   R.M. Dauwe, C.J.M. Wingerden and J.P. Zeeuwen, Experimental investigation into the blast effect produced by unconfined vapour cloud explosion, In: 4th Int. Symp. on Loss Prevention and Safety Promotion in the Process Industries, Harrogate, 12–16 September, 1983. AIChE event 290 of EFCE, Pergamon Press, London, 1983, pp. D20–D29.

32 A.J. Harrison and J.A. Eyre, The effect of obstacles and jet ignition on the combustion of
    gas clouds, In: 5th Int. Symp. on Loss Prevention and Safety Promotion in the Process
    Industries, Cannes, September 1986. Société de Chimie Industrièlle, Paris, 1967, pp.
    38.1 38.13.

Methods for vapour cloud explosion blast modelling

A.C. van den Berg[a],* and A. Lannoy[b]

[a] *TNO Prins Maurits Laboratory, P.O. Box 45, 2280 AA Rijswijk 'The Netherlands)*
[b] *EDF—Direction des Etudes et Recherches, 25, Allée Privée, Carrefour Pleyel,*
93206 Saint-Denis Cedex 1 (France)

Abstract

The potential explosion hazard of fuels is quantified by methods in which the explosive potential of a flammable fuel–air mixture is expressed as an equivalent explosive charge whose blast characteristics are known. In this paper, the two most current methods are described and demonstrated in a simple case study. TNT-equivalency methods have been widely used for this purpose for a long time now. Generally speaking, TNT-equivalency methods state a proportional relationship between the quantity of fuel available and the weight of a TNT charge expressing the cloud's explosive potential. However, fundamental and practical objections are met if the TNT-equivalency concept is used for vapour cloud explosion hazard assessment. To some extent, these difficulties are remedied in an alternative approach, the multi-energy method. In the multi-energy method, a flammable fuel–air mixture is considered to be explosive only if it is in a partially confined, congested or obstructed area in the cloud. The explosive potential of the fuel–air mixture in the various partially confined, congested or obstructed regions can be expressed as a corresponding number of equivalent fuel–air charges. The multi-energy concept is shown to be a flexible concept which makes it possible to incorporate current experimental data and advanced computational methods into the procedure of vapour cloud explosion hazard analysis.

1. Introduction

The long list of vapour cloud explosions from the past indicates that the presence of a quantity of fuel constitutes a potential explosion hazard. If a quantity of fuel is released, it will mix with air and a flammable vapour cloud may result. If the cloud meets an ignition source, the flammable mixture will be consumed by a combustion process which, under appropriate conditions, may develop an explosive intensity and heavy blast. Therefore, safety measures are desirable.

Safe stand-off distances should be exercised between locations where large quantities of fuels are stored or handled and places where people live or work.

---

*To whom correspondence should be addressed.

Control buildings at chemical plants or refineries and safety related structures of nuclear power plants, for instance, should be designed in such a way that they can withstand the destructive power of a vapour cloud explosion in their vicinity.

To establish fair premium rates, underwriters need to know the property damage potential of a quantity of fuel. For all these purposes, blast modelling methods are required by which the explosive potential of a fuel–air cloud present in some given environment can be quantified. Such methods express the explosive power of a vapour cloud as an equivalent explosive charge whose blast characteristics are known. TNT-equivalency methods, for instance, state a proportional relationship between the quantity of fuel in the cloud and the weight of an equivalent TNT-charge expressing its explosive power. Up to this day, TNT-equivalency methods are widely used for this purpose. However, TNT-equivalency methods are becoming progressively less satisfactory as the understanding of blast generation vapour cloud explosions increases.

Methods which utilize an equivalent fuel–air charge to express the potential explosive power may overcome the imperfections of TNT-equivalency blast modelling to some extent. Such a charge can be characterized by, for instance, applying the multi-energy philosophy which reflects the current understanding of vapour cloud explosions. In addition, the multi-energy concept makes it possible to incorporate current experimental data and advanced computational fluid dynamics into the procedure of vapour cloud explosion hazard assessment.

In this paper, both these most current methods are described and briefly demonstrated in a simple case study – a vapour cloud explosion hazard assessment with regard to a storage site for liquefied hydrocarbons.

1.1 Statement of the problem

A view of the storage site is represented in Fig. 1. Three storage spheres containing liquefied propane are situated next to a large butane tank of 50 m
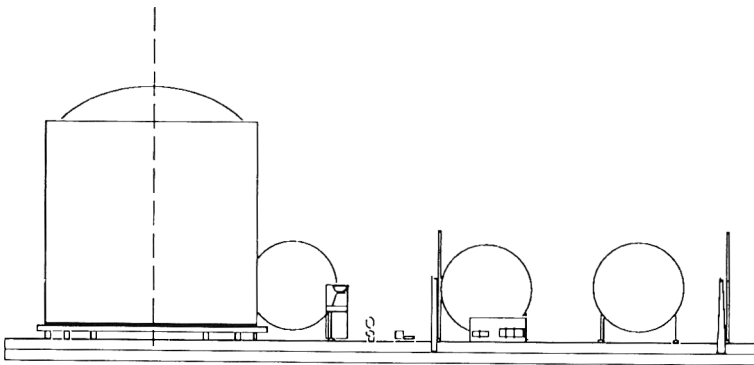

Fig. 1. View of a storage site for liquefied hydrocarbons.

diameter and 30 m height. To diminish heat inflow from the soil, the butane tank is placed 1 m above the earth's surface on a concrete pylon forest. In this environment a massive release of 20 tons of propane is anticipated. What blast effects can be expected if the propane forms a large flammable cloud blanketing the storage site and meets an ignition source?

For a complete description of blast loading, the full pressure–time history of the blast wave should be specified at any location in a vapour cloud explosion's environment. A blast model, on the other hand, defines a blast wave only in terms of the peak overpressure, the positive phase duration and the positive impulse, while the under-ambient pressure effects are neglected. These blast parameters are minimally required to calculate the behaviour of structures under blast loading or to assess explosion damage. Figure 2 plots idealized
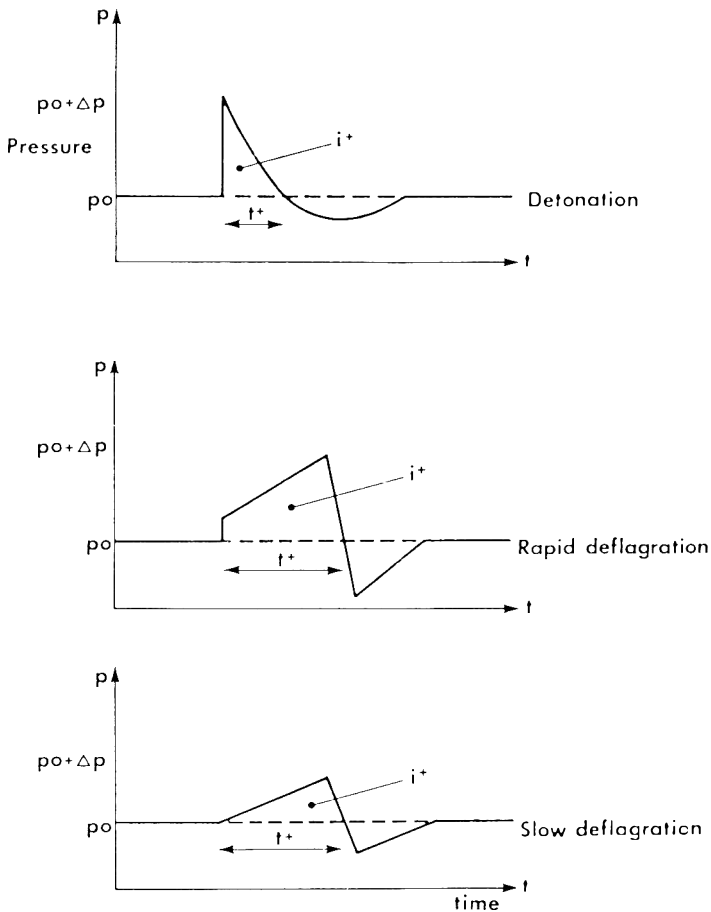

Fig. 2. Ideal blast wave structure (P_o = ambient pressure, Δp = peak overpressure, t^+ = positive phase duration, i^+ = positive impulse).

blast wave shapes and points out the parameters defining the blast load for structures.

2. TNT-equivalency methods

2.1 The basic concept

For a long time now, the military has been interested in the destructive potential of high-explosives. Therefore, extensive experimental data on the relation between TNT and damage have been available for many years. Consequently, it is quite obvious that the explosive power of accidental explosions, deduced from the damage patterns observed, was expressed as equivalent TNT-charge weights. Because the quantification of the potential explosive power of fuels was a necessity long before the mechanisms of blast generation in vapour cloud explosions were understood, it is fully comprehensible that the TNT-equivalency concept was also utilized to make predictive estimates for vapour cloud explosion hazard assessment.

Basically, the use of TNT-equivalency methods for blast predictive purposes is very simple. The available combustion energy in a vapour cloud is converted into an equivalent charge weight of TNT according to:

$$W_{TNT} = \alpha_e \, W_f Q_f / Q_{TNT}$$

where α_e denotes the TNT-equivalency, W_{TNT} the equivalent weight of TNT, W_f the total weight of fuel in cloud, Q_f the heat of combustion of fuel, and Q_{TNT} the heat of explosion of TNT (4.12–4.69 MJ/kg).

If the equivalent charge weight is known, the corresponding blast characteristics can be read from Fig. 3, which represents experimental TNT-blast data, an excerpt from the military technical manual TM 5-1300. Strictly speaking, the problem of vapour cloud explosion blast modelling is reduced to the determination of an appropriate value for the TNT-equivalency.

2.2 Blast modelling

Over the years many companies and authorities each developed their very own approach with regard to the use of the TNT-equivalency concept in vapour cloud explosion hazard assessment. Because all these methods differ only in details, only one of them is described here.

Within the framework of safety studies of nuclear power plants, where special importance was attached to the assessment of dangers which could arise from nearby industrial activities, in references [2–4] a statistical analysis is performed on more than 120 damage points of 23 accidents. A wide distribution of TNT equivalencies (0.02%–15.9%) with a median value of 3% was observed. 97% of the cases was covered by a TNT equivalency lower than or equal to 10%, while the mean value observed was a TNT equivalency of 4%, covering 60% of the cases.

The value of 10% corresponds approximately to a TNT equivalent of 1 kg of TNT for every kg of hydrocarbon released and to 5 kg of TNT for every kg of hydrocarbon mixed with air between the flammability limits. The latter value can be used if the flammable portion of the cloud is determined by means of dispersion calculations.

In addition, the analysis in references [3] and [4] showed that ignition delay and the presence of objects in the cloud are important factors in vapour cloud explosions and that blast effects are often asymmetric and directional.

TNT equivalency methods for vapour cloud explosion modelling should only be used for the assessment of blast effects in the far-field where the overpressure level is less than 30 kPa. In the near-field their use can lead to the
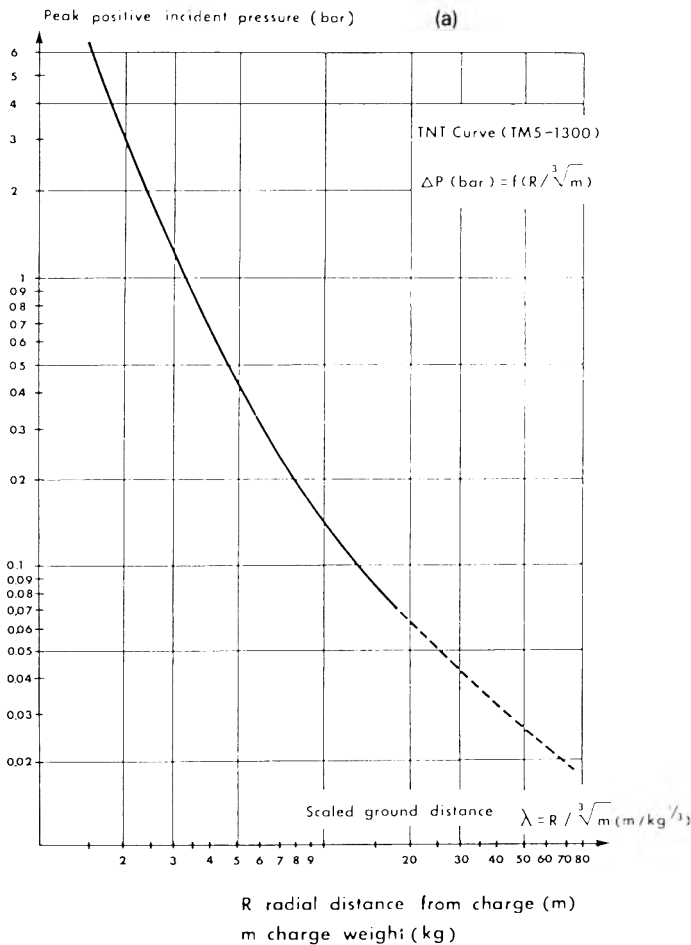

Fig. 3. (a) Blast peak incident overpressure for a hemispherical TNT charge at sea level [1]. (b) Blast positive phase duration for a hemispherical TNT charge at sea level [1]. (c) Blast positive incident impulse for a hemispherical TNT charge at sea level [1].

Scaled positive duration of positive phase   **(b)**

$$\frac{t+}{\sqrt[3]{m}} \left(\frac{10^{-3}s}{\sqrt[3]{kg}} \right)$$

Scaled ground distance $\lambda = \dfrac{R}{\sqrt[3]{m}} \; (m/\sqrt[3]{kg})$

Scaled positive incident impulse   **(c)**

$$\frac{t+}{\sqrt[3]{m}} \left(\frac{10^{-4}\,bar\cdot s}{\sqrt[3]{kg}} \right)$$

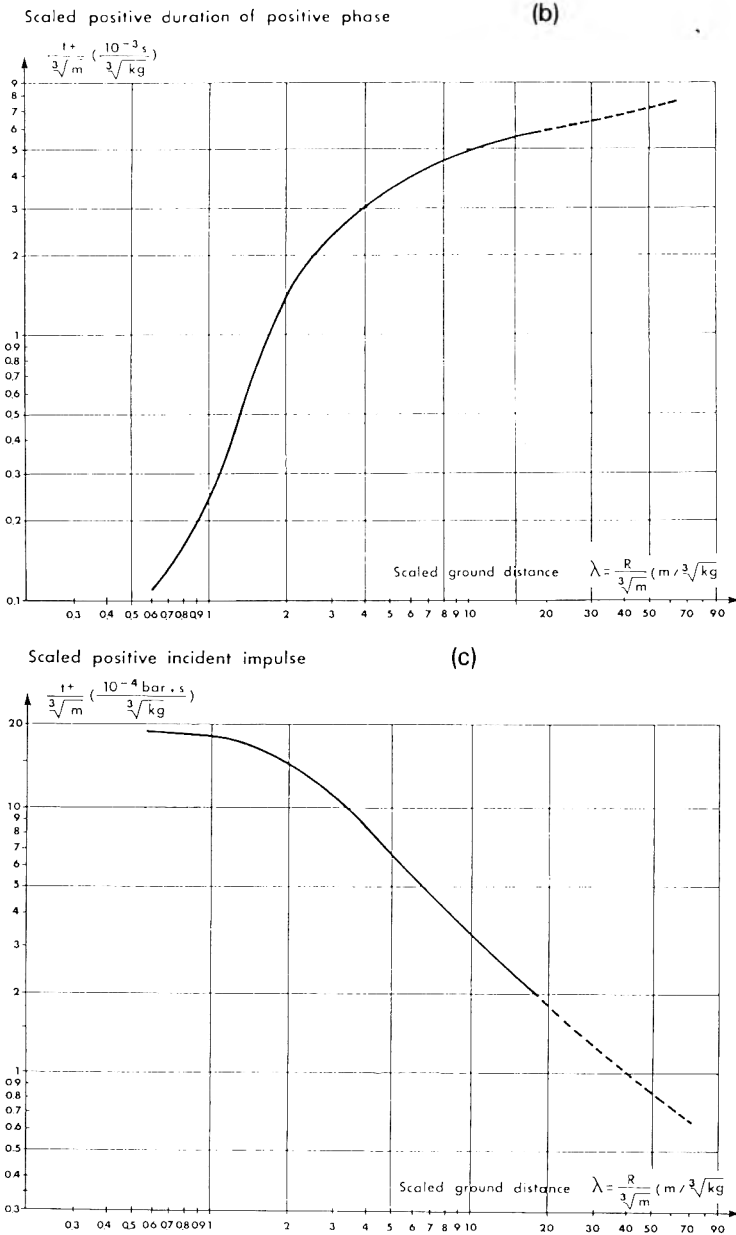Scaled ground distance $\lambda = \dfrac{R}{\sqrt[3]{m}} \; (m/\sqrt[3]{kg})$

Fig. 3. Continued.

overdesign of structures. Note that a French Authority Safety Rule [5] recommends the 10% equivalency for safety calculations and that the French Chemical Industry [6] recommends the 4% equivalency, both based on the full amount of fuel released.

TABLE 1

Comparison of blast characteristics modelled by both TNT-equivalency methods and the multi-energy method

Overpressure (kPa)	TNT equivalency				Multi-energy method energy	
	10%		4%		7330 MJ	
	Distance (m)	Positive phase duration (ms)	Distance (m)	Positive phase duration (ms)	Distance (m)	Positive phase duration (ms)
30	165	100	120	74	57	40
20	210	117	155	86	75	45
10	355	138	260	102	120	50
7	490	152	360	112	160	53
5	680	163	500	120	210	55

Application of the above recommendations to the case study on the liquefied hydrocarbons storage site results in the conclusion that the explosive potential of the 20 tons of propane can be expressed as:
(a) a 20 ton charge of TNT with a confidence level of 97%;
(b) an 8 ton charge of TNT with a confidence level of 60%.
The blast characteristics in the form of blast overpressures and positive phase durations at various distances to the charges are summarized in Table 1 together with the results of the multi-energy blast modelling.

2.3 Discussion
The basic assumption in TNT-equivalency methods – a relation between the amount of fuel available in the cloud and the TNT-charge weight expressing the cloud's explosive potential – is most questionable. This is reflected by the wide range of TNT equivalencies found if a large number of vapour cloud explosion incidents, involving only fuels whose heats of combustion are of the same order of magnitude as hydrocarbons, is analysed [3, 4, 7, 8].

Nevertheless, the TNT-equivalency concept makes it possible to model the blast effects of a vapour cloud explosion in a very simple and practical way. The great attractiveness of TNT-equivalency methods is the very direct, empirical relation between a charge weight of TNT and the attendant structural damage. Therefore, TNT equivalency is a useful tool if the property damage potential of vapour clouds is the major concern.

Values for the TNT equivalency, recommended for use in vapour cloud explosion hazard assessment, are deduced by statistical analysis from the damage observed in a limited number of major vapour cloud explosion incidents. From the wide distribution of TNT equivalencies observed, characteristic values such as an average (4%) and an approximate upper limit (10%)

were recommended to be used for predictive purposes [3, 4]. The average value of 4% is very near the TNT equivalency in the distribution where the majority of cases are found, i.e. a TNT equivalency of 4% corresponds to "an average major incident". Undoubtedly, "an average major incident" represents a situation where an accidental release of fuel is most likely such as, for instance, the site of a refinery or chemical plant or the site of a crowded marshalling yard during operations. Strictly speaking, by using an average value of the TNT equivalency, "average major incident conditions" are extrapolated to an actual situation. Therefore, TNT-equivalency methods give a reasonable estimate of far-field blast effects only if the actual conditions correspond more or less to "average major incident conditions".

TNT blast is a poor model for gas explosion blast. While a TNT charge produces a shock wave of a very high amplitude and a short duration, a vapour cloud explosion produces a blast wave, often shockless, of lower amplitude and longer duration. If the blast modelling is the starting point for the computation of structural response for, for instance, the design of blast resistant structures, TNT blast will be a less satisfactory model. Then the shape and the positive phase duration of the blast wave are important parameters which should be considered and the use of a more appropriate blast model is recommendable.

A practical value for TNT equivalency is an average, based on a wide statistical distribution of TNT equivalencies found in practice. As a consequence, a predictive estimate with TNT equivalency on the basis of an average value for the TNT equivalency has a very limited statistical reliability. A more deterministic estimate of blast effects is possible if a parameter could be found which correlates with the process of blast generation in vapour cloud explosions. In the multi-energy method such a parameter is introduced.

3. The multi-energy method

3.1 The basic concept

Presently, the belief is gaining ground that it is hardly possible to detonate an unconfined vapour cloud. The point is that the inhomogeneity of the fuel–air mixture, which is inherent to the process of atmospheric dispersion, prevents a possible detonation wave from propagating [9]. The heavy vapour cloud explosion on December 7, 1970 at Port Hudson (MO), USA where a substantial part of a large unconfined propane–air cloud detonated [10], should be blamed on a highly exceptional coincidence of circumstances. Lingering in a shallow valley under calm atmospheric conditions, the dense propane–air mixture had the opportunity to homogenize sufficiently by molecular diffusion during an exceptionally long ignition delay [9]. Therefore, in a vast majority of cases, the assumption of deflagrative combustion is a sufficiently safe approach in a vapour cloud explosion hazard assessment.
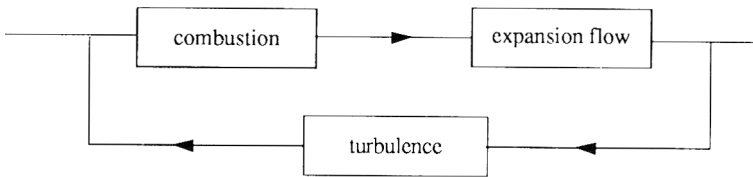
Fig. 4. Positive feedback, the basic mechanisms of a deflagrative gas explosion.

For blast generation in deflagrative premixed ccmbustion, turbulence generating (boundary) conditions are required. These boundary conditions trigger a positive feedback coupling in the process of flame propagation by which it develops more or less exponentially both in speed and pressure. A deflagrative gas explosion may be well defined as a process of combustion driven expansion flow in which the turbulent structure of the flow field is acting as an uncontrolled positive feedback (Fig. 4).

The consequence is that a turbulence generating environment is required for the development of explosive blast generating combustion. This statement has important consequences for the concept of a vapour cloud explosion which underlies the method of blast modelling. This basic concept, called the multi-energy concept, states that blast is generated in vapour cloud explosions only where the flammable mixture is partially confined and/or obstructed while, on the other hand, the unconfined/unobstructed mixture hardly contributes [11]. This concept is increasingly supported by both small-scale and large-scale experiments, including references [12–16]. So, contradictory to more conventional methods, in which a vapour cloud explosion is regarded as an entity, in the multi-energy concept a vapour cloud explosion is rather defined as a number of sub-explosions corresponding with the various partially confined/obstructed areas in the cloud.

3.1.1 Application

The space underneath the storage tank is the only location at the storage site where blast generating boundary conditions are found. For the space underneath the storage tank is an outstanding example of a combination of partial confinement by extended parallel planes and obstruction by the pylon forest which pre-eminently is a turbulence generating environment. On the other hand, the space underneath and in between the propane spheres is relatively open and unobstructed. Therefore, the multi-energy concept applied to this situation indicates that, if the entire storage site is blanketed in an extended flammable cloud, only the explosive combustion which develops underneath the storage tank is responsible for the blast produced upon ignition of the cloud. The blast effects produced by this gas explosion are mainly determined by the quantity of combustion energy present in the space underneath the butane tank and the intensity of the combustion process. Both are primarily determined by the size, shape and nature of the partially confined

and obstructed space. The reactivity of the fuel–air mixture is a factor indeed, but of secondary influence.

3.2 The blast model

To bypass the imperfections of TNT blast as a model for gas explosion blast, in the multi-energy method fuel–air charge blast is used for this purpose. Figure 5 shows the peak overpressure as well as the positive phase duration of the blast wave, produced by a hemispherical fuel–air charge of radius R_0 at the earth's surface, dependent on the distance to the blast centre in a Sachs-scaled representation. This blast model is generated by numerical simulation of spherical steady flame speed gas explosions. The heat of combustion of the fuel–air mixture was assumed to be 3.5 MJ/m^3, which is representative for an average stoichiometric hydrocarbon–air mixture.

The blast model reflects basic features of gas explosion blast. The initial blast strength is a variable expressed as a number ranging from 1 for insignificant to 10 for detonative strength. The initial blast strength can be defined as a consistent set of blast parameters at the location of the charge radius R_0. In addition, the model gives an indication for the blast wave shape. It is interesting to note that the detonative blast characteristics are in good agreement with experimental data according to [17].
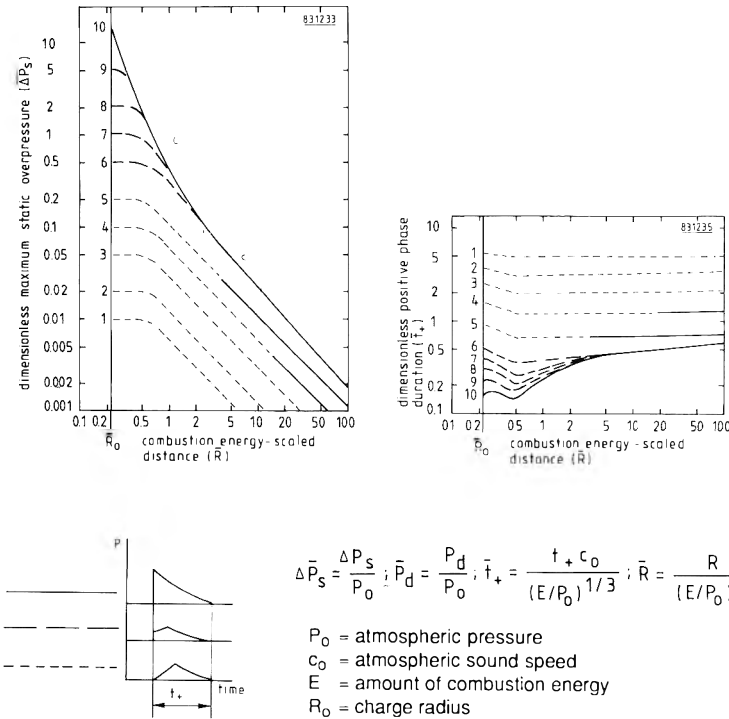

$$\Delta \bar{P}_s = \frac{\Delta P_s}{P_0} \; ; \; \bar{P}_d = \frac{P_d}{P_0} \; ; \; \bar{t}_+ = \frac{t_+ c_0}{(E/P_0)^{1/3}} \; ; \; \bar{R} = \frac{R}{(E/P_0)^{1/3}}$$

P_0 = atmospheric pressure
c_0 = atmospheric sound speed
E = amount of combustion energy
R_0 = charge radius

Fig. 5. Hemispherical fuel–air charge blast model [11].

The blast produced by the gas explosion underneath the storage tank can now be modelled by the blast from an equivalent hemispherical fuel–air charge which is characterized by a size and a strength.

3.3 The charge size

A safe and conservative estimate for the size of the charge can be made by assuming that the whole space underneath the tank is filled with a stoichiometric mixture which wholly contributes to the blast. Consequently, the radius of the hemispherical charge is approximately 10 m which corresponds with an energy of 7330 MJ (heat of combustion = 3.5 MJ/m^3).

3.4 The charge strength

A reasonable estimate for the strength of the blast is a more difficult problem which can be overcome in a variety of ways depending on the accuracy required.

3.4.1 Safe and conservative data

A safe and conservative estimate for the strength of the charge for near-field blast effects is 10, i.e. the assumption of detonative combustion (see Fig. 5). For far-field blast effects, on the other hand, the assumption of any strength higher than or equal to number 6 is sufficient because far-field effects are independent of the charge strength whether the explosion was a strong deflagration (number 6) or detonation (see Fig. 5).

If such a safe and conservative approach results in unacceptably high overpressures, a more accurate estimate for the initial blast strength may be found by consulting the growing body of experimental data on gas explosions or by performing an experiment tailored for the situation in question.

3.4.2 Experimental data

Since more than a decade ago, an increasing amount of experimental data (both on laboratory and full scale) on gas explosions in partially confined/obstructed environments becomes available. Many parameters were varied such as: degree of confinement, geometry, obstacle parameters, fuel reactivity and mixture composition. This growing body of experimental data offers the opportunity to compare actual situations with experimental data. It would be desirable to identify and collect these data, to structure a data base and to develop access to this information. It would be highly interesting, for instance, if these data could be parameterized, i.e. if the blast strength could be correlated to parameters such as: degree of confinement, obstacle configuration parameters and fuel reactivity.

For a good interpretation of the mostly small-scale experiments, a good understanding of scale effects in gas explosions is a necessity.

Experiments which could give a first indication of the overpressure to be expected from the gas explosion in the space underneath the butane tank are

reported by Van Wingerden [14]. A large number of obstacle configurations between parallel planes was investigated with regard to their blast generating capabilities. On the basis of these experimental data, a first estimate for the overpressure, generated underneath the butane tank, of 50 kPa to 200 kPa would be reasonable.

In addition, a good understanding of scaling effects offers the possibility of physical modelling, i.e. the estimation of overpressures by an experiment in a scaled down version of the actual situation.

3.4.3 Computational data

An approach which seems very promising for the near future is numerical simulation with advanced computational fluid dynamic computer codes such as FLACS [18, 19] and REAGAS [20, 21]. These codes are capable of simulating the basic mechanism of a gas explosion, the feedback coupling in the interaction of combustion, expansion flow and turbulence. Here, the REAGAS code is utilized to simulate the gas explosion in the space underneath the storage tank. The mathematical model which underlies the REAGAS code can be summarized as follows:

1. The gas dynamics is modelled as a gaseous fluid which expands as a consequence of heat addition. This is expressed in conservation equations for mass, momentum and energy.
2. The energy addition is supplied by combustion which is modelled as a simple one-step conversion process of unburnt mixture into combustion products. This is expressed in a conservation equation for the mixture mass fraction with a negative source term for the combustion rate.
3. The combustion rate, which is fully controlled by turbulent mixing of combustion products with unburnt mixture, is modelled by the Bray–Libby–Moss Unified Probability Function model [22].
4. The feedback in the interaction is closed by a k–ε model for turbulence which consists of conservation equations for the turbulent kinetic energy k and its dissipation rate ε.

The pylon forest underneath the butane storage tank was simplified into a two-dimensional obstacle environment, represented in a 130×65-node grid. The obstacles are placed in 11 concentric circles according to the pylon lay out (Fig. 6(a)). It is likely that the vapour cloud will meet an ignition source somewhere at the storage site outside the partially confined area. Then the combustion process in the obstacle configuration will be initiated from its edge. The present concept of the REAGAS code, however, cannot cope with edge-ignition. In an attempt to approximate an edge-ignited explosion the combustion process was initiated halfway between centre and edge. The results are represented in Figs. 6(a) and 6(b). Figure 6(a) shows the temperature distribution in the flow field at a few points of time during the development of the gas explosion. The temperature distribution is visualized by a pattern of isotherms, one for each change in temperature of 150 K. The temperature is, of course, a good indicator for the combustion process. The sequence of pictures

shows a behaviour which is characteristic for gas explosions, namely, a slow start followed by a more or less exponential development in speed and pressure once the feedback coupling in the process of flame propagation is triggered.

This behaviour can be readily recognized in the overpressure transients sampled at various locations in the axis of symmetry (Fig. 6(a)). The computations show that an overpressure of more than 70 kPa is observed in location 4 (Fig. 6(a)) where the combustion process attains its highest intensity. Higher overpressures are to be expected if the combustion process would be initiated closer to the edge.

(a)
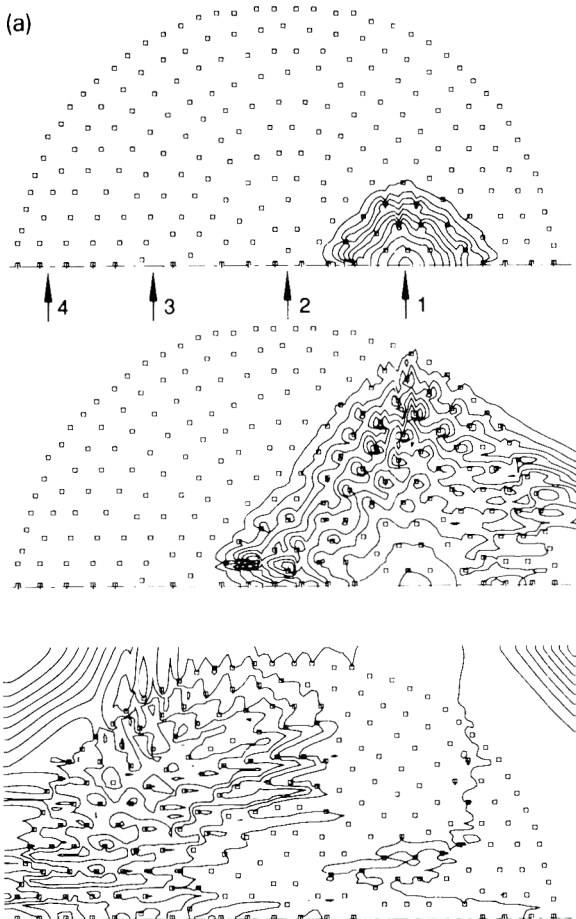
Fig. 6. (a) REAGAS simulation of a gas explosion developing in a concrete pylon forest underneath the butane storage tank. Temperature distribution visualized by an isotherm pattern, one isotherm for each change in temperature of 150 K. (b) Pressure transients sampled at four locations indicated in Fig. 6(a).
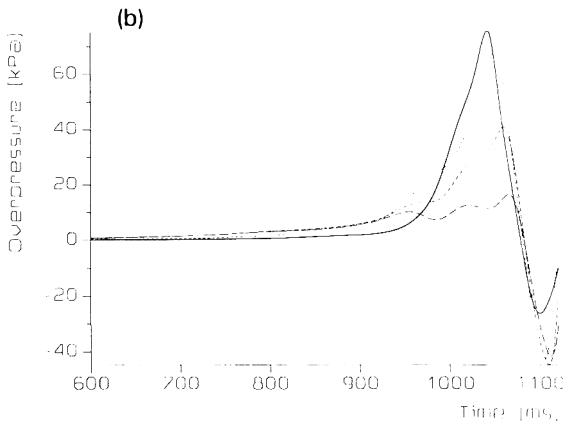
Fig. 6. Continued.

As a consequence, a maximum overpressure of approximately 100 kPa, generated by the gas explosion underneath the tank, is considered realistic. The overpressure corresponds to a blast strength of number 7 of the fuel–air charge blast model (Fig. 5).

3.5 Far-field blast effects

With the vapour cloud's explosive potential expressed as an equivalent fuel–air charge of a radius $R_0 = 10$ m ($E = 7330$ MJ) and a strength of number 7, the potential blast effects of the vapour cloud explosion can be found by substitution of these data in the Sachs-scaled fuel–air charge blast model (Fig. 5). Blast peak overpressures as well as durations of the blast wave's positive phase at several distances to the charge centre are presented in Table 1 beside the results of the blast modelling calculations on the basis of TNT-equivalency (Section 2.2).

The figures in the Table 1 show that, relative to the multi-energy method, the vapour cloud's explosive potential is strongly overestimated by TNT-equivalency methods. The problem is that conventional TNT-equivalency methods should not be used in situations such as in the present case study where the conditions at the storage site differ substantially from so-called "average major incident conditions", on which the used values for the TNT-equivalency were based (Section 2.3).

3.6 Near-field blast effects

After all, the representation of blast effects by means of a spherical model results in a highly idealized picture which may hold only for the far-field, at best. Blast effects produced by a partially confined space of such a large aspect ratio (length/height) as in the present situation are largely determined by the size of the opening through which the generated overpressure is vented from the confinement into free space. In addition, the partial confinement by extended

parallel planes induces a preferential direction in the combustion process. The consequence is that the near-field blast effects are highly directional, a well-known effect in the vapour cloud explosion literature. In addition, near-field blast effects are largely influenced by the interaction with nearby structures and objects. For the gas explosion in question, the near-field blast wave propagation is largely influenced by the presence of the butane storage tank itself.

These effects can be approximated by numerical simulation. In this paper, these effects are simulated with the BLAST code [23]. This code is capable of computing blast effects by the solution of the Euler equations in a two-dimensional space. The Euler equations describe the conservation of mass, momentum and energy for inviscid flow of a perfect gas. Flux-corrected transport [24] is used to capture and preserve shock phenomena.

For the problem in question, the code is initialized with a perfect gas in the space underneath the storage tank, pressurized up to a pressure and temperature so that a 100 kPa overpressure blast wave is formed on the burst. The computation is performed in a cylindrical grid consisting of 300 × 300 nodes. The results are represented in Figs. 7(a) and 7(b). The pressure distribution in the flow field at a few consecutive points of time is represented in Fig. 7(a). The
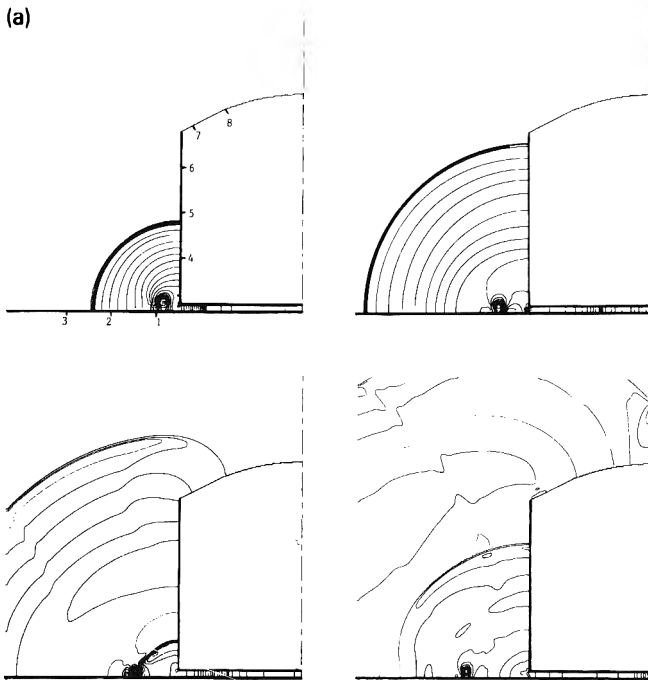
(a)

Fig. 7. (a) BLAST simulation of the near-field blast produced by the gas explosion underneath the butane storage tank. Pressure field visualized by an isobar pattern, one isobar for each change in pressure of 2.5 kPa. (b) Blast overpressures sampled at various locations in the vicinity of the gas explosion. The locations are indicated in Fig. 7(a).
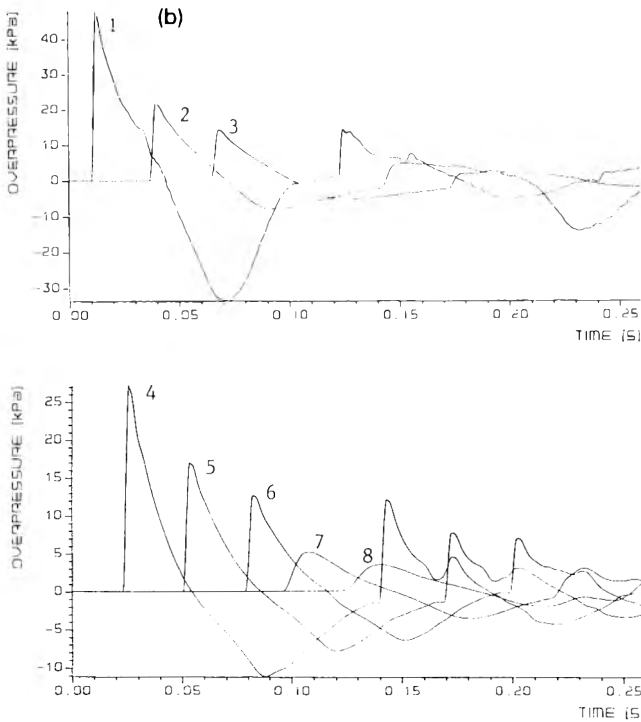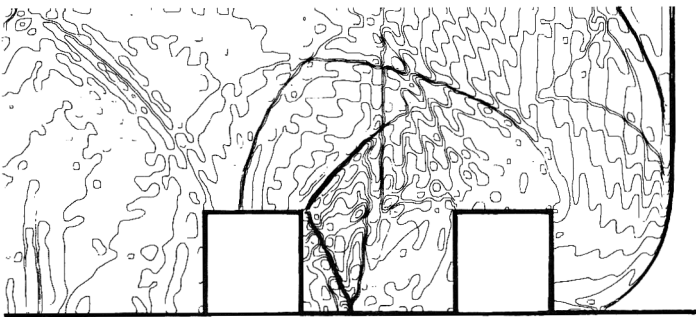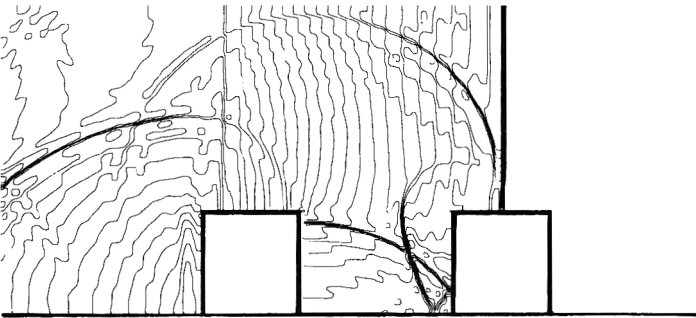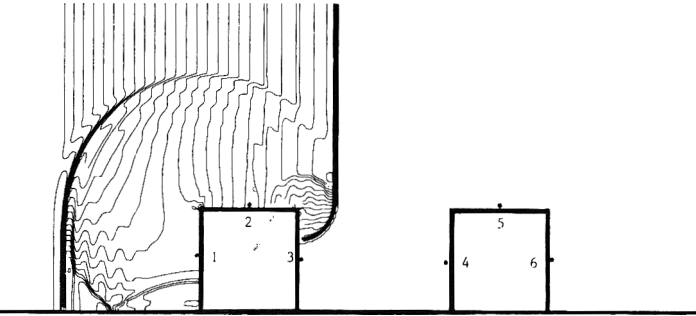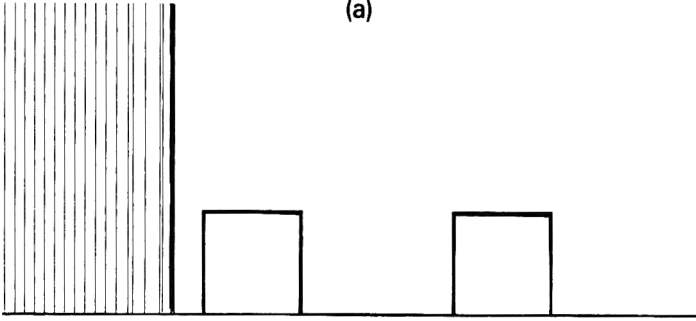
Fig. 7. Continued.

pressure distribution is visualized by a pattern of isobars, one for each change in pressure of 2.5 kPa. Shock phenomena are present where isobars accumulate. In addition, the overpressures sampled at various locations at the earth's surface as well as at the tank's wall and roof are represented in Fig. 7(b). Figures 7(a) and 7(b) show some features which are very characteristic of blast from gas explosions.

1. The blast wave shows a very pointed negative phase.
2. At the rim of the vent opening, a vortex structure is generated. Such a flow phenomenon is characterized by a substantial pressure dip in its centre.
3. The formation of a secondary wave. Blast is the result of fast expansion of combustion products. Because of the inertia of the expanding fluid, the

Fig. 8. (a) BLAST simulation of the blast wave reflection by a complex of two buildings. Pressure field visualized by an isobar pattern, one isobar for each change in pressure of 0.5 kPa. (b) Overpressures sampled in various locations in the buildings. Locations are given in Fig. 8(a).
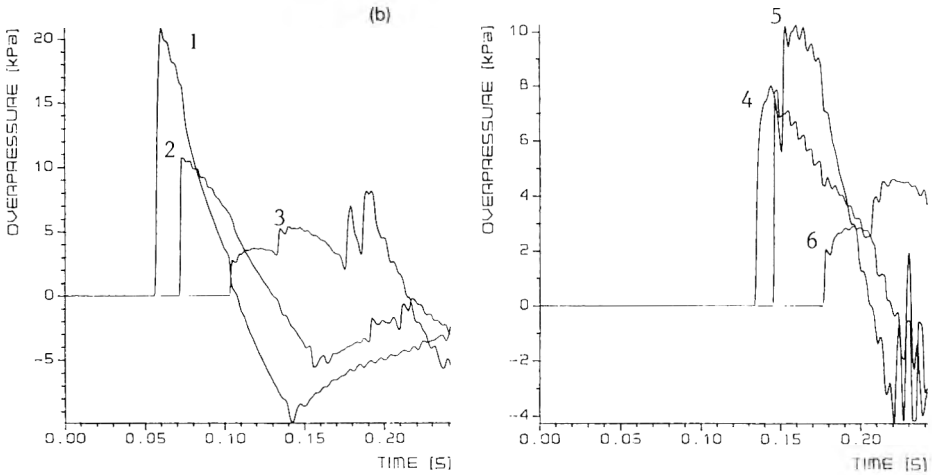
(a)

Fig. 8. Continued.

combustion products overexpand, while generating under-ambient pres-
sures in the blast centre. Consequently, the flow reverses which results in
recompression of the fluid in the blast centre. The subsequent expansion
produces a secondary wave.
These phenomena come alive in the sequence of pictures in Fig. 7(a) and can be
traced in the overpressure samples in Fig. 7(b).

3.7 Blast loading

Numerical simulation of blast may reveal all details of the blast loading
endured by any object of any shape at any distance from the explosion. To
demonstrate this, in Figs. 8(a) and 8(b) the results are presented of a BLAST [23]
simulation in a 350×150-node grid of a blast wave of 10 kPa overpressure and
60 ms duration falling in at two buildings located close behind one another. It
is to be expected that the blast loading at these buildings will be considerably
influenced by one another's presence.

In Fig. 8(a) the pressure field is represented which develops as a consequence
of the blast wave reflection at the configuration. At some consecutive points of
time the pressure distribution is visualized by means of an isobar pattern, one
isobar for each increase in pressure of 0.5 kPa. The pictures give a clear view of
how the blast loading is the result of a combination of wave reflection and
lateral rarefaction of reflected overpressures. In particular, they show how in
between the two buildings a complicated wave pattern develops, a consequence
of various reflections and wave interactions. The overpressures sampled at
three different locations in each building are graphically represented in Fig.
8(b). In the overpressure transients, the complicated wave pattern can be
readily recognized.

The overpressure build-up in transient number 3, for instance, sampled at the back wall of the first building shows a sequence of four shock phenomena which can be traced in the plots. The first corresponds with the passage of the shock of the infalling blast wave, diffracted around the building. The second corresponds with the same wave, after reflection by the ground.

The third corresponds with the infalling shock wave, reflected directly from the front of the second building. This shock phenomenon is immediately followed by a fourth which is the result of reflection by the second building and the ground.

The computation shows that the blast load at the front of the second building is considerably less than the reflected overpressure of the undisturbed blast wave endured by the front of the first building. In this way the effects of blast load reduction by sheltering effects can be quantified. Such calculations can provide the data required for the determination of the behaviour of structures under blast loading.

4. Conclusion

The two most current methods for vapour cloud explosion blast modelling are described and demonstrated in a simple case study. It shows that TNT-equivalency methods are easy to use. Because of the direct empirical relation between TNT and structural damage, they are particularly attractive if the vapour cloud's property damage potential is the major concern. They should only be used to determine far-field blast effects. TNT-equivalency methods, however, are unsatisfactory is several respects. In particular, they fail when the actual conditions to be modelled differ substantially from so-called "average major incident conditions", i.e. the conditions the used values for the TNT-equivalency were based on.

The multi-energy method is an alternative. Contradictory to TNT-equivalency, in the multi-energy concept, the fuel–air mixture is considered to be explosive only in partially confined, congested or obstructed areas of the cloud. In the multi-energy method, an extra parameter — the initial blast strength — is introduced which may be difficult to determine. However, even if the blast strength is conservatively estimated, the multi-energy method gives a more appropriate prediction of the explosive potential of a vapour cloud than TNT-equivalency methods. It should be emphasized that the multi-energy concept holds only if the possibility of unconfined vapour cloud detonation can be ruled out.

The multi-energy framework is a flexible concept which makes it possible to incorporate current experimental data and advanced computational techniques into the procedure of vapour cloud explosion blast modelling. In particular, the application of computational fluid dynamic codes such as REAGAS and BLAST are shown to contribute to a more and more sophisticated approach in vapour cloud explosion hazard analysis. Although the computational results

presented were obtained with two-dimensional methods, three-dimensional methods are fully operational.

In the near future, substantial progress in vapour cloud explosion blast modelling can be made by:

1. The development of a data base containing data on both vapour cloud explosion incidents and gas explosion experiments (small- and full-scale).
2. A further development of software for the computational simulation of the process of turbulent premixed combustion in gas explosions and blast effects.
3. The multi-energy concept applies only if the possibility of unconfined detonation can be ruled out. Therefore, the confidence in the multi-energy method for vapour cloud explosion blast modelling will increase substantially if the conditions under which the possibility of unconfined vapour cloud detonation should be considered, are further specified.

References

1   TM5-1300, Structures to Resist the Effects of Accidental Explosions, Technical Manual, Departments of the Army, Navy and Air Force, TM5-1300/NAFVAC-P 397/AFM 88 22, 1969.
2   T. Gobert and A. Lannoy, Analyse d'accidents dans l'industrie pétrolière. Determination de l'équivalent TNT'des hydrocarbures, SMIRT 4, San Francisco, CA, 1977.
3   A. Lannoy, Analyse des explosions accidentelles réelles. Evaluation du rendement d'explosion pour la prévision des effets de surpression, Revue Générale de Thermique, March, 1982.
4   A. Lannoy, Analyse des explosions air–hydrocarbure en milieu libre. Etudes déterministe et probabiliste du scénario d'accident; prévision des effets de surpression, Bulletin de la Direction des Etudes et Recherches d'Electricité de France-Série A, No. 4, Saint Denis, 1984.
5   French Authority Safety Rule, Règle fondamentale de Sureté I.2.d Prise en compte des risques liés à l'environnement industriel et aux voies de communication. Ministère de l'industrie, Paris, 1982.
6   French Chemical Industry, Cahier de sécurité: Explosion de gaz en milieu non confiné, Union des Industries Chimiques, 1986.
7   K. Gugan, Unconfined Vapour Cloud Explosions, The Institution of Chemical Engineers, London, 1979.
8   D.K. Pritchard, A review of methods for predicting blast damage from vapour cloud explosions, J. Loss Prev. Process Ind., 2(4) (1989) 187–193.
9   A.C. van den Berg, On the possibility of vapour cloud detonation, TNO Prins Maurits Laboratory Report No. PML 1987-IN-50, Rijswijk, The Netherlands, 1987.
10   D.S. Burgess and M.G. Zabetakis, Detonation of a flammable cloud following a propane pipeline break on December 9, 1970 in Port Hudson, MO, USA, U.S. Bureau of Mines Report of Investigations No. 7752, Washington, DC, 1971.
11   A.C. van den Berg, The Multi-Energy Method – a framework for vapour cloud explosion blast prediction, J. Hazardous Mater. 12 (1985) 1–10.
12   J.P. Zeeuwen, C.J.M. van Wingerden and R.M. Dauwe, Experimental investigation into the blast effect produced by unconfined vapour cloud explosions, In: 4th Int. Symp. on Loss Prevention and Safety Promotion in the Process Industries, Harrogate, UK, 1983, pp. D20–D29.

13   A.J. Harrison and J.A. Eyre, The effect of obstacle arrays on the combustion of large premixed gas/air clouds, Combustion Sci. Technol., 52 (1987) 121–137.
14   C.J.M. van Wingerden, Experimental investigation into the strength of blast waves generated by vapour cloud explosions in congested areas, In: 6th Int. Symp. on Loss Prevention and Safety Promotion in the Process Industries, Oslo, 1989, pp. 26–1/26–16.
15   A. Lannoy and A. Leroy, A practical way of assessing semi-confined explosion effects, In: 6th Int. Symp. on Loss Prevention and Safety Promotion in the Process Industries, Oslo, 1989, pp. 99–1/99–14.
16   R.J. Harris and M.J. Wickens, Understanding vapour cloud explosions — An experimental study, In: 55th Autumn Meeting of the Institution of Gas Engineers, 27–28 November, 1989, Kensington, UK.
17   J. Brossard et al., Air blast from unconfined gaseous detonations, Prog. Astronaut. Aeronaut., 94 (1984) 556–566.
18   B.H. Hjertager, Simulation of transient compressible turbulent reactive flows, Comb. Sci. Technol., 27 (1982) 159–170.
19   B.H. Hjertager, Simulation of gas explosions, Mod. Ident. Control, 10(4) (1989) 227–247.
20   A.C. van den Berg, Current research at TNO on vapour cloud explosion modelling, In: Int. Conf. on Vapour Cloud Modelling, Cambridge, MA, 1987, pp. 687–711.
21   A.C. van den Berg, REAGAS — A code for numerical simulation of reactive gas dynamics, TNO Prins Maurits Laboratory Report No. PML 1989-IN-48, Rijswijk, The Netherlands, 1989.
22   K.N.C. Bray, Turbulent flows with premixed reactants, In: Turbulent Reacting Flows, Springer-Verlag, New York, 1980.
23   A.C. van den Berg, BLAST — A code for numerical simulation of multi-dimensional blast effects, TNO Prints Maurits Laboratory Report, Rijswijk, The Netherlands, 1992.
24   E.S. Oran and J.P. Boris, Numerical Simulation of Reactive Flow, Elsevier, New York, 1987.

Review

Computer modelling of turbulent gas explosions in complex 2D and 3D geometries

Bjørn H. Hjertager

Telemark Institute of Technology (TMIH) and Telemark Technological R & D Centre (TEL-TEK), Kjølnes, N-3900 Porsgrunn (Norway)

Abstract

Numerical simulation methods capable of predicting flame and pressure development in turbulent gas explosions are presented. Special attention is given to methods which adopt the $k - \varepsilon$ model of turbulence. Several verification calculations are presented, which include a variety of geometrical layouts as well as a range of different fuel–air mixtures. Comparisons between simulated and measured explosion data are in general in good agreement.

1. Introduction

1.1 The problem

Gas explosion hazard assessment in flammable gas handling operations is crucial in obtaining an acceptable level of safety. In order to perform such assessments, good predictive tools are needed. These tools should take account of relevant parameters, such as geometrical design variables and gas cloud distribution. A theoretical model must therefore be tested against sufficient experimental data prior to becoming a useful tool. The experimental data should include variations in geometry as well as gas cloud composition and the model should give reasonable predictions without use of geometry or case-dependent constants.

1.2 Relevant works

It has in the past been usual to predict the flame and pressure development in vented volumes or unconfined vapour clouds by modelling the burning velocity of the propagating flame. This may be successful if we have a simple mode of flame propagation such as axial, cylindrical or spherical propagation in volumes *without obstructions* in the flow. If these are present, however, it is almost impossible to track the flame front throughout complex geometries. It has been

apparent that in these situations it is more useful to model the propagation by calculating the rate of fuel combustion at different positions in the flammable volume. It is also important to have a model which is able to model both subsonic and supersonic flame propagation to enable a true prediction of what can happen in an accident scenario. One such model, which in principle meets all these needs, has been proposed by Hjertager and coworkers [1–5] and Bakke and Hjertager [6–8]. The model has been tested against experimental data from various homogeneous stoichiometric fuel–air mixtures in both large- and small-scale geometries. Similar models for gas explosions have subsequently also been proposed by Kjäldman and Huhtanen [9], Marx et al. [10], Martin [11] and Van den Berg [12]. All the above models are similar in nature. They use finite-domain approximations to the governing equations. Turbulence influences are taken account of by the $k - \varepsilon$ model of Launder and Spalding [13] and the rate of combustion is modelled by variants of the 'eddy dissipation' model of Magnussen and Hjertager [14]. The Bakke and Hjertager models are incorporated in two computer codes named FLACS (FLame Acceleration Simulator) and EXSIM (EXplosion SIMulator). The solution method used is the SIMPLE technique of Patankar and Spalding [15]. The model of Kjäldman and Huhtanen uses the general PHOENICS code of Spalding [16]. Whereas the model of Marx et al. uses the CONCHAS–SPRAY computer code which embodies the ICE–ALE solution technique [17]. The model of Van den Berg is similar to the Hjertager model and is incorporated into a code named REAGAS. Finally, the model of Martin which is embodied in a computer code named FLARE uses the flux-corrected transport (FCT) of Boris and Book [18].

1.3 Objectives

This paper will review the EXSIM simulation model, show some validation calculations and present some predicted scaling characteristics.

2. Governing equations

2.1 Mass and momentum

The problem of turbulent explosion can be handled by solving for the time-mean evolution of time-mean values of the dependent variables in the domain of interest. The time-mean of a variable varying with time, t, may be expressed as:

$$\Phi(t) = \frac{1}{T} \int_t^{t+T} \varphi(\tau) \, \mathrm{d}\tau \tag{1}$$

where $\Phi(t)$ is the time-mean of the instantaneous value $\varphi(t)$ averaged over the time interval T. T must satisfy two competing demands. First, it must be small enough not to smear out the sought time dependence of the system under consideration. Secondly, it must be large enough to be able to produce

sufficient information to enable relevant time-mean values in the interval. This means that time-mean values of both the relevant variables and their second order correlations must be obtainable in the time interval T. This is often possible since conversely, turbulence has higher frequencies than the large-scale motion which generates turbulence. The equations of motion and the energy equation can thus be expressed in tensor notation as:

$$\frac{\partial}{\partial t}\rho + \frac{\partial}{\partial x_j}(\rho U_j) = 0 \tag{2}$$

$$\frac{\partial}{\partial t}(\rho U_i) + \frac{\partial}{\partial x_j}(\rho U_j U_i) = -\frac{\partial p}{\partial x_i} + \frac{\partial}{\partial x_j}(\sigma_{ij}) + \rho g_i \tag{3}$$

$$\frac{\partial}{\partial t}(\rho h) + \frac{\partial}{\partial x_j}(\rho U_j h) = -\frac{\partial}{\partial x_j}(J_{h,j}) + \frac{Dp}{Dt} + S_h \tag{4}$$

Here $\partial \cdot/\partial t$ is the partial derivative, $D \cdot/Dt$ the substantial derivative, U_j is the velocity component in the x_j coordinate direction; p is the pressure, ρ is the density; h is the enthalpy; σ_{ij} and $J_{h,j}$ are the turbulent fluxes of momentum and energy; g_i is the gravitational acceleration in the x_i-direction and S_h is the additional source term for enthalpy.

2.2 Chemical species

The combustion is treated as a single-step irreversible chemical reaction with finite reaction rate between fuel and oxygen. Hence, the reaction scheme may be written as:

$$1 \text{ kg fuel} + s \text{ kg oxygen} \longrightarrow (1+s) \text{ kg products} \tag{5}$$
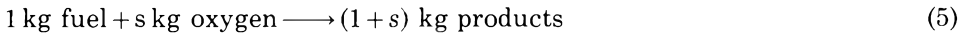
Here s is the stoichiometric oxygen requirement to burn 1 kg of fuel. This simple reaction scheme results in the mixture composition being determined by solving for only two variables, namely, mass fraction of fuel, Y_{fu}, and the mixture fraction, f.

$$\frac{\partial}{\partial t}(\rho Y_{fu}) + \frac{\partial}{\partial x_j}(\rho U_j Y_{fu}) = -\frac{\partial}{\partial x_j}(J_{fu,j}) + R_{fu} \tag{6}$$

$$\frac{\partial}{\partial t}(\rho f) + \frac{\partial}{\partial x_j}(\rho U_j f) = -\frac{\partial}{\partial x_j}(J_f) \tag{7}$$

Here R_{fu} is the time-mean rate of combustion of fuel, whereas $J_{fu,j}$ and $J_{f,j}$ are the diffusive fluxes in the x_j-direction. The basis for this to be valid is that the Schmidt numbers are equal for all species, an approximation which is often found in turbulent flows.

The mixture fraction is defined as:

$$f = \frac{\xi - \xi_\infty}{\xi_0 - \xi_x} \tag{8}$$

where ξ is a conserved combined variable of, for example, mass fraction of fuel, Y_{fu} and mass fraction of oxygen, Y_{0_2}, expressed as:

$$\xi = Y_{fu} - \frac{Y_{0_2}}{s} \tag{9}$$

ξ_0 is the value of ξ at a fuel-rich reference point, for example, a fuel leakage point in the domain, and ξ_{∞} is the value of ξ at an oxygen-rich reference point, for example, the ambient air condition. For a homogeneous premixed system the mixture fraction will be constant in the domain of interest and consequently only the Y_{fu} equation needs to be solved.

3. Turbulence and combustion models

3.1 General

To solve the governing equations (2), (3), (4), (6) and (7) given above the fluxes, σ_{ij} and $J_{\Phi,j}$, and the rate of combustion. R_{fu}, have to be modelled together with specification of relevant boundary conditions. Both the fluxes and the combustion rate are time-mean averaged values of fluctuating quantities. The fluxes can, for a general variable, Φ, and a velocity component U_j, be expressed as:

$$J_{\Phi,j} = -\overline{\rho u_j \varphi} \tag{10}$$

and

$$\sigma_{ij} = -\overline{\rho u_i u_j} \tag{11}$$

where u_i and φ are the instantaneous fluctuations around the time-mean values U_i and Φ, respectively. The overbar indicates time-mean value over the time interval T as defined in expression (1). When modelling the correlations given in (10) and (11) it is usual to relate these to the product of time-mean gradients of the relevant variables and an effective turbulent transport coefficient. For a general scalar variable Φ and a velocity component U_j the relations are:

$$J_{\Phi,j} = -\frac{\mu_{eff}}{\sigma_\Phi} \frac{\partial \varphi}{\partial x_j} \tag{12}$$

and

$$\sigma_{ij} = \mu_{eff} \left(\frac{\partial U_i}{\partial x_j} + \frac{\partial U_j}{\partial x_i} \right) - \frac{2}{3} \delta_{ij} \left(\rho k + \mu_{eff} \frac{\partial U_k}{\partial x_k} \right) \tag{13}$$

respectively.

Here $\delta_{ij} = 1$ if $i = j$ and $\delta_{ij} = 0$ if $i \neq j$. An effective viscosity μ_{eff} and the kinetic energy of turbulence have been introduced in the above expressions, together with an effective Prandtl/Schmidt number σ_Φ. The kinetic energy of turbulence, k, is related to the fluctuating turbulence velocity components in the

three coordinate directions as:

$$k = \tfrac{1}{2}(\overline{u_1^2} + \overline{u_2^2} + \overline{u_3^2}) \tag{14}$$

The effective turbulence viscosity is given by two turbulence parameters, the isotropic turbulence velocity u_t and a length scale, l as:

$$\mu_{\text{eff}} = \mu_l + \rho u_t l \tag{15}$$

μ_l is the molecular viscosity. The determination of the turbulence velocity and length scale are done by use of a turbulence model.

3.2 Two-parameter turbulence model

The determination of u_t and l are done by application of the so-called $k - \varepsilon$ model of turbulence given by Launder and Spalding [13]. The turbulence velocity is related to the kinetic energy of turbulence, k, as:

$$u_t = \sqrt{\frac{2}{3}k} \tag{16}$$

and the length scale, l, is related to the kinetic energy of turbulence, k, and its rate of dissipation ε, as:

$$l \sim \frac{k^{3/2}}{\varepsilon} \tag{17}$$

Inserting eqs. (16) and (17) into expression (15) gives as the result:

$$\mu_{\text{eff}} = \mu_l + C_\mu \rho \frac{k^2}{\varepsilon} \tag{18}$$

C_μ is a constant taken to be 0.09 (Launder and Spalding [13]). The conservation equations that determine the distribution of k and ε read as:

$$\frac{\partial}{\partial t}(\rho k) + \frac{\partial}{\partial x_j}(\rho U_j k) = \frac{\partial}{\partial x_j}\left(\frac{\mu_{\text{eff}}}{\sigma_k}\frac{\partial k}{\partial x_j}\right) + G - \rho\varepsilon \tag{19}$$

$$\frac{\partial}{\partial t}(\rho\varepsilon) + \frac{\partial}{\partial x_j}(\rho U_j\varepsilon) = \frac{\partial}{\partial x_j}\left(\frac{\mu_{\text{eff}}}{\sigma_\varepsilon}\frac{\partial \varepsilon}{\partial x_j}\right) + C_1\frac{\varepsilon}{k}G - C_2\rho\frac{\varepsilon^2}{k} \tag{20}$$

The two new constants appearing above C_1 and C_2, are given the values 1.44 and 1.79 respectively. The Schmidt numbers σ_k and σ_ε are given the values 1.0 and 1.3, respectively, whereas the other Schmidt/Prandtl numbers are put equal to 0.7. The generation rate of turbulence is given by:

$$G = \sigma_{ij}\frac{\partial U_j}{\partial x_i} \tag{21}$$

These production terms take account of turbulence produced by shear and compression/expansion. If buoyancy production or Rayleigh–Taylor instability production is important additional terms may be added.

3.3 Rate of combustion

The rate of combustion may be modelled according to the 'eddy-dissipation' concept by Magnussen and Hjertager [14] with the ignition/extinction modification introduced by Hjertager [2] and the quasi-laminar combustion modification introduced by Bakke and Hjertager [6].

If the local turbulent Reynolds number, based on the turbulent velocity and length scale, is less than a critical value the rate of combustion is calculated according to:

$$R_{fu} = -A_{lam}n_t \frac{S_{lam}}{\delta_f} \rho Y_{lim} \tag{22}$$

Here n_t is the enhancement factor related to the wrinkling of the laminar flame and this factor is proportional to the radius of flame propagation up to a maximum radius of 0.5 m. The enhancement factor is 1.0 for a radius of 0 m and is 2.5 for radii larger than 0.5 m. S_{lam} and δ_f are the laminar burning velocity and thickness of the laminar flame, A_{lam} is a constant.

If the local turbulent Reynolds number is larger than the critical value, the rate of combustion is calculated according to the eddy dissipation approach modified by the extinction/ignition criteria.

Two time scales are defined, namely, the turbulent eddy mixing time scale, $\tau_e = k/\varepsilon$, and the chemical time scale:

$$\tau_{ch} = A_{ch} \exp\left(\frac{E}{RT}\right)(\rho Y_{fu})^a (\rho Y_{O_2})^b \tag{23}$$

Also, an ignition/extinction criterion is defined when the two time scales are in a certain ratio $(\tau_{ch}/\tau_e)^* = D_{ic}$. The rate of combustion is thus calculated as:

$$\begin{aligned} R_{fu} &= 0 \quad \text{when} \quad \frac{\tau_{ch}}{\tau_e} > D_{ic} \\ R_{fu} &= -\frac{A}{\tau_e}\rho Y_{lim} \quad \text{when} \quad \frac{\tau_{ch}}{\tau_e} < D_{ic} \end{aligned} \tag{24}$$

where Y_{lim} is the smallest of three mass fractions, namely, fuel, Y_{fu}, oxygen Y_{O_2}/s, or mass fraction of fuel already burnt, $Y_{fu,b}$, A and D_{ic} are two constants.

4. Modelling of complex geometries

Many geometries found in industrial practice may contain a lot of geometrical details which can influence the process to be simulated. Examples of such geometries are heat exchangers with thousands of tubes and several baffles, and regenerators with a lot of internal heat absorbing obstructions, etc. In the present context, the geometries found inside modules on offshore oil and gas-producing platforms and geometries found in refineries constitute relevant examples of the complex geometries at hand. There are at least two routes for

describing such geometries. First, we may choose to model every detail by use of very fine geometrical resolution, or secondly, we may describe the geometry by use of some suitable bulk parameters. Detailed description will always need large computer resources both with regard to memory and calculation speed. It is not feasible with present or even with future computers to implement the detailed method for solving such complex problems. We are therefore forced to use the second line of approach, which incorporates the porosity/distributed resistance formulation of the governing equations. This method was proposed by Patankar and Spalding [19] and has been applied to analysis of heat exchangers, regenerators and nuclear reactors. Sha et al. [20] have extended the method to include advanced turbulence modelling.

The presence of geometrical details modifies the governing equations in two ways. First, only part of the total volume is available to flow and secondly solid objects offer additional resistance to flow and additional mixing in the flow. The modified equations for use in high density geometries may be expressed by:

$$\frac{\partial}{\partial t}(\beta_V \rho \phi) + \frac{\partial}{\partial x_i}(\beta_i \rho U_i \phi) = \frac{\partial}{\partial x_i}\left[\beta_i \Gamma \frac{\partial \phi}{\partial x_i}\right] + \beta_V(S_\phi + R_\phi) \tag{25}$$

Here ϕ denotes a general variable. β_V is the volume fraction occupied by the fluid, β_i is the area fraction available for flow in the x_i-direction and R_ϕ is the additional resistance or additional mixing or heat transfer caused by solid obstructions in the flow. All the volume/area fractions (porosities) may take values between 0.0, completely blocked, or 1.0, completely open. Some R_ϕ functions may be found in a report by Sha and Launder [21]. These functions depend on parameters like velocity, porosity, typical dimension, pitch between obstacles, obstacle shape and orientation.

5. Solution procedures

It is noted that all conservation equations mentioned above can be written in the following general form (all porosities are set equal to unity for clarity):

$$\frac{\partial}{\partial t}(\rho \Phi) + \frac{\partial}{\partial x_j}(\rho U_j \Phi) = \frac{\partial}{\partial x_j}\left(\Gamma_\Phi \frac{\partial \Phi}{\partial x_j}\right) + S_\Phi; \qquad \Gamma_\Phi = \frac{\mu_{eff}}{\sigma_\Phi} \tag{26}$$

$$\text{I} \qquad\quad \text{II} \qquad\qquad \text{III} \qquad\quad \text{IV}$$

This means, equations with four distinct terms, namely, I transient, II convection, III diffusion and IV source terms. A summary of all the equations needed for a typical calculation of flows with chemical reaction is given in Table 1. Solution of these equations are performed by finite-domain methods. Details of the computation methods are given by Hjertager [1] and Bakke and Hjertager [7]. Only a brief description of the solution method adopted by Hjertager [1, 2] is given here.

TABLE 1

Conservation equations

Conservation of	Φ	σ_Φ	S_Φ
Mass	1.0	∞	0
Velocity in x-direction	U	1.0	$-\dfrac{\partial p}{\partial x} + \dfrac{\partial}{\partial x}\left(\mu_{eff}\dfrac{\partial U}{\partial x}\right) + \dfrac{\partial}{\partial y}\left(\mu_{eff}\dfrac{\partial V}{\partial x}\right) + \dfrac{\partial}{\partial z}\left(\mu_{eff}\dfrac{\partial W}{\partial x}\right) - \dfrac{2}{3}\dfrac{\partial}{\partial x}\left(\mu_{eff}\cdot\nabla\cdot U + \rho k\right)$
Velocity in y-direction	V	1.0	$-\dfrac{\partial p}{\partial y} + \dfrac{\partial}{\partial x}\left(\mu_{eff}\dfrac{\partial U}{\partial y}\right) + \dfrac{\partial}{\partial y}\left(\mu_{eff}\dfrac{\partial V}{\partial y}\right) + \dfrac{\partial}{\partial z}\left(\mu_{eff}\dfrac{\partial W}{\partial y}\right) - \dfrac{2}{3}\dfrac{\partial}{\partial y}\left(\mu_{eff}\cdot\nabla\cdot U + \rho k\right)$
Velocity in z-direction	W	1.0	$-\dfrac{\partial p}{\partial z} + \dfrac{\partial}{\partial x}\left(\mu_{eff}\dfrac{\partial U}{\partial z}\right) + \dfrac{\partial}{\partial y}\left(\mu_{eff}\dfrac{\partial V}{\partial z}\right) + \dfrac{\partial}{\partial z}\left(\mu_{eff}\dfrac{\partial W}{\partial z}\right) - \dfrac{2}{3}\dfrac{\partial}{\partial z}\left(\mu_{eff}\cdot\nabla\cdot U + \rho k\right)$
Kinetic energy of turbulence	k	σ_k	$G - \rho\varepsilon$
Rate of dissipation	ε	σ_ε	$\dfrac{\varepsilon}{k}(C_1 G - C_2 \varepsilon)$
Enthalpy	h	σ_h	$\dfrac{\partial p}{\partial t} + U\dfrac{\partial p}{\partial x} + V\dfrac{\partial p}{\partial y} + W\dfrac{\partial p}{\partial z}$
Mass fraction of fuel	Y_{fu}	σ_{fu}	R_{fu}
Mixture fraction	f	σ_f	0

$$G = \mu_{eff}\left\{2\left[\left(\frac{\partial U}{\partial x}\right)^2 + \left(\frac{\partial V}{\partial y}\right)^2 + \left(\frac{\partial W}{\partial z}\right)^2\right] + \left(\frac{\partial U}{\partial y}+\frac{\partial V}{\partial x}\right)^2 + \left(\frac{\partial U}{\partial z}+\frac{\partial W}{\partial x}\right)^2 + \left(\frac{\partial W}{\partial y}+\frac{\partial V}{\partial z}\right)^2\right\} - \frac{2}{3}\nabla\cdot\bar{U}(\mu_{eff}\cdot\nabla\cdot U + \rho k)$$

$$\nabla\cdot U \equiv \frac{\partial U}{\partial x}+\frac{\partial V}{\partial y}+\frac{\partial W}{\partial z}$$

The calculation domain is divided into a finite number of main grid points where pressure p, density ρ, mass fraction of fuel, Y_{fu}, mixture fraction f, and the two turbulence quantities k and ε are stored. The three velocity components U, V and W are, on the other hand, stored at grid points located midway between the main points. The conservation equations are integrated over control volumes surrounding the relevant grid points in space, and over a time interval, Δt. This integration is performed using upwind differencing and implicit formulation.

The result of this is a set of non-linear algebraic equations, which are solved by application of the well known tri-diagonal matrix algorithm used along the three coordinate directions. Special care has been taken to solve the pressure/velocity/density coupling of the three momentum equations and the mass balance. The 'SIMPLE' method developed by Patankar and Spalding [15] for three-dimensional incompressible parabolic flow has been extended by Hjertager [1] to compressible flows and is used to handle this coupling. The method introduces a new variable, the so-called pressure correction which makes the necessary corrections to the velocity components, pressure and density to make them obey the mass balance constraint at the new time level. The pressure correction is determined by solution of a set of algebraic equations derived from the linearized momentum equations and the mass balance equation.

6. Validation calculations

6.1 Tube

Calculations of flame and pressure development have been performed for three different homogeneous fuel–air mixtures contained in two different tube geometries. The methane–air and propane–air data [22–24] used are taken from a large-scale explosion study in a $50\,\mathrm{m}^3$ tube of 2.5 m diameter and 10 m length with five orifice rings of variable blockage ratios.

The hydrogen/air data used are taken from a small-scale experimental study performed by Lee et al. [25]. This geometry was a tube, 5 cm in diameter and 3 m in length, having orifice rings which blocked off 60% of the free tube area and with distance between rings of 5 cm. These tests comprise a fairly large span in both scale and fuel type and are thus suited for our present validation needs.

The chemical times are taken from Burcat et al. [26] and Schott and Kinsey [27], and the relevant parameters used in expression (23) are compiled in Table 2.

Figure 1 shows a comparison between experiments and predictions of peak pressures versus blockage ratio $(\mathrm{BR}=1-(d/D)^2)$ for methane–air and propane–air mixtures. The figure shows that the large difference in peak pressures between methane–air and propane–air explosions is fairly well predicted. The present prediction method also gives the correct behaviour of pressure versus blockage ratio. There is, however, some underprediction for propane–air at

TABLE 2

Fuel	A_{ch}	a	b	E/R (K^{-1})	Reference
Methane	3.62×10^{-14}	0.33	-1.03	23.300	Burcat et al. [26]
Propane	4.40×10^{-14}	0.57	-1.22	21.210	Burcat et al. [26]
Hydrogen	2.25×10^{-11}	0	-1.0	9.132	Schott and Kinsey [27]
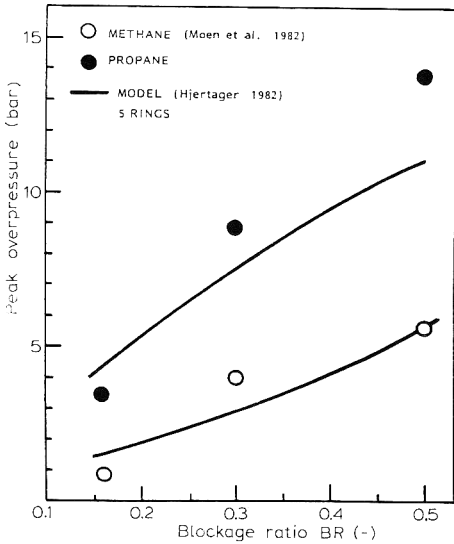
Fig. 1. Peak measured [22, 23] and predicted pressures in the 50 m³ combustion tube as a function of blockage ratio, $BR = 1 - (d/D)^2$. Propane–air and methane–air mixtures.
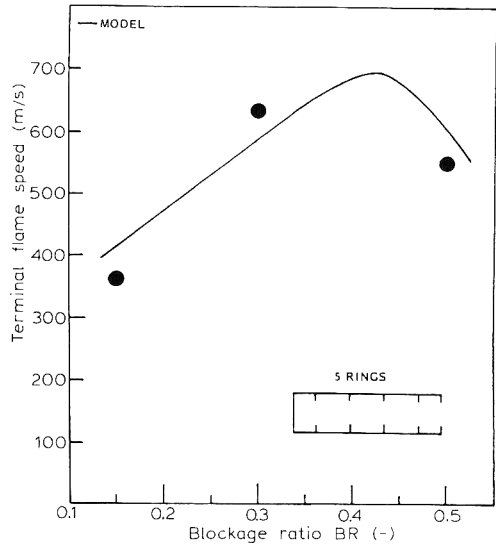
Fig. 2. Comparison between measured (Hjertager et al. [23]) and predicted variations of terminal flame speed with blockage ratio.

blockage ratio 0.5. It should also be mentioned that the original combustion rate model [1] would only show a 20% difference between methane and propane. This clearly demonstrates that only changes in thermodynamic properties and the infinite chemical kinetics assumption are incapable of reproducing the experimental differences between methane–air and propane–air explosions.

Figure 2 shows a comparison between the computation model and the experiments of the terminal flame speed for propane–air as a function of blockage ratio. It is seen that the agreement is satisfactory and that the
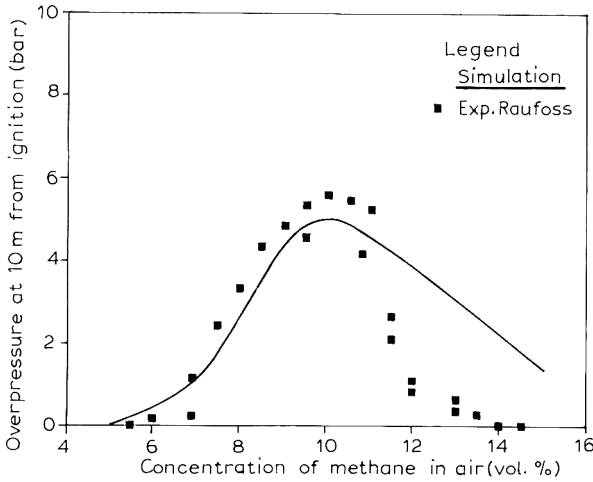
Fig. 3. Comparison of measured [24] and predicted peak overpressures at the exit of the 50 m³ tube versus concentration of methane.
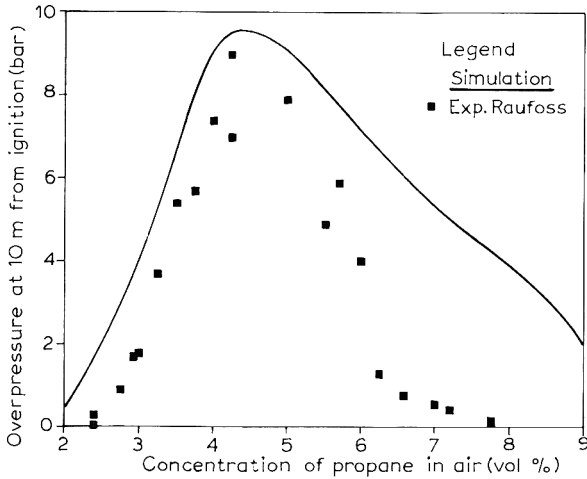

Fig. 4. Comparison of measured [24] and predicted peak overpressures at the exit of the 50 m³ tube versus concentration of propane.

model predicts the optimum flame speed at a blockage ratio equal to approximately 0.4.

Figures 3 and 4 show a comparison between predicted and measured peak pressures for variable concentrations of methane–air and propane–air explosions in the 50 m³ tube. Good agreement between predictions and

experiments can be observed for the lean mixtures of methane–air and propane–air, whereas less agreement is seen for both gases at the rich side of stoichiometry. There is a good correspondence between measured and predicted concentrations for optimum pressure build-up. Both mixtures exhibit this maximum at slightly rich mixtures. This is the same trend as found in detonation sensitivity studies in both methane–air and propane–air mixtures [28]. The predicted maximum peak pressures are approximately 5 bar for methane and 9.5 bar for propane. This difference has come about mainly because of different reaction times. Figures 5 and 6 elucidate this in more detail. These figures show local distributions within the tube of velocity, flame contours and reaction rate contours for both fuels. In Figs. 5(a) and (b) the conditions after the flame has passed the first obstacle are shown. We can see that the local distribution of all variables is almost identical for both gases. However, in Figs. 6(a) and (b), which show the situation after the flame has propagated over the second obstacle, some differences can be observed. At this position of the flame the turbulent mixing time, τ_e, has diminished to a value which corresponds to quenching in some regions where the shear in the flow is
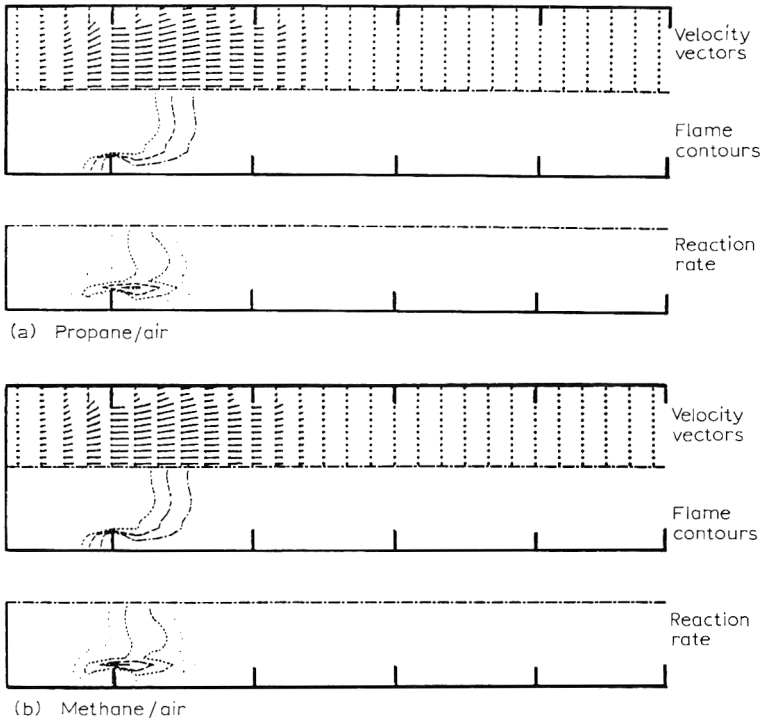

Fig. 5. Distribution of velocity, flame and reaction rate for (a) propane–air and (b) methane–air explosions after the flame has passed the first obstacle.
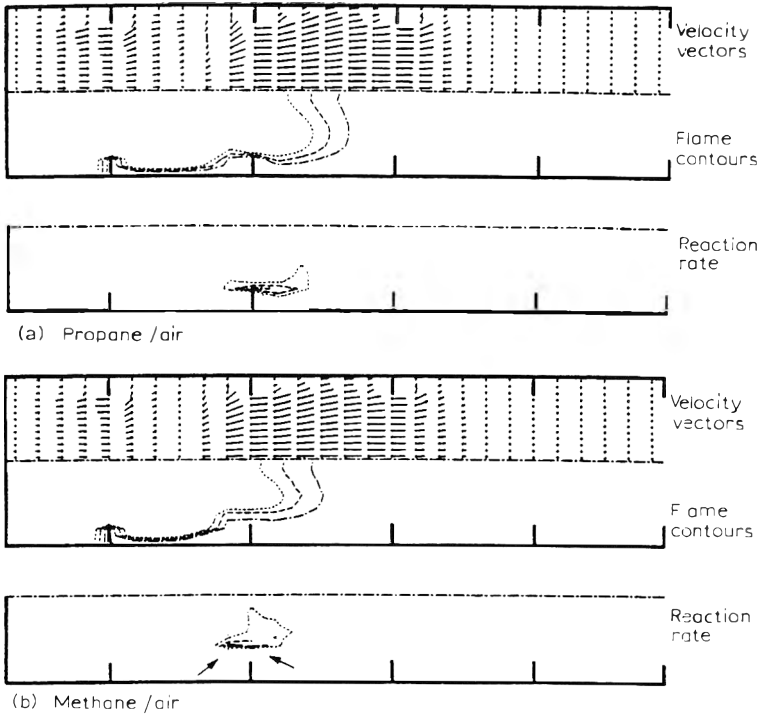
Fig. 6. Distribution of velocity, flame and reaction rate for (a) propane–air and (b) methane–air explosions after the flame has passed the second obstacle. Arrows indicate quenched regions.

large. Obviously, as seen in Fig. 6, this quenching is most pronounced for the methane–air mixture, since the chemical induction time is much larger for methane compared to propane. The arrows in Fig. 6(b), indicate the extinction region of the methane–air flame. This difference in flame propagation between methane and propane continues also for the rest of the flame travel. The net result of this is as shown in Figs. 3 and 4, that the pressures produced in methane–air explosions are lower by a factor of approximately 2 compared to propane–air explosions for identical geometries.

In Figs. 7 and 8 the comparisons between predictions and measurements are shown of flame speed and pressure produced in different hydrogen–air mixtures. It is seen that the agreement is in general good. The overall behaviour is well predicted for both quantities. However, if we look at the details, there are some discrepancies. These are especially notable close to stoichiometry where the experimental data show a sudden jump to a quasi-detonation. This is not seen in the corresponding predictions. Also, the experimentally observed jump in flame speed close to 13% hydrogen concentration is not well predicted. However, the predicted curve in Fig. 7 gives a good indication of the trend. As
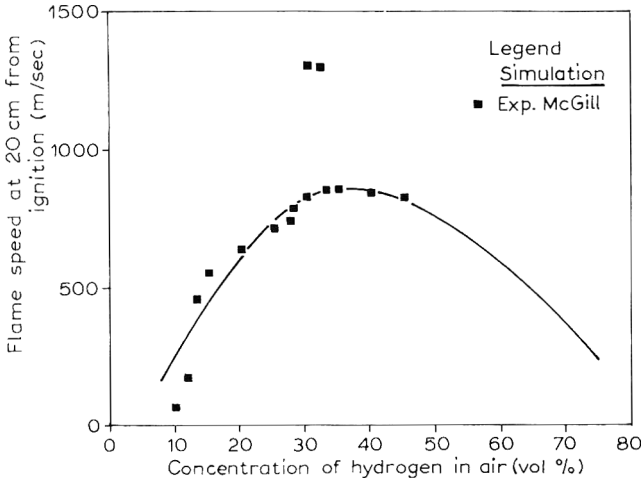
Fig. 7. Comparison of measured [25] and predicted flame speeds at 20 cm from ignition as a function of hydrogen concentration.
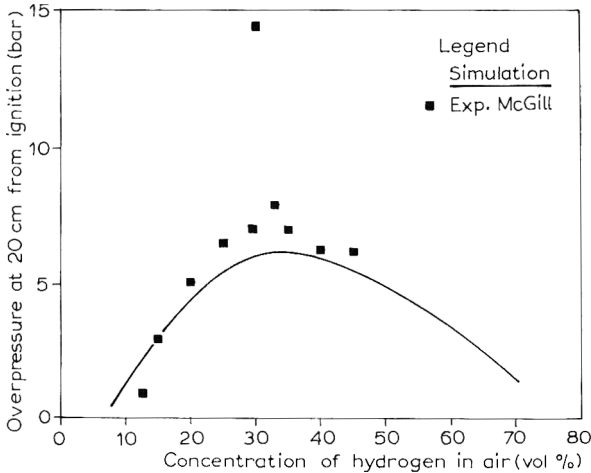

Fig. 8. Comparison of measured [25] and predicted peak overpressures at 20 cm from ignition as a function of hydrogen concentration.

noted by Lee et al. [25] the sudden jump in flame speed in Fig. 7 is probably due to a sudden change in reaction times. In order to model this correctly, a much more detailed reaction kinetic scheme than the simple induction time formula presently used, would be required.
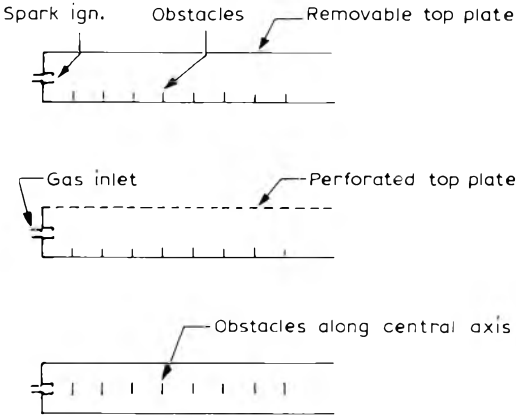
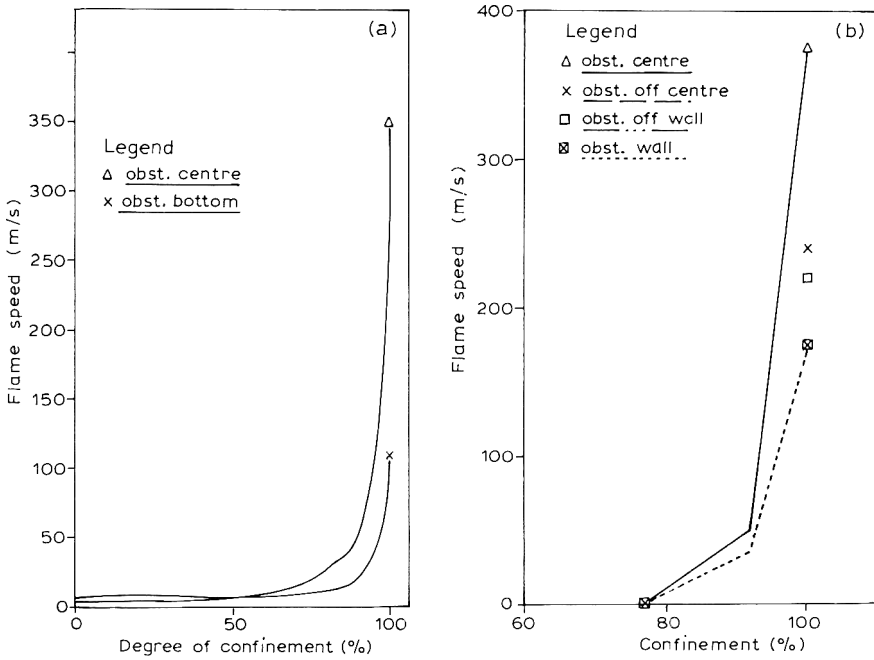Fig. 9. Schematics of experimental apparatus (Chan et al. [29]).

Fig. 10. (a) Measured flame speeds vs. confinement. Measured 1 m from ignition. (Chan et al. [29]). (b) Predicted flame speed vs. confinement. Calculated 1 m from ignition (Bakke and Hjertager [7]).
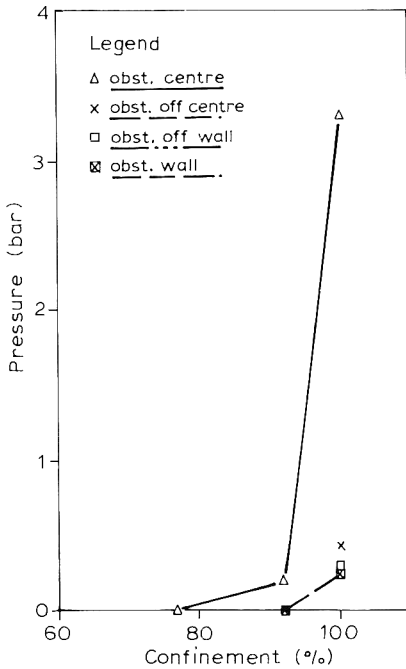
Fig. 11. Pressure vs. confinement. Monitored near lid and open end; maximum value (Bakke and Hjertager [7]).

6.2 Vented channel

As can be seen from the previous confinement on either side of the flame propagation path, high flame speeds and pressures are produced. Chan et al. [29] have performed a small scale study in which they investigated the influence of variable venting in a channel along the propagation path. The layout of their channel is shown in Fig. 9. The length of the channel was 1.22 m and the height was 0.203 m with sharp edged repeated obstacles which block off approximately 25% of the free channel area. The experiments were performed using a homogeneous stoichiometric mixture of methane in air. They found that the flame speed was drastically reduced by reducing the top confinement. This is shown in Fig. 10(a). Bakke and Hjertager [7] used these data in a validation study of the model presented above. Figure 10 shows a comparison between the measured and predicted variation of flame speed versus degree of confinement. The figure shows that there is close agreement between predictions and experiments. Both the decrease in flame speed and the difference between obstacles along the wall and along the centre line are fairly well reproduced. Also shown in Fig. 10 is the influence of moving the obstacles off the wall and off the centre line. Both of these cases show flame speeds in between the two extremes. Figure 11 shows the predicted peak pressures versus confinement. We observe
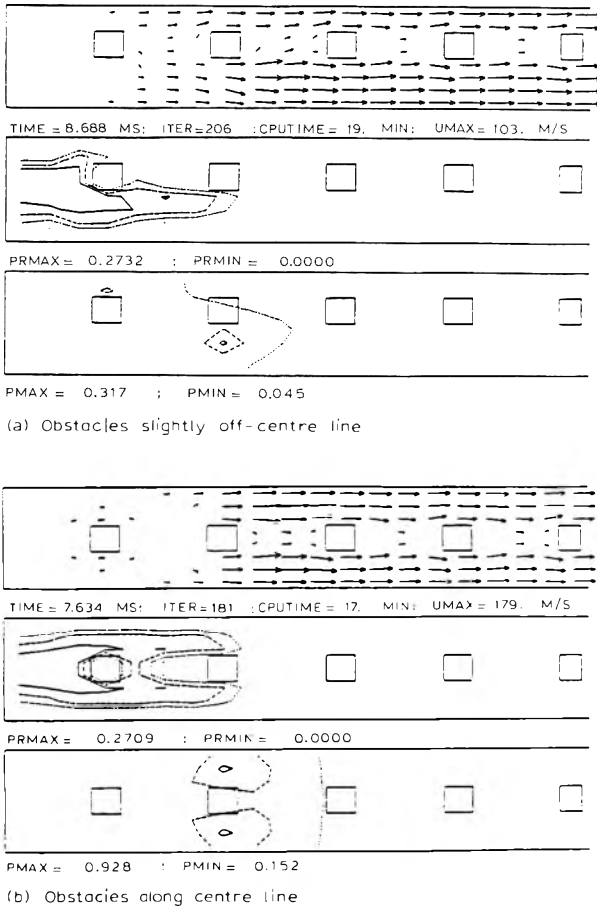
Fig. 12. Distribution of velocity vectors, flame contours and pressure distribution for 100% confinement and two different obstacle arrangements (Bakke and Hjertager [7]): (a) obstacles slightly off centre line; (b) obstacles along centre line.

that the maximum pressure of over 3 bars is obtained by placing the obstacles along the centre line, whereas moving the obstacles towards the wall reduced the pressures by a factor of 10 in this particular geometry. This shows that the maximum effectiveness of two shear layers are only obtained when the obstacles are exactly in the centre line. Figure 12 shows the predicted distribution of flow velocities, flame contours and pressure contours for these two situations.

Moen et al. [30] have reported results from large-scale tests performed in a top-vented channel of 1.8 m × 1.8 m in cross section and 15.5 m in length with repeated obstacles. Results are given for three different stoichiometric fuel–air clouds, namely, acetylene, propane and hydrogen sulphide. Moen et al. [30]

TABLE 3

Fuel	A_{ch}	a	b	E/R	Reference
Acetylene	3.31×10^{-12}	0	-1.0	8.597	Kistiakowsky and Richards [31]
Hydrogen sulphide	5.0×10^{-13}	-0.45	-0.33	13.100	Frenklach et al. [32]
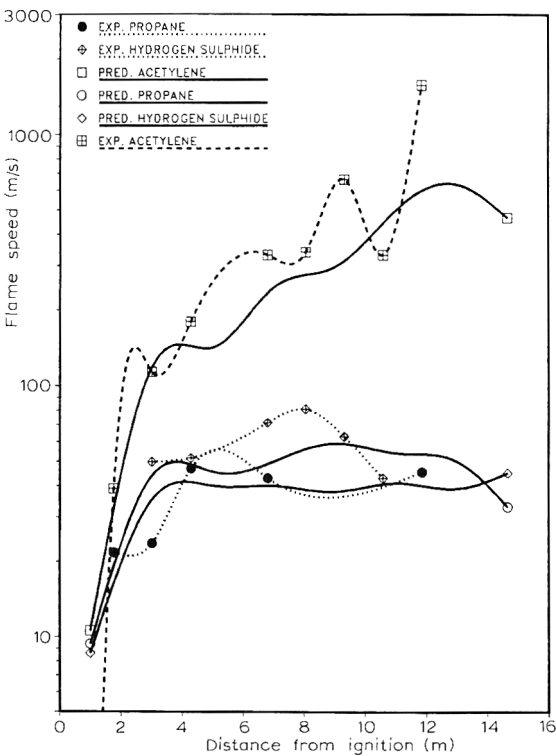
Fig. 13. Comparisons of measured and predicted (Moen et al. [30]) flame speeds along the 15.5 m vented channel.

also include results from application of the FLACS model to some of the experimental tests. The induction time data used in the calculations for acetylene and hydrogen sulphide are given in Table 3. Calculations are performed for one geometrical layout consisting of obstacles of diameter 0.5 m, pitch equals 1.25 m and a height above ground of 0.9 m.
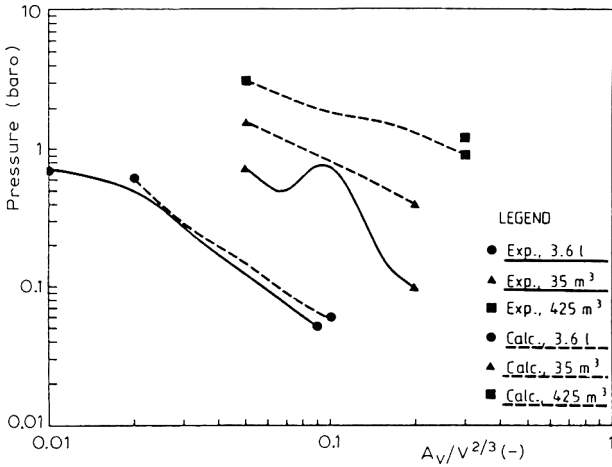
Fig. 14. Measured [33] and predicted (Bakke and Hjertager [8]) peak pressures as a function of the vent parameter for three different empty vessels.

Figure 13 shows comparisons between predicted and measured flame speeds along the 15.5 m length of the obstructed channel. The general characteristics of the observed differences between the three fuels seem to be well predicted. Propane and hydrogen sulphide explosions exhibits much lower flame acceleration compared to acetylene which accelerates to detonation at the end of the channel. The model is not able to predict this sudden transition to detonation due to the fact that only a turbulent combustion mode is included.

6.3 Empty volumes

All the cases presented above contain internal obstructions inside the volume. Bakke and Hjertager [8] have applied the model to the empty volume propane–air tests of Solberg [33]. These tests included three different vessels without obstacles with volumes ranging from 3.6 l and up to 425 m^3.

Figure 14 shows a comparison between predicted and measured variation of the explosion pressure as a function of the scaled vent area. As we can see, the predictions are in reasonable agreement with measurements for all three volumes.

6.4 Module geometries

Hjertager et al. [4] have incorporated the model given above into a 3D computer code and used this to simulate the module data of Hjertager et al. [34]. The compressor module was modelled by using a grid of $42 \times 14 \times 14$ points in the length, height and width directions respectively. The internal equipment was modelled using approximately 100 obstructions. Figure 15 gives a summary of the simulated and measured peak pressure data in the 1:33 and 1:5 scale compressor modules. The figure shows a variation of
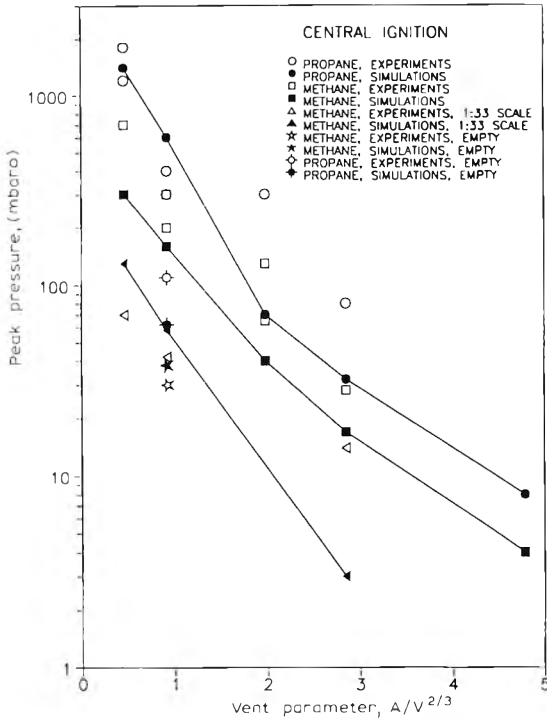
Fig. 15. Peak pressure as a function of vent parameter for centrally ignited explosions in the 1:5 scale compressor module   comparison between experiments and simulations. (Reproduced from [4] by permission of the publishers, Butterworth Heinemann Ltd. © 1992)

peak explosion pressures inside the module for centrally ignited clouds as a function of the vent parameter. It can be noted that the predicted general trends are in good accordance with the measurements. The computer model is able to predict the following characteristics found in the experiments:
1. The variation of peak pressures with the vent parameter.
2. The difference between pressure build-up in methane–air and propane–air explosions.
3. The influence of two scales, i.e. 1:33 and 1:5.
4. The influence of internal process equipment on the violence of the explosion.

Although the general trends are predicted well, it is also noted that there are discrepancies between experiments and simulations. This is especially seen for the cases with vent parameters larger than about 2.0 and for the 1:5 scale methane–air test with a vent parameter of about 0.5.

6.5 Scenario calculations

Hjertager et al. [5] have used the 3D gas explosion code to analyse the Piper Alpha accident. The geometrical and other data were taken from the interim

TABLE 4

Case	Peak pressure (bar)
1	4.7
2	0.68
3	0.86
4	0.15

report from the investigation of the Piper Alpha accident [35]. The explosion in the module C – the compression module – was modelled using a grid of $47 \times 17 \times 9$ points in the length, width and height directions. The internal equipment was modelled using about 55 obstructions.

Four different cases were simulated with a fixed ignition point located centrally in the module, namely stoichiometric homogeneous cloud filling:
1. the whole free space.
2. the right half of the free space.
3. the lower half of the free space.
4. one quarter of the free space located at the lower right position.

Table 4 gives the peak pressures that were found for the four cases: The table indicates a range of pressure loads from 150 mbar to 4.7 bar. The Piper Alpha report indicates that the pressures must have been larger than about 300 mbar. The model simulations indicate that three of the cases produce pressure loads larger than that. Even the case with one quarter of the module filled with flammable gas produces an explosion pressure that may produce significant damage.

Hjertager et al. [36] have demonstrated a scenario analysis of gas explosions on an onshore process plant. The results show that the explosion pressures for the four cases considered ranged from 0.2 bars and up to 9 bars. The highest pressure was found when ignition is in a partially confined area, thus producing an initially fast flame. The peak flame speeds range from approximately 200 m/s and up to 1200 m/s.

7. Scaling characteristics

This last section will report on some predicted scaling characteristics of fuel–air explosions contained in tubes with length over a diameter ratio $L/D = 4.0$ and with five orifice rings (obstacles) which block off 30% of the free tube area, and in channels with $L/D = 6.0$ and five obstacles which block off 25% of the free channel area. The obstacles are evenly distributed along the
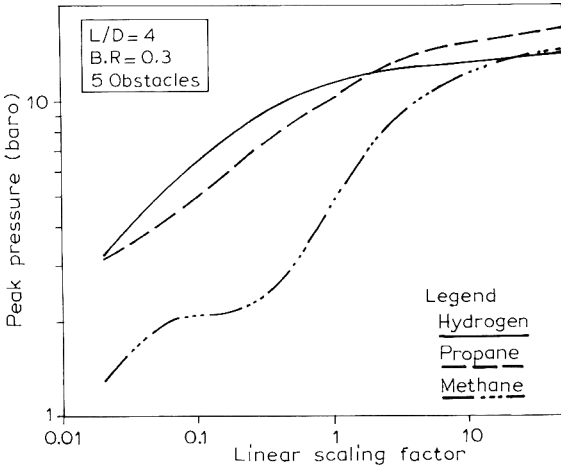
Fig. 16. Variation of peak overpressure in stoichiometric mixtures of methane air, propane–air and hydrogen air with scaling. Scaling factor of 1.0 indicates 10 m of flame travel over five obstacles.
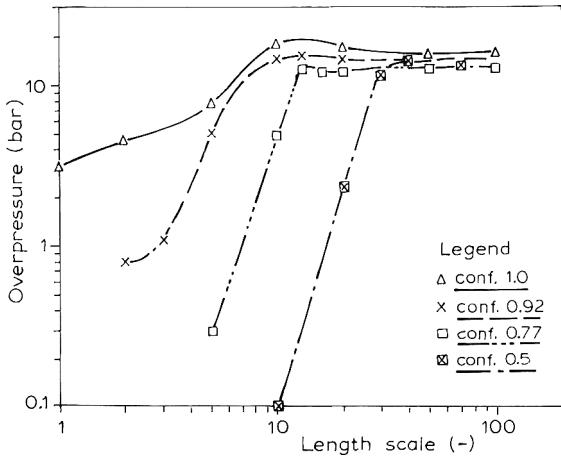
Fig. 17. Maximum overpressure vs. length scale. Obstacles along central axis of channel (Bakke and Hjertager [8]).

enclosure axis from the closed end to the open end, and ignition occurs at the closed end. The tube with a length of 10 m and diameter of 2.5 m we take as our base case and define a linear scaling factor of 1.0 for this geometry. If we, for example, increase the length of the geometry to 100 m and the diameter to 25 m,

Erratum

Editorial — Three papers on vapour cloud explosions
(J. Hazardous Mater. 34(1993)121)

Above editorial inadvertently mentioned it had been written by Rex Britter. This should have been: Dr. H. Phillips, formerly of the Explosion and Flame Laboratory, Research Services Division, Health and Safety Executive, Harpur Hill, Buxton, Derbyshire, SK17 9JN, UK. The journal regrets this error has happened.

we have for this situation, a linear scaling factor of 10. Explosion calculations have been performed over a range of scaling factors which cover three orders of magnitude, from 0.02 to 50. This corresponds to lengths of flame propagation from 20 cm to 500 m.

The channel with length of 1.22 m and height of 0.203 m (Chan et al. [29]) we take as the base and define a length scale of 1.0 for this geometry. If we for this case increase the length to 122 m and the height to 20.3 m we obtain a scaling factor of 100.

Figure 16 shows the predicted peak overpressure produced in stoichiometric mixtures of methane-air, propane-air and hydrogen-air as a function of the linear scaling factor. It can be seen that all three gases exhibit a strong dependence of peak pressure on scaling. The larger the scale, the higher the explosion pressure. Both hydrogen and propane produce larger pressures than methane. It is observed that the difference in peak pressure ratio between propane and methane in a 0.5 m tube (linear scaling equals 0.05) is 2.0, a value which is in good accordance with the experimental results reported by Hjertager [24] in a 0.5 m radial geometry.

Figure 17 shows the predicted peak overpressure produced by stoichiometric methane-air mixtures in a vented channel as function of length scale. The figure shows that the effectiveness of venting is reduced with increasing scale. For example, will a vessel of length approximately 3.6 m (scale 3) and confinement fraction on a top wall of 0.92 (8% porosity) produces a pressure of 1 bar. A scale-up of this geometry to a vessel with length of 25 m (scale 20) would produce a pressure of over 10 bars. In order to reduce the pressure to below 1 bar a confinement fraction of the top wall smaller than 50% should be chosen (porosity larger than 50%). This indicates that larger scales need larger vent areas to reduce the pressure to acceptable values.

8. Concluding remarks

A summary of a computer model capable of analysing the processes which occur in turbulent gas explosions inside complex congested geometries is presented. Several computations are reported which compare the computer model against several sets of experimental data relevant for offshore situations. The agreement between predictions and measurements is in general good. However, more work is needed: (1) to develop and verify the porosity/distributed resistance model for explosion propagation in high density obstacle fields; (2) to improve the turbulent combustion model and (3) to develop a model for deflagration to detonation transition. More experimental data are needed to enable verification of the model in high-density geometries using homogeneous as well as non-homogeneous fuel-air clouds and to validate model predictions at large and full scale. This is particularly needed for onshore process plant geometries.

Acknowledgement

References

1　B.H. Hjertager, Simulation of transient compressible turbulent reactive flows, Comb. Sci. Technol., 41 (1982) 159–170.

2　B.H. Hjertager, Numerical simulation of flame and pressure development in gas explosions, SM study No. 16, University of Waterloo Press, Waterloo, Ont., 1982, pp. 407–426.

3　B.H. Hjertager, Simulation of gas explosions, Modeling, Identification Control, 10 (1989) 227–247.

4　B.H. Hjertager, T. Solberg and K.O. Nymoen, Computer modeling of gas explosion propagation in offshore modules, J. Loss Prev. Process Ind., 5(3) (1992) 165–174.

5　B.H. Hjertager, T. Solberg and J.E. Førrisdahl, Computer simulation of the 'Piper Alpha' gas explosion accident, paper to be published, 1993.

6　J.R. Bakke and B.H. Hjertager, Quasi-laminar/turbulent combustion modelling, real cloud generation and boundary conditions in the FLACS-ICE code, CMI No. 865402-2, Chr. Michelsen Institute, 1986. Also in J.R. Bakke D. Sc. thesis, Numerical simulation of gas explosions in two-dimensional geometries, University of Bergen, Bergen, 1986.

7　J.R. Bakke and B.H. Hjertager, The effect of explosion venting in obstructed channels, In: Modeling and Simulation in Engineering, 1986, pp. 237–241.

8　J.R. Bakke and B.H. Hjertager, The effect of explosion venting in empty volumes, Int. J. Num. Meth. Eng., 24 (1987) 129–140.

9　L. Kjäldman and R. Huhtanen, Numerical simulation of vapour cloud and dust explosions, In: Numerical Simulation of Fluid Flow and Heat/Mass Transfer Processes, Vol. 18, Lecture Notes in Engineering, 1986, pp. 148–158.

10　K.D. Marx, J.H.S. Lee and J.C. Cummings, Modeling of flame acceleration in tubes with obstacles, Proc. of 11th IMACS World Congress on Simulation and Scientific Computation, Vol. 5, 1985, pp. 13–16.

11　D. Martin, Some calculations using the two-dimensional turbulent combustion code FLARE, SRD Report R373, UK Atomic Energy Authority, Warrington, 1986.

12　A.C. Van den Berg, REAGAS a code for numerical simulation of 2-D reactive gas dynamics in gas explosions, PML-TNO Report PML 1989-IN48, Rijswijk, The Netherlands, 1989.

13　B.E. Launder and D.B. Spalding, The numerical computation of turbulent flows, Comp. Methods Appl. Mech. Eng., 3 (1974) 269–289.

14　B.F. Magnussen and B.H. Hjertager, On the mathematical modeling of turbulent combustion with special emphasis on soot formation and combustion, 16th Symp. (Int.) on Combustion, The Combustion Institute, Pittsburgh, PA, 1976, pp. 719–729.

15　S.V. Patankar and D.B. Spalding, A calculation procedure for heat, mass and momentum transfer in three-dimensional parabolic flows, Int. J. Heat Mass Transfer, 15 (1972) 1787–1806.

16　D.B. Spalding, A general purpose computer program for multi-dimensional one- and two-phase flow, Mathematics Computers Simulation, IMACS, XXII (1981) 267–276.

17　L.D. Cloutman, J.K. Dukowicz, J.D. Ramshaw and A.A. Amsden, CONCHAS-SPRAY: A computer code for reactive flows with fuel sprays, Los Alamos National Laboratory Report LA-9294-MS, Los Alamos, NM, May 1982.

18　J.P. Boris and D.L. Book, Flux-corrected transport I: Shasta-A fluid transport that works, J. Comp. Phys., 11 (1973) 38.

19　S.V. Patankar and D.B. Spalding, A calculation procedure for the transient and steady-state behavior of shell-and-tube heat exchangers, In: N.H. Afgan and E.V. Schlünder (eds.), Heat Exchangers: Design and Theory Sourcebook, McGraw-Hill, New York, 1974, 155–176.

20　W.T. Sha, C.I. Yang, T.T. Kao and S.M. Cho, Multi dimensional numerical modelling of heat exchangers, J. Heat Transfer, 104 (1982) 417–425.

21　W.T. Sha and B.E. Launder, A Model for Turbulent Momentum and Heat Transport in Large Rod Bundles, ANL-77-73, 1979.

22　I.O. Moen, J.H.S. Lee, B.H. Hjertager, K. Fuhre and R.K. Eckhoff, Pressure development due to turbulent flame propagation in large-scale methane–air explosions, Comb. Flame, 47 (1982) 31–52.

23　B.H. Hjertager, K. Fuhre, S.J. Parker and J.R. Bakke, Flame acceleration of propane–air in large-scale obstructed tube, 9th International Colloquium on Dynamics of Explosions and Reactive Systems, Poitiers, France, 3–8 July, 1983. See also Prog. Am. Inst. Aeronaut. Astronaut., 94 (1984) 504–522.

24　B.H. Hjertager, Influence of turbulence on gas explosions, J. Hazardous Mater., 9 (1984) 315–346.

25　J.H.S. Lee, R. Knystautas and A. Freiman, High speed turbulent deflagrations and transition to detonation in H_2–air mixtures, Comb. Flame, 56 (1984) 227–239.

26　A. Burcat, R.W. Crossley and K. Scheller, Shock tube investigation of ignition in ethane–oxygen–argon mixtures, Comb. Flame, 18 (1972) 115–123.

27　G.L. Schott and J.L. Kinsey, Kinetic studies of hydroxyl radicals in shock waves. II. Induction times in the hydrogen–oxygen reaction, J. Chem. Phys. 29 (1958) 1177–1182.

28　D.C. Bull, Concentration limits to the initiation of unconfined detonation in fuel–air mixtures, Trans. I. Chem. E., 57 (1979) 219–227.

29　C. Chan, I.O. Moen and J.H.S. Lee, Influence of confinement on flame acceleration due to repeated obstacles, Comb. Flame, 49 (1983) 27.

30　I.O. Moen, A. Sulmistras, B.H. Hjertager and J.R. Bakke, Turbulent flame propagation and transition to detonation in large fuel air clouds, Presented at the 21st Int. Symp. on Combustion, Munich, Germany, August 3–8, 1986.

31　G.B. Kistiakowsky and L.W. Richards, Emission of vacuum ultraviolet radiation from the acetylene–oxygen and the methane–oxygen reactions in shock waves, J. Chem. Phys., 36 (1962) 1707.

32　M. Frenklach, J.H.S. Lee, J.N. White and W.C. Gardiner, Oxidation of hydrogen sulphide, Comb. Flame, 41 (1981) 1–16.

33　D.M. Solberg, Gas explosion research related to safety of ships and offshore platforms, Fuel–Air Explosions, SM Study No. 16, University of Waterloo Press, Waterloo, Ont., 1982, pp. 787–819.

34　B.H. Hjertager, K. Fuhre and M. Bjørkhaug, Gas explosion experiments in 1: 33 and 1: 5 scale offshore separator and compressor modules using stoichiometric homogeneous fuel/air clouds, J. Loss Prev. Process Ind., 1 (1988) 197–205.

35　J.R. Petrie, Piper alpha technical investigation, Interim report, Department of Energy, September 1988.

36　B.H. Hjertager, S. Enggrav, J.E. Førrisdahl and T. Solberg, A case study of gas explosions in a process plant using a 3D computer code, Paper prepared for inclusion as Appendix in Guidelines for Evaluating Consequences of Fires and Explosions from Vapor Clouds and BLEVE's, to be published by the CCPS of the AIChE, New York, 1993.

Information support for the incineration of chemical waste in cement kilns

S.A. Glažar, A. Kornhauser* and A. Musar

University of Ljubljana, International Centre for Chemical Studies, P.O. Box 18/1, 6100 Ljubljana (Slovenia)

Abstract

A specialised information system on industrial (hazardous) waste management has been developed and applied in Slovenia. It is composed of (1) computerised waste registry, (2) reference database on waste and waste water management, (3) relational database on river water pollution, (4) a prediction of waste generation module, and (5) an expert system for determination and prevention of river water pollution. Incineration of hazardous waste in cement kilns was identified as an efficient solution for over 20% of chemical waste accumulated. A specialised database on analytical control for this incineration was created, with the files on sampling, sample preparation, waste characteristics, and methods for proximate, survey and directed analyses. The method of structuring information into systems for the recognition of relationships and patterns was applied, resulting in a model system for analytical control of waste incineration in cement kilns presented in Fig. 4. The vertical branches of the system give the succession order of analyses for (1) cement raw materials, (2) primary fuel, (3) waste blended as secondary fuel, (4) stack gas, (5) dust from electrofilters, and (6) cement produced. The hierarchical organisation enables recognition of key analyses and pathways, as well as of optional procedures.

1. Introduction

The efficiency of research and development can be considerably increased by organising information, which is usually available in bits, into well-structured schemes. The structuring of information enables a better definition of parameters and recognition of their hierarchical order and relations. This can lead to the design of patterns of knowledge which enables hypotheses of higher probability to be formed [1, 2].

For the structuring of information into patterns of knowledge, comprehensive information must be available. If a problem is of a complex nature, the amount and diversity of information should be high, and a computerised information system is needed. This is certainly true for chemical (hazardous) waste management.

---

* To whom correspondence should be addressed. Fax: 38-61-226-170.

2. Specialised information system on chemical (hazardous) waste management

In the effort to find high efficiency and low cost solutions to the chemical waste problem which had accumulated in Slovenia, a highly specialised information system was first developed [3, 4] (Fig. 1). The system is intended to support research, development and environmental decision making. It is installed on PC which enables wide transferability. The system is fed by collection and analysis of primary documentation from national and international sources. The results are compared and completed by processing six international databases.

2.1 Information system for special waste management

The Waste Registry is a factual relational database covering the specific needs of the Republic of Slovenia with two million inhabitants and a chemical industry with about ten thousand employees. This database includes statistical data on (1) waste generators, (2) waste processing and waste disposal options based on Republic waste regulations, (3) qualitative and quantitative characteristics of waste, (4) waste storage, processing and final disposal, and (5) production processes generating waste needed for building of waste generation prediction models.

The system was built using dBASE III PLUS and CLIPPER programming language on IBM compatible PC as relational databases consisting of five modules. The connection among modules is provided by a waste and company coding system. Recently the system has been transferred into PARADOX version 3.5 database management system, and modules links were provided by the PASCAL programming language.

The processing of the Registry enables the recognition of several dimensions of the waste problem, e.g. accumulation of different types of waste in different locations, trends in waste generation, relationships between total quantities of raw materials, products and total waste generated, etc. The information provided by the Registry serves in the planning of waste minimisation, waste transport, blending and incineration.

2.2 Reference database on waste and waste water management

These segments are built on IBM compatible PC using UNESCO CDS/ISIS Information Storage and Retrieval System, and connected via keywords. This software package also enables the non-specialist user to have easy access to all segments of the reference database.

2.3 Bibliographic database

This covers printed publications (selected books, scientific papers, patents, standards, industrial reports, project reports, regulations, etc.), as well as "grey" literature (e.g. theses). The database is regularly updated by target-oriented search and selection of new information. It contains over 4500
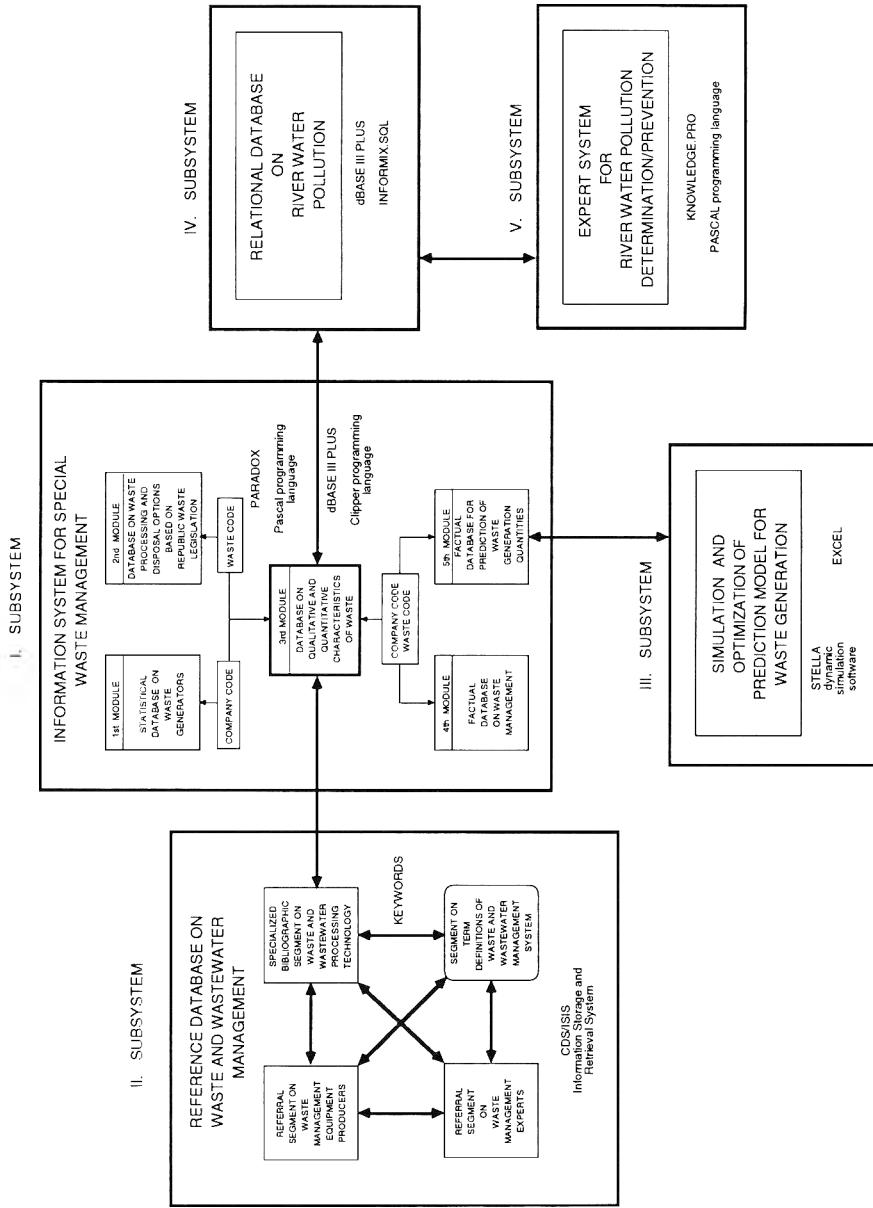
Fig. 1. Integrated information system for pollution determination and prevention.
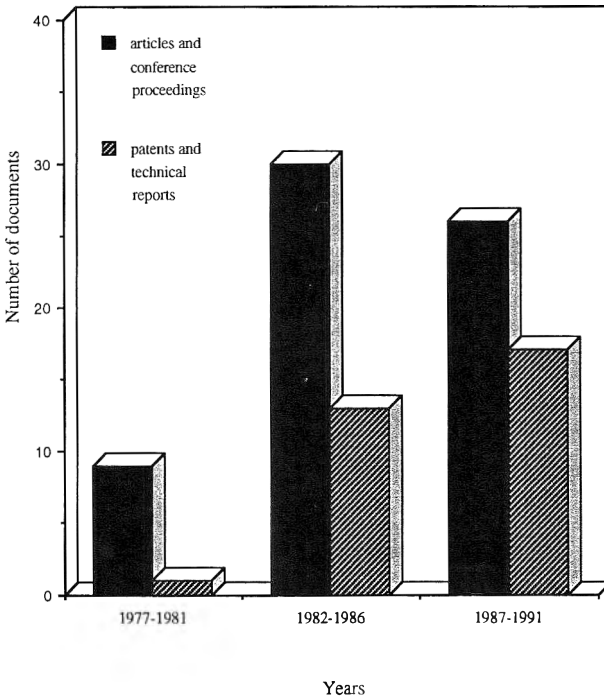
Fig. 2. Number of documents on hazardous waste incineration in cement kilns by types and years.

documents (January 1992) and has been accessible on-line from 1988 on the national host IZUM at the University of Maribor.

The processing of the database not only provides information for selected questions, but also enables trends to be followed. An example is given in Fig. 2.

3. Information database on the analytical control of waste incineration in cement kilns

In countries burdened by economic crises, which is particularly serious in Eastern/Central Europe, there is little hope of acquiring investments into special waste incinerators which cost 50 million U.S. dollars or more [5]. There is also a strong "green peace" movement against transborder transport of hazardous waste, for which some claim that it would bring foreign investors to the country. The incineration of waste in cement kilns seems to be more realistic. Cement industries are widely available in most countries, and the investment in adaptation of cement kilns is less than 2 million US\$. Cement kilns are reported to enable high destruction of organic hazardous constituents (greater than 99.99%) [6], neutralisation of acid gases by alkaline clinker, long retention time, absorption of toxic metals into non-leaching mineral

matrices of clinker, no residues and considerable energy savings [7]. Waste organic solvents, used motor oils, as well as cooling and lubricating oils, and even pulverised waste can all be incinerated. The wet cement production process is also suitable for concentrated residual waste waters that contain small amounts of combustible organic compounds. They can be added to the raw mix feed [8–11].

However, there is an *a priori* mistrust from the cement producers and consumers who are worried about the deterioration of production lines and product quality, and, in particular, of the general public who may fear air and water pollution linked with health hazards [12]. A thorough analysis of the initial situation, and setting up regular control of the incineration of chemical waste in cement kilns is therefore a *conditio sine qua non* [13, 14].

A detailed study of the available documentation on analytical methods and techniques for the control of chemical waste incineration in cement kilns was carried out first, and a database on analytical procedures built. Based on the study of EPA regulations pertaining to this field [15], a specialised database "Sampling, sample preparation and analysis" has been built. The database was designed for an IBM compatible PC, using software package CDS/ISIS.

The following *structure of records* was designed.

1. *Method number*

    Each method is marked with a 4–5 character code.

    The first character is a letter denoting the field of activity:

    S–sampling methods

    P–sample preparation procedures

    C–analytical methods for determination of waste physical character-
    istics

    A–analytical method for determination of waste chemical character-
    istics

    In these specific fields the methods are described with a three character number and sometimes also by a letter (a, b, c) denoting the method variant.

2. *Method name*

    From the method name, which is taken from the original document, it is usually possible to determine target compound(s) and the main analytical method used.

3. *Analytical method*

    One or more main analytical methods are listed (e.g. liquid/liquid extrac-
    tion, GC/MS).

4. *Matrix*

    Matrices for which the method is applicable are listed.

5. *Analytical equipment*

    This field includes basic data on necessary analytical equipment and is divided into three subfields:

    ^t–apparatus type, general name of apparatus (e.g. HPLC/UV, graph-
    ite furnace)

$^\wedge$i–exact data on the producer and model of apparatus if at all
   mentioned in primary document
$^\wedge$o–other data not applicable to other two subfields

6. *Parameters of analytical methods*
   Text field with a more detailed description of each analytical method,
   including equipment parameters (e.g. for GC exact data on column, work-
   ing temperature, carrier gas).

7. *Detection limits of analytical method*
   The field consists of four subfields:
   $^\wedge$e – unit of detection limits, e.g. mg/l, ppm
   $^\wedge$n – lower detection limit
   $^\wedge$x – upper detection limit
   $^\wedge$o – other additional data

8. *Compounds and standards*
   The field contains the list of compounds for which the method is appli-
   cable, or a list of suitable standards.

9. *References*
   The field contains basic data on primary documents describing the
   method.

The database consists of 98 records on methods in both English (ANI) and
Slovene (ANS) versions. The database files are:

1. File: Sampling (12 records)
2. File: Sample preparation (22 records)
3. File: Analysis of waste (64 records)
   3.1. Subfile: Waste characteristics (4 records)
   3.2. Subfile: Waste analysis (60 records)
        3.2.1.: Proximate analysis (6 records)
        3.2.2.: Survey analysis (8 records)
        3.2.3.: Directed analysis (46 records)

The structure of the database is shown in Fig. 3.

1. *File: Sampling*
   In this file standard methods for sampling waste and stack gases are de-
scribed. Methods of stack gas sampling are divided into: (1) continuous samp-
ling (O_2, CO, CO_2, SO_2, NO_x, TOC); (2) EPA–MM5 method of sampling of
solid particles, organic substances, metals and chlorine; (3) VOST method of
sampling volatile organic substances, found in stack gas in low concentration.

2. *File: Sample preparation*
   The collected sample, regardless of its state of matter, must be converted into
a matrix which is compatible with the final analysis methods needed for
measurement of the designated POHC(s). The types of samples which could be
collected during the evaluation of a hazardous waste incineration include:
(1) permanent gases and stack gases collected as comprehensive sampling
train components, (2) liquid samples: aqueous liquids (including process
waters) and organic liquids, (3) sludges (including suspensions, slurries, and
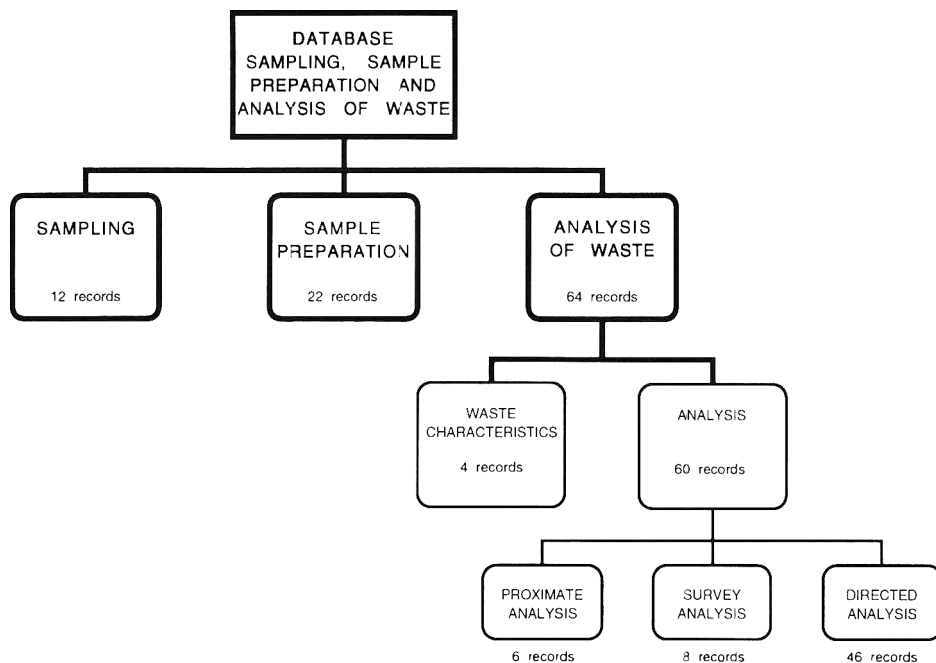
Fig. 3. Structure of the database "Sampling, sample preparation and analysis".

gels), (4) solids (including particles from filters, solid residues, and sorbents). Methods described in this file are divided into: (1) preparation of representative aliquots from field samples, (2) recovery measurements, (3) sample extraction of organic compounds, (4) concentrating solvent extracts, (5) digestion for metals' analysis, and (6) sample cleanup procedures.

3. *File: Analysis of waste*

This file refers to waste and by-products of incineration. In the first part, methods for determining basic waste characteristics are given for ignition, corrosivity, reactivity (explosivity, possible reactions with other substances) and toxicity based on leaching tests.

The second part describes analytical methods for determining waste composition and by-products of incineration. The composition is analysed in three steps: proximate analysis, survey analysis and directed analysis. Proximate analysis defines consistency (viscosity), calorific value, humidity content, dry matter and ash, and elemental composition (carbon, hydrogen, nitrogen, sulphur, phosphorus and halogens). Elemental composition is essential for the prediction of possible hazardous organic compounds in waste. This segment is supported by a referral database "Chemical Compounds Characteristics" [16]. The database contains data relevant for incineration of 362 organic compounds which are frequently present in waste. With the combination of element composition and the data on compounds in the database, it is possible to predict possible hazardous organic compounds in waste.

Following proximate analysis, the content of organic and inorganic substances, especially metals in waste, are determined by survey analysis. During experimental incineration of waste the content of organic and inorganic substances is determined with by-products of thermal destruction in stack gas [17].

Since it is not possible to control quantities of all organic compounds in waste, one to a maximum of six hazardous substances in waste are selected [12], based on the results of proximate analysis, POHC (Principal Organic Hazardous Constituents). The destruction factor and removal efficiency, DRE, is determined [18, 19].

By directed analysis by-products of incineration of selected POHC compounds in stack gas samples are determined, after which the DRE factor can be calculated.

4. Structuring of information into systems: An example for analytical control of waste incineration in cement kilns

The aims of structuring information on analytical procedures for the control of waste incineration in cement kilns were:
(1) *to identify the existing methods* for sampling, sample preparation and analyses in order to determine parameters which influence environment or product quality, either in input (raw materials, primary fuel and secondary fuel from waste) or output (cement, stack gas, electrofilter and other ash, scrubber solutions);
(2) *to develop a hierarchical structure* of these procedures which would show gaps and call for amendments with additional or alternative procedures; and
(3) *to recognize key analyses* for monitoring an environmentally and production-wise safe process, the frequency of their application, and the cost of analyses.

4.1 Identification of methods
The basis for the first draft structuring were sampling and analysis methods for hazardous waste combustion, identified by EPA [15]. Apart from methods for determination of dangerous/toxic compounds in special/hazardous waste and stack gas, the scheme also incorporates appropriate methods for determining parameters, which can have impact on environment and/or product quality for raw materials, primary fuel (coal), electrofilter or other ash, scrubber solutions and product (cement) [12].

The above methods [15] are mostly standard ASTM (American Society for Testing and Materials) and official EPA methods. Other standard methods for sampling, sample preparation and analytical methods, collected from different sources, e.g. other ASTM, VDI (Verein Deutscher Ingenieure, Germany) [20], UNICHIM (Associazione per l'Unificazione nel Settore dell'Industria Chimica,

Italy) standard methods, were incorporated in the scheme. They filled the gaps in the scheme or represent alternatives to existing methods.

4.2 Development of a hierarchical structure

After identification of relevant methods, the basic structure of the scheme was set up. Appropriate horizontal and vertical lines were identified. The *horizontal lines* in the scheme are:

- sampling
- sample preparation
  - representative aliquots from field samples
  - surrogate addition to aliquots for organic analysis
  - preparation procedure for determination of metals
  - extraction of organics
  - determination of total chromatographable organics
  - concentration of extracts
  - extract purification
- analysis
  - determination of basic waste characteristics
  - proximate analysis
  - survey analysis
  - directed analysis

The *vertical lines* include input and output from the cement production process, using special/hazardous waste as a secondary fuel:

- raw materials
- primary fuel (coal)
- secondary fuel (special/hazardous waste)
  - solids
  - sludges
  - organic liquids
  - aqueous liquids
- incineration by-products
  - stack gas
    - gas
    - scrubber solutions
  - electrofilter or other ash
- product (cement)

By verticals it is possible to follow appropriate methods for determination of relevant parameters from sampling to directed analysis (Fig. 4, Tables 1 and 2).

4.3 Recognising key analyses — Identifying levels of analysis

Methods in the scheme are arranged in three levels according to their sequence, relevance and accuracy:

(1) Obligatory procedures: It is necessary to carry these out for every charge of waste at its incineration. They include key methods ("fingerprint" analyses) for determination of parameters important for dosage of secondary fuel (waste)
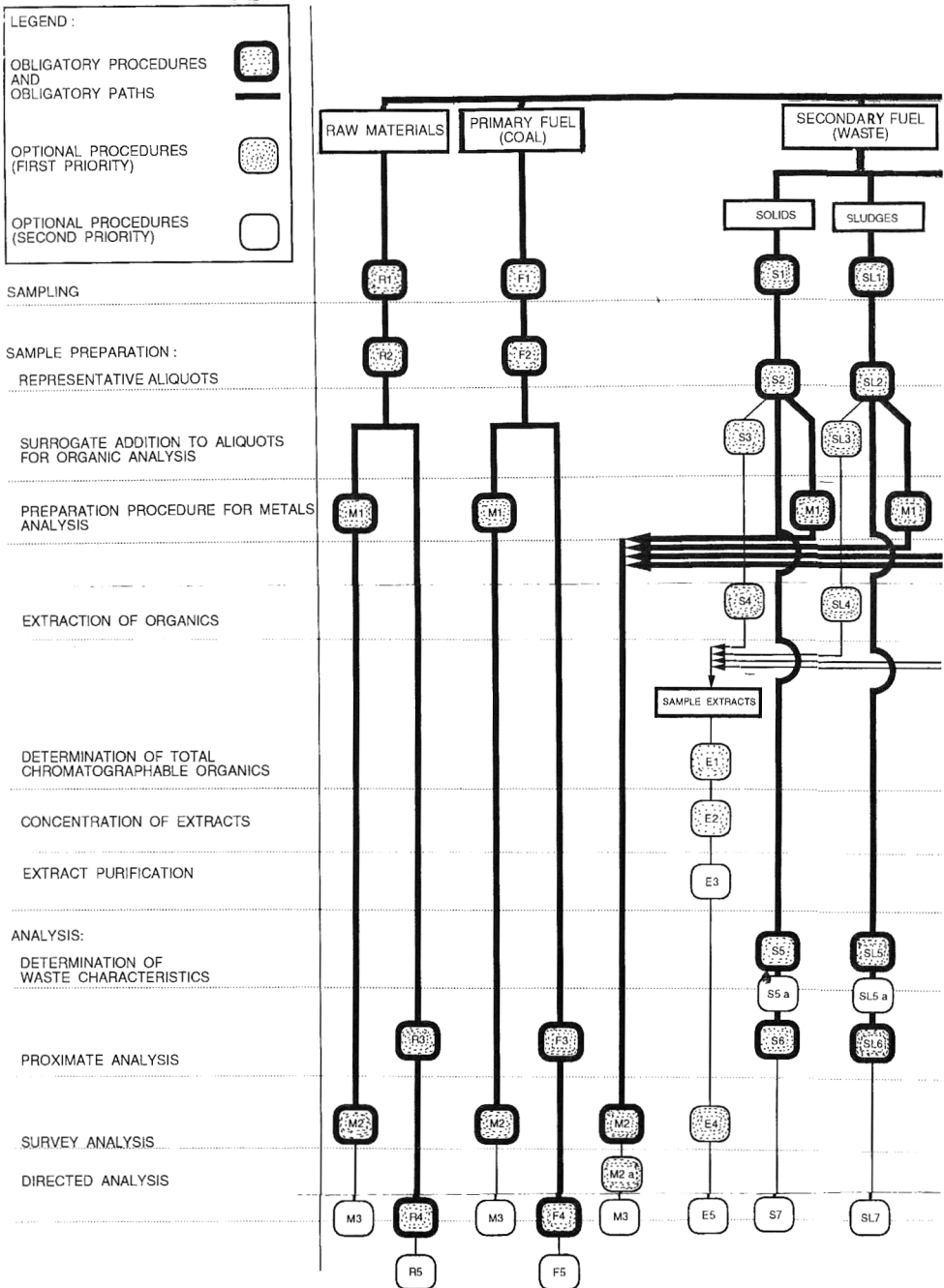
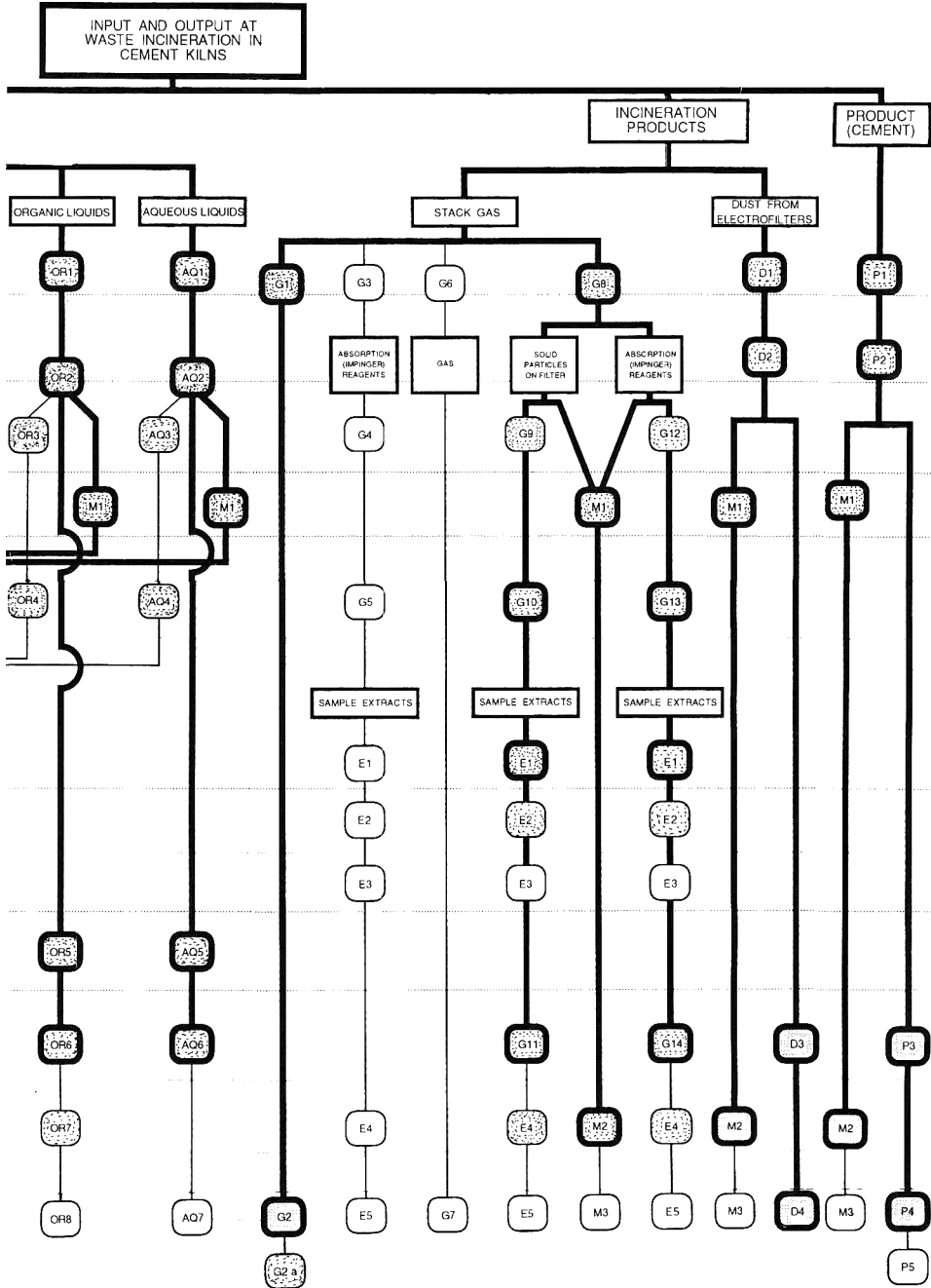Fig. 4. Analytical procedures at waste incineration. (See Table 1 for legend.)

Fig. 4. Continued.

TABLE 1

Analytical procedures at waste incineration

Raw materials				
R1	R2	R3	R4	R5
5,6	15	39–41	102–105	106

Vertical in the scheme (Figure 4)	
	Code in the scheme (Figure 4)
	Number of applicable methods (Table 2)

Primary fuel (coal)				
F1	F2	F3	F4	F5
5, 6	15	41 100,101	102–105	106

Solids							
S1	S2	S3	S4	S5	S5a	S6	S7
5–7	15	16–19	25–27	35–37	38	39–41 44	56, 81–95, 97, 98

Sludges							
SL1	SL2	SL3	SL4	SL5	SL5a	SL6	SL7
6	14	16–19	22, 23	35–37	38	39–41 44	56, 81–95 96, 97

Organic liquids							
OR1	OR2	OR3	OR4	OR5	OR6	OR7	OR8
1–4	13	16–19	24	35–37	39–41 43,44	47, 48	53, 63, 70–73 75–79 81–95, 97

Aqueous liquids						
AQ1	AQ2	AQ3	AQ4	AQ5	AQ6	AQ7
1–4	13	16–19	20, 21	35–37	39–44	54, 60 63 81–95, 96

TABLE 1. Continued

Stack gas							
G1	G2	G2a	G3	G4	G5	G6	G7
109	110–113	108, 114	12	16–19	20, 21, 24	10, 11	64–69 74, 80
G8	G9	G10	G11	G12	G13	G14	
8, 9, 99	16–19	25–27	41, 42	16–19	20, 21, 24	41, 42	

Dust from electrofilters			
D1	D2	D3	D4
5, 6	15	39–41	102–104 106, 107

Product (cement)				
P1	P2	P3	P4	P5
5	15	39–41	102–105 107, 108	106

Analysis of metals			
M1	M2	M2a	M3
29	52	81–95	104, 106

Analysis of extracts				
E1	E2	E3	E4	E5
45	28	30–34	46–52	57–61 70–73 75–79, 96

and/or blending different kinds of waste according to its moisture, solid and ash content, heating value, elemental composition, metals content. These results together with data on the waste origin are usually sufficient for determination of incineration parameters.

(2) Optional procedures (first priority): Their implementation depends on (a) properties of the sample (as determined by obligatory procedures), (b) special requirements for following some of the parameters and (c) in the case when the results of the obligatory procedures fall out of the usual value range (at "fingerprinting"). Among these procedures are also methods for survey analysis of organics (e.g. GC/MS, IR). It is recommended to carry out one of them for every charge of waste to be incinerated.

(3) Optional procedures (second priority): These procedures are carried out (a) at thorough analysis of new sample (primary characterisation to determine "fingerprint" parameters and their value ranges), (b) to follow some of the

TABLE 2

Methods for sampling, sample preparation and analysis

No.	Method name
1	Coliwasa
2	Dipper (pond sampler)
3	Weighted bottle
4	Tap
5	Thief (grain sampler)
6	Trier (sample corer/waste pile sampler)
7	Trowel (scoop)
8	MM5 train
9	SASS train
10	Gas bulb
11	Gas bag
12	VOST – Volatile Organics Sampling Train
13	Representative aliquots from field samples
14	Representative aliquots from field samples
15	Representative aliquots from field samples
16	Surrogate addition to aliquots for organic analysis
17	Surrogate addition to aliquots for organic analysis
18	Surrogate addition to aliquots for organic analysis
19	Surrogate addition to aliquots for organic analysis
20	Extraction of semivolatiles from aqueous liquids
21	Extraction of volatiles from aqueous liquids
22	Extraction of semivolatiles from sludges
23	Extraction of volatiles from sludges
24	Semivolatiles from organic liquids
25	Extraction of semivolatiles from solids
26	Extraction of semivolatiles from solids
27	Extraction of volatiles from solids
28	Drying and concentrating solvent extracts
29	Digestion procedure for metals
30	Florisil column chromatography
31	Biobeads SX-3
32	Silica gel chromatography
33	Alumina column chromatography
34	Liquid/liquid extraction
35	Ignitability
36	Corrosivity
37	Reactivity
38	Extraction procedure toxicity
39	Moisture, solid and ash content – macroscale
40	Moisture, solid and ash content – microscale
41	Elemental composition – organic
42	Total org. carbon (TOC), total org. halogen (TOX)
43	Viscosity
44	Heating value of waste
45	Organic content by TCO
46	Organic content by GRAV
47	Organic content – volatiles

TABLE 2. Continued

No.	Method name
48	Compound class type by infrared analysis
49	Mass spectrometric analysis
50	Specific major components by GC/MS
51	Specific major components–HPLC/IR or LRMS
52	Survey analysis for inorganics
53	Volatiles
54	Volatiles
55	Volatiles
56	Volatiles
57	Extractables
58	HPLC/UV – generalised procedure
59	HPLC/UV – generalised procedure
60	Aldehydes – derivatisation procedures
61	Aldehydes – HPLC analysis
62	Carboxylic acids
63	Alcohols
64	Phosphine
65	Fluorine
66	Gases – cyanogens and phosgene
67	Gases – mustard
68	Gases
69	Acid chlorides
70	Aflatoxins
71	Brucine
72	Citrus red No. 2
73	Cycasin
74	Ethylene oxide
75	2-fluoroacetamide
76	Lasiocarpine
77	Phenacetine
78	Strychnine
79	Oximes
80	Tris(1-aziridinyl)phosphine sulphide
81	Antimony
82	Arsenic
83	Barium
84	Beryllium
85	Cadmium
86	Chromium
87	Lead
88	Mercury
89	Nickel
90	Osmium
91	Selenium
92	Silver
93	Strontium
94	Thallium
95	Vanadium

TABLE 2. Continued

No.	Method name
96	Anions
97	Total cyanides
98	Phosphides
99	UNICHIM gas sampling train, Italy
100	ASTM D-240: determination of heating value
101	ASTM D-482: determination of ash content
102	ASTM D-808: chlorine determination
103	ASTM C-25: sulphure determination
104	X-ray determination of Na
105	X-ray determination of Mg
106	X-ray determination of K
107	Determination of dioxins and PCBs by GC/MS
108	Determination of organic compounds by TOC
109	Continuous sampling of gas
110	Continuous analysis of O_2
111	Continuous analysis of CO
112	Continuous analysis of NO_x
113	Continuous analysis of SO_x
114	Continuous analysis of CO_2

parameters (e.g. for DRE determination) or (c) for additional analysis, depending on the sample. Some of them can be also obligatory, according to regulations or special properties of the sample (e.g. determination of volatile organics in stack gases in USA by Volatile Organics Sampling Train) [21].

5. Conclusions

An integrated information support for hazardous chemical waste management can significantly contribute to waste reduction, the safety of waste storage and processing, and to the economic efficiency of these processes. The Computerised Waste Registry proved to be the first step, allowing for waste to be followed "from cradle to grave" and thus minimising the danger of inadequate waste disposal. Knowledge of locations and quantities of waste enables better planning of waste processing, and the information on the costs of the latter helps to highlight the need for waste reduction at the source. Bibliographic and reference databases catalyse the international transfer of waste management know-how and technologies.

Higher levels of information processing – particularly the structuring of information into systems for the recognition of parameter hierarchy, relations and patterns of knowledge – promote efficient application in the control of

processes, as presented in this work and as illustrated by the example of cost-efficient analytical control design for the incineration of chemical hazardous waste in cement kilns.

References

1   A. Kornhauser and M. Vrtačnik, Speciality chemicals – information support for research and development, Bull. Slov. Chem. Soc., 37(4) (1990) 383–405.
2   A. Kornhauser and B. Boh, Information support for research and development, in: E.J. DaSilva, C. Ratledge and A. Sasson (Eds.), Biotechnology: Economic and Social Aspects, Cambridge University Press, 1992, pp. 309–353.
3   S.A. Glažar, A. Kornhauser and R. Olbina, Waste management information system: its role in pollution prevention and introducing cleaner technologies and products, Abstracts, International Conference on Pollution Prevention: Clean Technologies and Clean Products, Washington, DC, June 10–13, 1990, T-43.
4   M. Vrtačnik, D. Dolničar, A. Cizerle, P. Čok, S.A. Glažar and R. Olbina, Design of an expert system for water pollution determination/prevention, in: J. Liebowitz (Ed.), Expert Systems World Congress, Orlando, Florida, USA, December 16–19, 1991, Pergamon Press, New York, 1992, Vol. 1, pp. 917–928.
5   A. Beekwilder, Development of central hazardous waste treatment facilities in the Netherlands, Waste Manag. Res., 6(3) (1988) 314–320.
6   C. Benestad, Incineration of hazardous waste in cement kilns, Waste Manag. Res., 7(4) (1989) 351–361.
7   R.E. Mournighan, Hazardous waste combustion in cement and lime kilns, Waste Manag. Res., 6(4) (1988) 400–402.
8   J.F. Chadbourne and H.M. Freeman, Hazardous waste as fuel in cement kilns, In: R. Abbou (Ed.), Proc. World Conference Hazardous Waste: Detection, Control, Treatment, 1987, Elsevier, Amsterdam, 1988 Vol. Pt. B, pp. 1315–1324.
9   J.F. Chadbourne and A. Helmstetter, Burning hazardous waste in cement kilns, In: Proc. First International Conference Industrial and Hazardous Wastes, Toronto, Ont., Oct., 19–21, 1982, pp. 19–39.
10 P. Waage, The role of cement kilns in hazardous waste management – Norwegian experience, in: Proc. First International Conference Industrial and Hazardous Wastes, Toronto, Ont., Canada, Oct. 19–21, 1982, pp. 52–65.
11 S.A. Glažar, A. Kornhauser, M. Vrtačnik, R. Olbina, A. Cizerle, A. Musar and D. Dolničar, Hazardous waste as fuel for cement kilns, United States Environmental Protection Agency, Project (JFP) 884, Second Annual Report, 1991.
12 M.W. Black, Impact of use of waste fuels upon cement manufacturing, In: Proc. First International Conference Industrial and Hazardous Wastes, Toronto, Ont., Oct., 19–21, 1982, pp. 40–51.
13 Burning of hazardous waste in boilers and industrial furnaces, United States Environmental Protection Agency, Washington, DC, USA, Federal Registry, 56(35) 7134–7239, 21 Feb., 1991.
14 A.J. Buonicore, Experience with air pollution control equipment and contiuous monitoring instrumentation on hazardous waste incinerators, J. Hazardous Mater., 22(2) (1989), pp. 233–242.
15 J.C. Harris, D.J. Larsen, C.E. Rechsteiner and K.E. Thrun, Sampling and analysis methods for hazardous waste combustion, Report U.S. EPA Contract No. 68-02-3111, 1983.
16 S.A. Glažar, A. Kornhauser, M. Vrtačnik, R. Olbina, A. Cizerle and I. Cerar, Hazardous waste as fuel for cement kilns, United States Environmental Protection Agency, Project (JFP) 884, First Annual Report, 1990.

17   S.L. Daniels, Products of incomplete combustion (O_x, CO_x, HO_x, NO_x, SO_x, RO_x, MO_x and PO_x), J. Hazardous Mater., 22(2) (1989) 161–173.

18   Y. Zeng and D. Okrent, Assessment of off-normal emissions from hazardous waste incinerators, Part I. Assessment of off-normal emissions frequency and duration. J. Hazardous Mater., 26(1) (1991) 47–62.

19   Y. Zeng and D. Okrent, Assessment of off-normal emissions from hazardous waste incinerators, Part II. Assessment of off-normal emissions intensity and total emission, J. Hazardous Mater., 26(1) (1991) 63–80.

20   H. Keinhorst, Environmental protection requirements in the cement industry, Zement Kalk Gips, 41(3) (1988) 72–73.

21   E.M. Hansen, Protocol for the collection and analysis of volatile POHCs (Principal Organic Hazardous Constituents) using VOST (Volatile Organic Sampling Train), Report US EPA-600/8-84-007, Order No. PB84-170042, 1984.

Durability study of a solidified mercury-containing sludge

Gordon C.C. Yang

Institute of Environmental Engineering, National Sun Yat-Sen University, Kaohsiung (Taiwan)

Abstract

To more efficiently dispose of hazardous wastes, the durability of a solidified mercury-containing sludge was studied. A sludge sample was obtained from a chloro-alkali plant and solidified using a commercially available sludge treatment agent (STA II). The solidified monoliths were then subjected to physical and chemical durability tests. The physical durability tests (the freezing and thawing test and the wetting and drying test) were followed by the measurements of unconfined compressive strength and mercury concentration resulting from the toxicity characteristic leaching procedure (TCLP), if possible. The multiple TCLP (MTCLP), developed by this author, was employed for the chemical durability test. It was found that the smaller the sludge-to-binder ratio (S/B) was, the better the physical and chemical properties of a solidified monolith would have. This conclusion was a result of the various durability tests, unconfined compressive strength measurements, and TCLP test. All solidified specimens were broken during the freezing and thawing test except the one with S/B = 0.5, which was found to be degraded in terms of compressive strength and leaching toxicity as well. Results of the wetting and drying test also showed that all solidified specimens were degraded as evidenced by the compressive strength and TCLP leachate concentration measurements. The multiple TCLP test was carried out to determine the long-term stability of the solidified specimens subjected to cyclic erosion and leaching by acid precipitation. The test results in this study showed that solidification with the binder STA II has reduced the cumulative amount of mercury leached from 10.57% to less than 0.66% by weight.

1. Introduction

Mercury is the only metal in liquid form at ambient temperatures. Generally, mercury can exist in any of the following three forms: zero valence (elemental mercury), positive monovalence, and positive bivalence. Mercury is a very toxic heavy metal. When mercury is in an organic form, it would give rise to the greatest toxicity comparing the inorganic and metallic forms. Mercury can easily enter the human bodies via the bioconcentration and foodchain.

The content of mercury is very low in the natural environment. For example, the average content of mercury ranges from 0.06 to 0.08 µg/g for

soils; 0.3–0.41 μg/g for freshwater, estuarine and marine sediments; and 0.01–0.05 μg/g for water [1, 2].

In Taiwan, there used to be eight chloro-alkali plants employing the mercury process to generate chlorine gas, hydrogen gas and caustic soda. The residue from the following reactions in the mercury process is the so-called "mercury-containing sludge" employed in this study:

$$NaCl + xHg \rightarrow NaHg_x + \frac{1}{2}Cl_2(g)$$

$$NaHg_x + H_2O \rightarrow NaOH + \frac{1}{2}H_2(g) + xHg$$
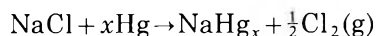
Approximately 30,000 metric tons of mercury-containing sludge were generated by the chloro-alkali plants in Taiwan. Although no longer used after August 1989, this waste still remains to be managed in a proper manner or it will pose severe threats on the environment and human health.

The objective of this work was to determine whether the chemical solidification of the aforementioned mercury-containing sludge would yield a durable monolith. The durability of the solidified monolith was evaluated by the freezing and thawing test, the wetting and drying test, and a cyclic leaching test.

2. Experimental

2.1 Materials

A composite sample of mercury-containing sludge was obtained from a chloro-alkali plant, which has stopped generating such waste when it began using an ion exchange membrane (IEM) process instead. In this work, a commercially available sludge treatment agent (STA II) was used as the binder for sludge solidification. STA II, a cement-based binder with some proprietary additives, is a product of the Taiwan Cement Company.

All chemicals used in this study were reagent grades as specified in various standard methods adopted by R.O.C. EPA and/or the U.S. EPA for evaluating solid wastes. The water used in this work was deionized water.

2.2 Methods

The original sample was characterized by various standard methods for evaluating solid wastes recommended by the U.S. EPA and R.O.C. EPA [3, 4]. The measured properties included moisture content, ash content, combustible content, density, total contents of heavy metals of interest, and heavy metal concentrations of the leachate resulting from the Toxicity Characteristic Leaching Procedure (known as TCLP test).

Sludge solidification was carried out by: (1) mixing the sludge, binder and water in a Hobart mixer for a few minutes; (2) pouring the mortar into an adequate size of PVC molds of cylindrical shape; (3) curing under the ambient conditions for one day; (4) demolding; (5) curing in an environmental chamber

maintaining 20 °C and 90% relative humidity for a desired length of time. After curing, the solidified specimens were tested for a variety of purposes. In this work, solidification was conducted according to CNS 1230 A3043; unconfined compressive strength measurement, CNS 1232 A3045; wetting and drying test, ASTM D4843-88; freezing and thawing test, ASTM B553-79; leaching toxicity, TCLP test; heavy metals concentration, atomic absorption spectroscopy (AAS); and mercury concentration, a cold-vapor atomic absorption method (Method 7471, SW-846, U.S. EPA) [3].

Multiple TCLP (designated MTCLP), developed by this author, was the repetitive leaching test employed in this work. This test basically is a combined technique of TCLP and Multiple Extraction Procedure (MEP; Method 1320, SW-846, U.S. EPA) [3]. In MTCLP, the first leaching test is exactly the same as the conventional TCLP test, which uses glacial acetic acid as the extraction fluid. The solid portions of the sample that remain after the first leaching are generally re-extracted nine times using a synthetic acid rain extraction fluid (sulfuric acid/nitric acid = 60/40 wt% mixture).

3. Results and discussion

3.1 Characterization of the mercury-containing sludge

Characterization results for the composite sample of the mercury-containing sludge are given as follows: moisture content, 41.24%; ash content, 37.18%; combustible content, 21.58%; true density, 2.39; and pH, 9.9. The total contents of heavy metals ($\mu g/g$) were found to be: Hg, 174.4; Zn, 192.5; Pb, 202.3; Cd, 11.5; Cr, 40.2; Cu, 108.6; and Ni, 89.6. On the other hand, the heavy metal concentrations (mg/l) of the TCLP leachate were: Hg, 0.81; Zn, 0.15; Pb, <0.2; Cd, <0.03; Cr, <0.2; Cu, <0.1; and Ni, 0.53. The result of TCLP test indicates that the mercury concentration is greater than the R.O.C. regulatory threshold of 0.25 mg/l. Thus, the sludge sample studied is classified as a hazardous waste.

3.2 Characterization of solidified monolith prior to durability tests

As expected, an increase in the quantity of binder in the solidified monolith would increase its unconfined compressive strength. The smaller the weight ratio of sludge to binder (S/B), the greater the compressive strength (see Table 1). In the case of S/B = 0.5 and weight ratio of water to binder of 0.5, the compressive strength for the specimen 28 days old was 124.5 kg/cm^2.

Solidification indeed decreased the leaching toxicity of mercury in the sludge. Prior to solidification, the mercury concentration of the TCLP leachate for the sludge specimen was 810 ppb. After solidification, such as S/B = 0.5, the mercury concentration of the TCLP leachate was found to be 3.4 $\mu g/L$.

The effect of the binder quantity on the TCLP leaching toxicity was clearly shown in Table 2. A specimen solidified with a greater amount of binder would give rise to a greater compressive strength, which in turn would result in a lower leached concentration for each hazardous constituent. Besides,

TABLE 1

Effects of physical durability tests on unconfined compressive strength of a mercury-containing sludge solidified with the binder STA II

Sludge-to-binder ratio (wt%)	Unconfined compressive strength (kg/cm^2)		
	No durability test	Freezing and thawing test	Wetting and drying test
0.5	124.5	70.2	64.5
1.0	57.2	N.A.	24.5
1.5	24.6	N.A.	14.6
2.0	20.5	N.A.	10.5
3.0	18.7	N.A.	8.7

Note: N.A. means the solidified monolith has failed in the test.

TABLE 2

Effects of physical durability tests on leaching toxicity of a mercury-containing sludge solidified by the binder STA II

Sludge-to-binder ratio (wt%)	Mercury concentration of the TCLP leachate (μg/L)		
	No durability test	Freezing and thawing test	Wetting and drying test
0.5	3.4	34.3	8.5
1.0	8.9	59.5	17.9
1.5	10.8	73.4	34.7
2.0	17.4	85.7	58.2
3.0	30.6	99.4	69.1

a greater quantity of a cementitious binder would indeed reduce the leaching capability of the extraction fluid due to a partial neutralization resulting from a rather high pH of the binder.

3.3 Freezing and thawing test

Effects of the freezing and thawing test on unconfined compressive strength of solidified specimens are shown in Table 1. Except for the case of S/B = 0.5, all solidified specimens were cracked or broken into smaller pieces during the test. This makes the compressive strength measurement impossible (see Table 1).

The negative effect of the freezing and thawing test on leaching toxicity is depicted in Table 2. In this work, the leached mercury concentration compared with the sample subjected to this test has been found to be three to ten folds after the freezing and thawing test.

3.4 Wetting and drying test

Table 1 shows also the results of the compressive strength measurement for the sludge solidified with the binder STA II and then subjected to the wetting and drying test. From this table, it is clear that the wetting and drying test would lower the compressive strength of a solidified specimen. But the degradation of the solidified monolith due to the weathering effect of this test was found to be less than that of the freezing and thawing test.

The influence of the wetting and drying test on the leaching toxicity of the solidified specimen is shown in Table 2. As indicated above, this test would cause the degradation of the solidified monolith, which in turn would make the extraction of hazardous constituents easier. Again, in terms of leaching toxicity, the weathering effect of the wetting and drying test is not as significant as the freezing and thawing test.

3.5 MTCLP test

Based on the same design principles of Multiple Extraction Procedure (MEP), this author has combined TCLP and MEP tests to develop a new leaching test designated Multiple TCLP (MTCLP). Since MTCLP is a modification of MEP, its design function should be very similar to, if not the same as, that of MEP. MEP is designed to simulate the leaching that a solid waste will undergo from repetitive precipitation of acid rain on an improperly designed sanitary landfill [3]. In a similar manner, MTCLP should reveal the highest concentration of each hazardous constituent that is likely to leach in a harsh, natural environment.

TABLE 3

Results of multiple TCLP test for a mercury-containing sludge and its solidified monolith

Sequence no. of MTCLP	Mercury-containing sludge unsolidified			Solidified specimen		
	Hg conc. ($\mu g/L$)	Wt of Hg leached (mg)	% of Hg leached (wt%)	Hg conc. ($\mu g/L$)	Wt of Hg leached (mg)	% of Hg leached (wt%)
1	810	1.620	9.31	30.6	0.061	0.47
2	21.90	0.044	0.25	0.63	0.001	0.01
3	8.95	0.018	0.10	1.13	0.002	0.02
4	11.30	0.023	0.13	0.84	0.002	0.02
5	9.74	0.019	0.11	0.91	0.002	0.02
6	12.60	0.025	0.14	2.09	0.004	0.03
7	10.60	0.021	0.12	2.41	0.005	0.04
8	6.51	0.013	0.07	0.63	0.001	0.01
9	27.90	0.056	0.32	1.69	0.003	0.02
10	1.51	0.003	0.02	1.25	0.003	0.02

Note: All calculations were based on 100 g of solid sample in 2000 ml of extraction fluid.

Table 3 shows the results of MTCLP for a mercury-containing sludge before and after solidifying with the binder STA II. For ease of comparison, the weight of mercury leached has been determined on the same basis that 100 g of solid sample is leached in 2000 ml of extraction fluid. As shown in Table 3, for both unsolidified and solidified specimens, the first leaching (Sequence No. 1) of MTCLP yielded the highest concentration of mercury. Starting from the Sequence No. 2 towards the end of the test, each leaching sequence gave only a very small increment (less than 0.3 wt%) of mercury leached. The cumulative amounts of mercury leached were found to be 10.57% and 0.66% by weight for unsolidified and solidified (S/B = 3) specimens, respectively. Thus, it is evident that solidification of the mercury-containing sludge with the binder STA II is capable of providing long-term stability for the waste disposed in this manner. A further study for the same sludge solidified with the same binder (S/B = 0.5) and 1 wt% (S + B) of a styrene–butadiene rubber (SBR) has indicated that the cumulative amount of mercury leached is reduced to 0.20 wt%.

4. Conclusions

In this work, properties of a mercury-containing sludge solidified by a commercially available binder STA II were characterized. The effects of physical and chemical durability tests on solidified monoliths were investigated as well. The former durability tests include the freezing and thawing test and the wetting and drying test, whereas the latter is a newly developed Multiple TCLP (MTCLP).

Experimental results indicate that physical durability tests would degrade the solidified monolith when their degradation was measured by unconfined compressive strength and TCLP leachate concentration of mercury. Except for the case of S/B = 0.5, all solidified monoliths were cracked or broken during the freezing and thawing test. The weathering effect of the wetting and drying test is not as strong as that of the freezing and thawing test.

Results of MTCLP show that the first leaching (the conventional TCLP) is the most significant step in the entire MTCLP test. In this leaching step, approximately 70–90 wt% of total leached mercury would be extracted. Only a rather small increment of leached mercury will be obtained for each of the subsequent leaching steps. For the unsolidified sludge specimen, the cumulative amount of mercury leached is 10.57%. Solidification of the same sludge with the binder STA II would reduce the cumulative amount of mercury leached to 0.66% by weight, or even smaller depending on the solidification conditions.

As indicated above, Sequence No. 1 leaching dominates the overall leaching of MTCLP. Whether this finding is applicable to other wastes solidified with other binders still remains uncertain. Further studies in this regard are therefore needed.

Acknowledgements

References

1   U.S. EPA, An Assessment of Mercury in the Environment, PB 83-111625, U.S. EPA, Washington, DC, 1977.
2   R.O.C. EPA, An Investigation on Heavy Metal Contents of Soils in Taiwan Area, EPA 044780569, R.O.C. EPA, Taipei, Taiwan 1990 (in Chinese).
3   U.S. EPA, Test Methods for Evaluating Solid Waste, SW-846, 3rd edn., U.S. EPA, Washington, DC, 1986.
4   R.O.C. EPA, Analytical Methods for Solid Wastes, Environmental Protection Communication Service, Taipei, Taiwan, 245 pp., 1990 (in Chinese).

The investigation of a devastating accident — An accidental explosion of 40 tons of TNT

Guo-Shun Zhang[a] and Ming-Jun Tang[b,*]

[a]*China North Industries Group, Beijing (China)*
[b]*Chemical Engineering Department, East China Institute of Technology, Xiao Ling Wei No 200 Nanjing [210014] (China)*

Abstract

A disastrous explosion accident with the force of 40 tons of TNT occurred on February 9, 1991. The explosion origin was defined by witness testimony, material evidence and field investigation. Two primary causes of the explosion were identified through "event tree analysis" by eliminating non-relevant factors and conducting a detailed study on relevant factors. It has been concluded that this was a "human element accident" which occurred due to poor safety in production. Lessons learned from this accident are summarized.

1. Background

TNT, a high explosive, is produced from toluene (methylbenzene) through a nitrating reaction by nitro-sulfuric acid [1]. The nitrating reaction comprises three stages: the first stage is to nitrate toluene into mononitrotoluene (MNT), which is accomplished by four nitrating reactors connected in parallel; the second stage is to nitrate mononitrotoluene to dinitrotoluene (DNT), which is accomplished by two nitrating reactors connected in parallel; the third stage is to nitrate dinitrotoluene into trinitrotoluene (TNT), which is accomplished by eleven nitrating reactors and their separators by series connection.

Equations of chemical reactions corresponding to the three stages are as follows:

---

*To whom correspondence should be addressed.

$$CH_3C_6H_5 + HNO_3 \xrightarrow{H_2SO_4} CH_3C_6H_4(NO_2) + H_2O$$

$$CH_3C_6H_4(NO_2) + HNO_3 \xrightarrow{H_2SO_4} CH_3C_6H_3(NO_2)_2 + H_2O$$

$$CH_3C_6H_3(NO_2)_2 + HNO_3 \xrightarrow{H_2SO_4} CH_3C_6H_2(NO_2)_3 + H_2O$$
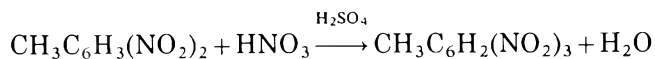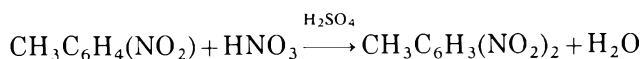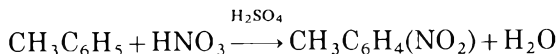
The third nitrating stage is much more difficult to accomplish than the other two stages. It requires longer reaction time and hence is performed in a series of many interconnected nitrating reactors. The process must be operated under higher temperature and by nitro-sulfuric acid of higher concentration. As a result, the third stage is the most dangerous in the process.

2. The accident

On February 9, 1991 at 7.30 p.m., a massive and devastating explosive accident occurred in the TNT production line of a factory in Liaoning province, China. Seventeen workers were killed and 107 injured, among them 13 in critical condition. Buildings of an area of 50,000 m² were totally demolished, 58,000 m² were seriously destroyed and 176,000 m² were damaged. 951 pieces of process equipment were completely destroyed. Direct property damage was 22.66 million RMB (ca. $5 million) and indirect property loss due to the interruption and rebuilding of this and neighboring production lines was enormous. The schematic of the production process is shown in Fig. 1.

By determining the quantity of explosives in each process equipment, the total amount of explosives exploded in this incident was estimated to be the equivalence of 40 tons of TNT. This figure is in agreement with damage analysis from buildings surrounding the explosion center and the size and shape of the crater.

The nitrating workshop, where the explosion occurred, consisted of three connected buildings. In the middle there was a three-layer, reinforced concrete building with the dimensions $9 \times 40 \times 15$ m³ and an arched roof. The side buildings east and west of the central building were 8×40 m² and 12×40 m², respectively. Most nitrating reactors were placed in the west building and the laboratory for physical and chemical analysis was in the east building. The three buildings were surrounded by a soil barricade of 3 m in height. The entrance to the workshop was through culverts which penetrated the barricade. After the explosion, the workshop was completely eliminated leaving a huge crater of 40 m in diameter and 7 m in depth (Fig. 2).
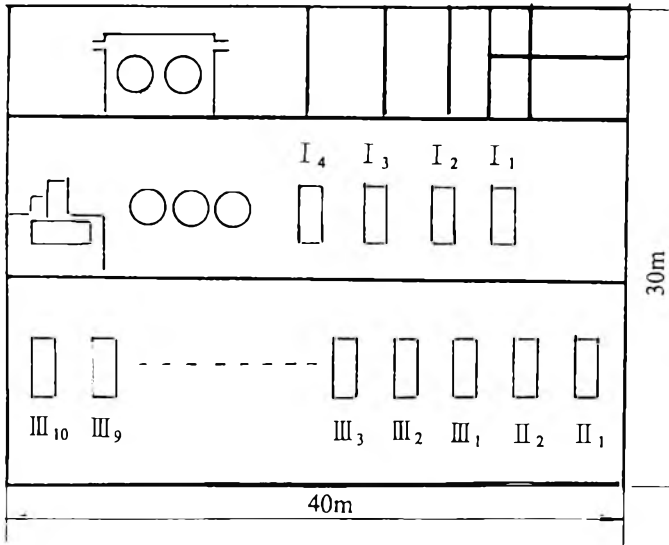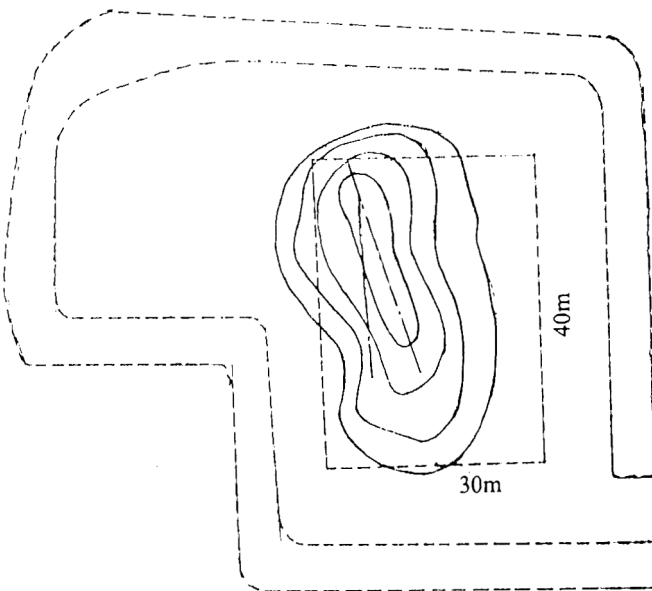
Fig. 1. Schematic of TNT production line.

Fig. 2. Schematic of the crater. (—) Isohypers of the crater, (· · ·) locations of the nitrating buildings and the barricades before the accident, and (· - ·) symmetry line of the crater or the reactors before the explosion.

The explosion not only demolished the nitrating workshop, but also serious-
ly destroyed the refining and packaging buildings, the compressor station and
the office building of the plant. Neighboring plants were also significantly
damaged. All buildings within 600 m of the explosion center were destroyed,
those within 1200 m were significantly damaged and those within 3000 m were
partially damaged. Thousands of trees in this area were damaged by blast waves.

Most of the debris from the demolished buildings and equipment was depos-
ited in an area of 300 m in radius around there. However, some debris was
found very far from the center of the blast. For instance, a steel rod 0.8 m long
and 8 cm in diameter was thrown 1685 m; a chunk of reinforced concrete, which
was originally a part of the arched roof of the central building and weighing 50
tons, was found 487 m from the center. Pieces of debris weighing 50 kg, which
had been a part of the concrete wall, penetrated the roof of a building 310 m
from the center and seriously injured two workers inside the building. Water
pipes 40 cm in diameter and 2 m depth under the ground were broken so that
running water filled the crater to a depth of 2.7 m.

3. The investigation

The investigation, which was initiated immediately after the accident, was
conducted by a team selected by the authorities, government labor department,
workers' Union and regional administrators. The investigation into the origin
and the causes of the explosion were very difficult because the production
buildings and process equipment were completely demolished. Very few pieces
of material evidence could be found since the scene was a large crater partially
filled with water. Fortunately, there were 17 survivors among the 34 workers
on the shift. During the extensive interview process they provided valuable
information about conditions at the workshop immediately prior to the
explosion.

In the course of the investigation, a large number of blueprints and docu-
ments were reviewed and simulating experiments were conducted by the
investigation team. After detailed analysis on equipment conditions, work
practices, raw material quality, process technology and production manage-
ment, the origin of the explosion was determined to be the separator of No.
2 nitrating reactor in the third nitrating stage.

The determination of the origin was based on following facts.

(1) Witness statements. The operator of the No. 2 reactor said that at 7.00
p.m. he took samples from the reactor and sent the sample to the laboratory.
Upon returning to his post at about 7.15 p.m. he found that the separator was
smoking. He activated the shower cooler and provided cooling water to reduce
the temperature. Meanwhile, he went to the control room to report his findings
to the shift supervisor.

The shift supervisor agreed that at about 7.15 p.m., upon receiving the
report, he took two other workers with him and went into the nitrating

building. They observed that the separator of the No. 2 reactor was smoking heavily. He instructed the workers to open the valve to add concentrated sulphuric acid to the reactor in order to further reduce the temperature. Unfortunately, this measure was not successful. At this time, the building was full of nitride smoke. So, he and other workers withdrew to the door and observed fire bursting from the gap between the separator and its lid. They immediately ran towards the barricade, and upon reaching the culvert exit they heard a loud explosion.

The operator of reactor No. 10 said that he saw the separator of the No. 2 reactor smoking when returning to his post after sending samples to the laboratory at about 7.15 p.m. Then he observed the shift leader attempting to reduce the temperature and control smoke. Immediately, upon seeing the nitride smoke getting denser and fire bursting from the reactor, he ran through nearby culvert and managed to escape.

(2) Material evidence. Pieces of process records were found at the site of the collapsed control room. The records indicated that at 7.00 p.m. of February 9, the concentration of nitric acid in the reactors of the third nitrating stage was too high: 7.09% and 12.6% for No. 2 and No. 5 reactors respectively, while they should have been 1.0–3.5% and 2.0–4.0% according to standard operating procedures manuals [2]. Thus, the recorded concentrations were two to three times higher than the standard values. This would cause off-specification conditions and cause the lowest melting point to occur earlier than normal in the process. In other words, the most violent reaction occurred in the No. 2 reactor instead of in later reactors. The discovery of high concentrations of nitric acid again supported the witness testimony of the first appearence of smoke, fire and explosion in No. 2 reactor.

(3) Crater analysis. The ground mapping showed that there was an angle of $5°$ between the main axis of the crater and the axis of the original location of nitrating reactors. These data indicated that the explosion originated in the first few reactors, which is in agreement with witness testimony that smoke and fire were first observed in the No. 2 reactor. After the first explosion, displacement of other reactors resulted due to the shock waves produced by the explosion of No. 2 reactor. Then sympathetic detonations followed. Different displacements of each reactor before sympathetic detonation resulted in a tilt between the axes of the crater and the location of reactors before the incident.

4. Causes of the event

The method of "event tree analysis" was adopted and found effective by the investigation team. A flow chart was drawn by the experts to include all possible causes of combustion and explosion. Logical relationships among all factors which might result in the accident were also indicated in the analyses. Then, the status and effectiveness of each factor were examined.

After eliminating non-relevant factors and conducting a detailed study of relevant factors, causes of the accident were verified.

In the analysis non-relevant factors such as: leakage of cooling water, interruption or insufficient supply of cooling water, stirrer problems, breakdown of instrumentation and the presence of foreign matters in raw materials, etc. were eliminated. Then, two "cause-result chains" were formed from the few relevant factors, as shown in Fig. 3.

In the first "cause-result chain", the key is "incorrect reactant ratio and off-specification operating conditions", which were the result of "excessive concentration of nitric acid". Due to the violent reaction, the contents in the reactor flowed to the separator where they continued reacting violently. However, there were no cooling tubes or stirrer in the separator where local overheating might easily develop into dissociation and combustion. It was found during the investigation that the off-specification operating conditions were present prior to the accident. On the day shift of February 9, nitric acid valves of No. 6 and No. 7 reactors were found to be leaking. After the next shift took over at 4.30 p.m. maintenance workers repaired the valves at 5.00 p.m. Nevertheless, the leakage already resulted in an excessive concentration of nitric acid in the nitrating system. For instance, the nitric acid concentration in the No. 2 reactor reached 7.09%, which is two or three times above the concentration of No. 1 reactor – 3.5% according to the standard operating procedures manuals.

In the second "cause-result chain", the key is "contact of reactants with foreign combustibles", since combustibles such as cotton yarn, lubricant oil, rubber gloves or rubber spacer, etc. will react violently with nitric acid and the
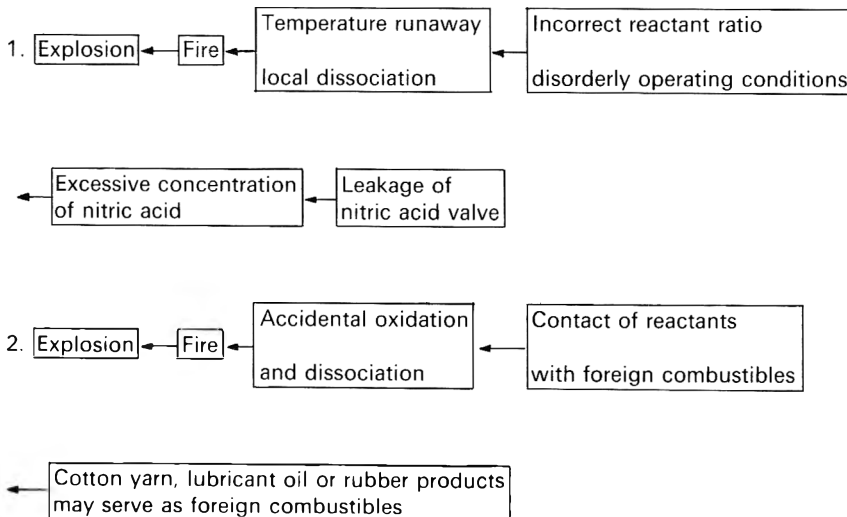

Fig. 3. Cause-result chains for a 40 tons TNT accidental explosion.

oxidation reaction may result in smoking or even fire. In the investigation, no foreign combustibles were determined to have entered the reactor before the explosion. However, it was discovered by further investigation that unapproved asbestos cord was used as the filler between the top of the separator and its upper lid. This asbestos cord might have served as the igniter of the fire when contacting nitro-sulfuric acid of high temperature and high concentration. Particularly, a large amount of concentrated sulphuric acid had been added into No. 2 reactor as a safety measure. In contrast with the original attempt, the addition of sulfuric acid would increase the chance for interaction between the asbestos cord and the concentrated nitro-sulfuric acid.

In general, asbestos cord is incombustible. However, the remainder of this asbestos cord found on the scene and that in storage could both be ignited by a match. The analysis report by the inspection center for labor safety and health in Liaoning province showed that this asbestos cord contained only 50% asbestos with combustible fiber and grease as the rest. In order to verify the interaction of this cord and nitro-sulfuric acid, simulation tests were conducted by the investigation team. It was proved in the experiments that this cord reacted violently with nitro-sulfuric acid of concentration specified by the standard operating manual. During the reaction, the production of large amount of yellow smoke and the sudden rise of temperature from 110 °C to 150 °C were observed. In contrast, process-acceptable asbestos cord hardly reacted in the same test. It was concluded, thus, that the application of the inappropriate asbestos cord as the filler in separators, which took place in June 1990 during the maintenance, might cause the ignition of nitro-compounds.

It was also found in the investigation that the fire starting in the No. 2 separator was propagated and transmitted through the venting system and the low wooden roof panels.

The transition from fire to explosion was due to the staff not taking the appropriate safety measure of emergency dumping. According to regulations, a nitrating reactor should be equipped with remote control, automatic and manual dumping devices in order to immediately open safety valves and let the contents of the reactor flow into the safety pool in case of emergency. Unfortunately, there was no automatic dumping device in the reactor because this was an old factory which was poorly equipped and did not have adequate automatic safety measures. In other words, this factory had poor safety conditions. In addition, the fact that the operator and the shift leader failed to manually dump the reactor, allowed the fire to develop and result in detonation.

The causes of the accident are summarized below.

The incident started as a result of the leakage of nitric acid valves on No. 6 and No. 7 reactors, which lead to excessive concentrations of nitric acid in the nitrating system and brought forward the lowest melting point in the reactor system. Then, a violent reaction and the generation of a large amount of smoke in the No. 2 reactor resulted. The interaction of unacceptable asbestos cord containing a large percentage of combustible fiber and grease with

nitrating acid of high concentration and high temperature provided the igni-
tion source. Another source of ignition might be dissociation and ignition of
nitro-compounds due to local overheating resulted from violent reaction in No.
2 separator. Finally, the fire was able to transit to detonation because of the
lack of automatic dumping device and the failure of the operators to manually
dump the reactor.

Meanwhile, poor management is also responsible for this accident. Many
problems occurred prior to the explosion but had not been properly addressed.
For instance, the process equipment was not in good condition; workers had
not been properly trained and the wrong asbestos cord was used, etc.

In conclusion, this is a human element accident which occurred due to poor
safety conditions.

5. Lessons learned from the accident

The following lessons should be learned from the accident.

5.1 Regarding equipment and technology

(1) Buildings for producing explosives should meet the requirements for fire
and explosion protection.

In this incident, the nitrating line was located in the west building which
was constructed of wood and brickwork and the distance between the top of
separator and the wooden roof was only 1.7 m. This construction allowed the
wooden roof to become the medium for transmitting combustion. Moreover,
the main building of the workshop was of reinforced concrete roof. In the
explosion, the heavy roof yielded large pieces of debris which penetrated and
destroyed surrounding buildings and injured people inside them.

(2) The process control and safety conditions of production equipment
should be improved.

The production line should be equipped with protective devices such as an
automatic alarm system and an automatic dumping devices. The number of
process workers should also be reduced.

(3) The process flow should be well organized, not only for convenient
operating but also for safe evacuating.

(4) Sufficient safe distance between explosive building and its surrounding
buildings should be established.

The large number of casualties and significant property losses in this acci-
dent are directly related to improper factory layout which had insufficient
distances between buildings and an insufficient blast resistant capacities of
most buildings.

5.2 Regarding production and safety management

(1) Process equipment for producing explosives should be under strict con-
trol in order to reduce or even to eliminate leakage or other problems.

In the days preceding the explosion, according to the testimony of the workers, there had been many equipment problems, many cases of replacing and repairing valves and spacers, and frequent turning on and off the production. Unfortunately, the managers and engineers did not solve the problems in time and let them develop into a major event.

(2) A worker's training program should be conducted to increase their knowledge of safe production and increase their ability to prevent accidents, i.e. the correct safety measures to be taken in case of emergency.

In this accident burning was able to transit to detonation because the operator and the shift leader left the site without taking the safety measure of manual dumping.

(3) Material such as asbestos cord should be inspected for fire and acid resistance before use.

References

1   T. Urbanski, "Chemistry and Technology of Explosives", Pergamon, New York, 1964.
2   Standard operating procedures manuals for TNT production, Internal Document, China Inc. of Explosives and Propellants, 1990.

Environmental threats of discarded picture tubes and printed circuit boards

Gordon C.C. Yang

Institute of Environmental Engineering, National Sun Yat-Sen University, Kaohsiung (Taiwan, R.O.C.)

Abstract

Scrap picture tubes (television and monitor tubes) and printed circuit boards were invest- igated for their potential threat to the environment. First, a qualitative analysis of samples was carried out by atomic emission spectrophotometry. In addition, U.S. EPA Method 3050 (SW-846) and atomic absorption spectrophotometry (AAS) were employed to determine the total contents of heavy metals of interest. Finally, TCLP and AAS were used to evaluate the leaching toxicity of the samples. All color and amber picture tubes tested were found to be hazardous; whereas the green, white and paper-white picture tubes were not. For color picture tubes, lead and zinc concentrations of TCLP are greater than the current regulatory thresholds in Taiwan; while the amber one is hazardous because of its cadmium concentra- tion. The environmental threats of those hazardous picture tubes are ascribed to leaching of heavy metals from the phosphors that are deposited on the inner side of the viewing screen of each picture tube. All tested printed circuit boards also were found to be hazardous as evidenced by their TCLP lead, zinc and cadmium concentrations. The findings in this work show that disposal of discarded TV sets, personal computers, video-game sets, etc. should be managed properly to avoid contamination of soil and groundwater. Several recommenda- tions were made in this regard.

1. Introduction

Improper disposal of discarded television sets, personal computers, video- game sets, etc., is likely to cause soil and groundwater pollution due to the leaching of heavy metals within. Like many industrial countries, each year Taiwan discards several hundred thousand units of used TV sets, personal computers and so on. For color TV sets alone, it was estimated that at least 400,000 units were discarded annually for the past several years [1]. Part of these used home appliances may be reclaimed and recycled by domestic scrap processors. The remainder, that account for a good portion of the total, however, are still disposed of in an uncontrolled manner. In other words, a great quantity of picture tubes (television and monitor tubes) and printed circuit boards in those home appliances are not disposed of properly.

Improper disposal methods currently practiced include: (1) illegal dumping (not limited to "midnight dumping") in an open field, (2) illegal burning in an open field, and (3) disposal in a non-secure landfill. As a result, potential threats to human health and the environment are posed due to the pollution of air, soil and groundwater. An incident of illegal dumping and burning of defective printed circuit boards from a local manufacturer resulted in some 900 students in a nearby primary school being hospitalized or under medication on April 29, 1992 in Taiwan. The R.O.C. EPA immediately ordered the manufacturer to close the plant temporarily and to clean up the dump site of the incident.

The objective of this work was to study whether used/defective picture tubes and printed circuit boards generated by discarded home appliances and the manufacturers would be hazardous. Moreover, this investigation would ascertain whether soil and groundwater pollution problems can be caused by poor management of such wastes. This was determined by the TCLP leachate concentrations of heavy metals of interest.

2. Experimental

2.1 Materials

A total of 12 picture tube samples were studied in this work. Eight (defective 14" display/monitor tubes) were obtained from a local picture tube manufacturer; three were dismantled from used television sets (18" and 20" color ones and a 12" black/white one); and, one sample in powdered form was obtained from a domestic scrap picture-tube processor. The color shown on the viewing screen of a picture tube is of interest because it is used by this author to differentiate one picture tube from another. The displayed colors of the above picture tube samples are detailed in Table 1. To carry out various experiments, all picture tube samples except the Sample PT-1 were first crushed by a hammer, then ground with a mortar if needed.

Three printed circuit boards containing the resistors, capacitors, etc. were also studied in this work. These samples were obtained from the same TV sets mentioned above. The samples were first cut into three or four smaller pieces by a pair of big scissors. Further fragmentation was carried out by a German-made cutting mill (Retsch, Model SM-1).

2.2 Experiments

All samples of picture tube and the printed circuit board from a B/W TV set in triplicate were subjected to a qualitative analysis by atomic emission spectrophotometry (Baird Atomic, Model GX-1). In this test, generally, samples were ground very fine (-325 mesh) to have a better result.

To understand the heavy metal contents of each waste, specimens in triplicate were subjected to an acid digestion (Method 3050, SW-846, U.S. EPA), then analyzed by a Perkin-Elmer atomic absorption spectrophotometer. To evaluate

TABLE 1

List of displayed colors of picture tubes tested

Sample No.	Displayed color
PT1	*
PT2	Amber
PT3	Color
PT4	Color
PT5	White
PT6	Paper white
PT7	Color
PT8	Color
PT9	Green
PT10	Green
PT11	Paper white
PT12	White

*Sample PT1 was obtained, in powdered form, from a scrap picture-tube processor.

the leaching toxicity, the samples were first subjected to Toxicity Characteristic Leaching Procedure (known as the TCLP test) [2]. The leachates were acid-digested further (Method 3010, SW-846) before the determination of metals concentration by atomic absorption spectrophotometry (AAS).

3. Results and discussion

3.1 Picture tubes

Results of atomic emission spectrophotometry indicated that the major constituents of the samples were Si and Na; whereas minor constituents (less than 1%) were Al, Ba, Ca, K, Pb, and Sr. This finding is in accord with the typical glass compositions such as SiO_2, Na_2O, Al_2O_3, BaO, CaO, K_2O, PbO, and SrO.

In this work, results of atomic emission spectrophotometry also suggested this analysis was almost not able to detect the phosphor compositions except for Samples PT6 and PT11. Both PT6 and PT11 have a paper-white color emission. For these two specimens, a trace amount of In element was found. This is due to the fact that the paper-white color is emitted by the trichromatic phosphors blend. This phosphor blend is composed of $InBO_3$:Tb (green), $InBO_3$:Eu (red), and ZnS:Ag (blue). Normally, for a 14" picture tube/display tube, only about 2.26 g of relevant phosphors were deposited on the inner side of the viewing screen. It is possible that such a small amount of phosphors would be lost during sample preparation (crushing and grinding), which would result in the difficulty for detection.

Table 2 depicts the analytical results of pH, total heavy metals content, and TCLP leachate concentration. A review of these results shows high

TABLE 2

Total contents of heavy metals and their corresponding TCLP leachate concentrations for picture tubes tested

Item	Sample No.									
	PT1		PT2		PT3		PT4		PT5	
	A	B	A	B	A	B	A	B	A	B
Ni	20	<0.20	25	<0.20	10	<0.20	40	0.2	45	0.3
Cu	17.5	0.16	5	<0.10	7.5	<0.10	2.5	0.05	<0.05	<0.05
Cr	<0.2	<0.20	<0.20	<0.20	<0.2	<0.20	87.5	0.25	75	0.25
Cd	2.5	<0.20	278.2	0.86	1.4	<0.02	0.05	<0.02	71.65	0.02
Pb	345.6	6.60	96.4	1.50	4,126.5	113.5	10,000	21.3	86.4	1.7
Zn	79.5	1.40	15.9	0.23	506.8	216.3	775.5	32.62	506	0.36
Initial pH	—	10.03	—	9.28	—	7.70	—	9.65	—	9.19
Final pH	—	5.01	—	5.18	—	4.68	—	4.95	—	4.90

Item	Sample No.							
	PT6		PT7			PT8		
	A	B[a]	A	B[a]	B[b]	A	B[a]	B[b]
Ni	4.3	<0.05	76.9	1.31	<0.05	207.5	0.10	<0.05
Cu	1.1	<0.05	3.2	<0.05	<0.05	3.3	<0.05	<0.05
Cr	4.7	<0.05	1.0	<0.05	<0.05	2.8	<0.05	<0.05
Cd	4.2	<0.05	25.2	<0.05	<0.05	0.5	<0.05	<0.05
Pb	104.3	2.43	5,930	394.5	0.80	11,790	380.2	128.3
Zn	73.6	0.49	1,398	50.7	0.15	2,380	45.9	14.4
Initial pH	—	9.80	—	9.60	9.80	—	9.70	9.70
Final pH	—	5.15	—	5.20	5.18	—	5.08	5.08

TABLE 2. Continued

Item	Sample No.											
	PT9			PT10			PT11			PT12		
	A	B[a]	B[b]	A	B[a]	B[b]	A	B[a]	B[b]	A	B[a]	B[b]
Ni	14.5	<0.05	<0.05	5.2	0.06	<0.05	3.9	<0.05	<0.05	<0.10	0.3	<0.1
Cu	3.4	<0.05	<0.05	10.9	<0.05	<0.05	5.3	0.06	<0.05	<0.05	<0.05	<0.05
Cr	0.3	<0.05	<0.05	1.0	<0.05	<0.05	2.7	<0.05	<0.05	<0.20	<0.1	<0.1
Cd	0.9	<0.05	<0.05	0.6	<0.05	<0.05	20.7	<0.05	<0.05	78	0.05	<0.05
Pb	100	1.65	0.60	81.8	2.19	0.71	100.5	2.30	1.03	106	1.5	0.7
Zn	1,480	2.82	2.07	1,169	2.63	2.26	317.2	0.41	0.17	1,688	0.58	0.33
Initial pH	—	9.80	9.80	—	9.85	9.85	—	9.65	9.65	—	8.90	8.96
Final pH	—	5.15	5.15	—	5.15	5.15	—	5.18	5.18	—	4.96	4.94

Notes: 1. Column A denotes the total content of each heavy metal.
2. Column B denotes the TCLP leachate concentration of each heavy metal.
3. All figures are in mg/L units except pH.
[a] Denotes particle sizes <0.6 mm; [b] Denotes particle sizes in the range of 0.6–2.36 mm.

levels of regulated heavy metals (such as cadmium, lead and zinc) in the original wastes. A similar trend for the TCLP test was observed for the same specimens.

For color picture tubes (PT3, PT4, PT7 and PT8), TCLP leachate concentrations of Pb and Zn indicated that all these specimens would be considered hazardous. A color picture results from a joint effect of red, blue and green phosphors. Compositions for the above phosphors are $Y_2O_2S:Eu$, $ZnS:Ag$ and $ZnS:Cu, Al$ [or $(Zn, Cd)S:Cu, Al$], respectively. Thus, phosphors are responsible for a high concentration of Zn in the TCLP leachate. Besides, the leaching of frit seal ($PbO-B_2O_3-ZnO$) would explain high levels of Pb and Zn in the TCLP leachate. Normally, 14'' and 20'' picture tubes contain 30 g and 55 g of frit seal, respectively.

For the amber (or orange) picture tube (PT2), its leachate concentration of Cd is greater than the regulatory threshold. This is due to a high content (63.2 wt%) of Cd in the phosphor $Cd_5Cl(PO_4)_3:Mn$.

The finely ground sample of mixed picture tubes (PT1) also is considered hazardous because of its Pb concentration. This might be due to the leaching of frit glass in the specimen.

Each display tube with the white picture (PT4 and PT12) showed a high content of Zn in the sample. Normally, blue and yellow phosphors are deposited on the white picture tube. The compositions for these phosphors are $ZnS:Ag$ and $(Zn, Cd)S:Ag$, respectively. However, none of the heavy metals in the TCLP leachates exceeded the regulatory standards.

Monochrome green monitor tubes (PT9 and PT10) both showed a high content of Zn as well. Again, this is due to its green phosphor of $ZnS:Cu, Al$ [or $(Zn, Cd)S:Cu, Al$]. None the less, these two specimens are considered non-hazardous as evidenced by their metal concentrations in the leachates.

Further study was conducted to determine the effect of particle size on the TCLP test for PT6 through PT12. The coarser fraction consisted of particles passing through a No. 8 sieve (2.36 mm) but retained on a No. 28 sieve (0.6 mm). The finer fraction represented all particles under 0.6 mm. Results of TCLP tests showed a higher level of metal concentration in the finer fraction for the same picture tube.

3.2 Printed circuit boards

To better understand the potential environmental impacts of discarded printed circuit boards it is worth giving them a general description. A printed circuit board, consists of epoxy resin filled with glass cloth (fiber glass) and a brominated flame retardant. About one-third of the surface for each side is covered with a copper layer (about 70 μm thick), which is partially covered with 8 μm thick of tin lead (60/40). If the finish is bare copper, a thin layer (about 0.5 μm) of alkylimidazole can cover the copper part. Each side is covered with 35 μm of a resin solder mask: acrylic resin (screening process), or epoxy resin (photo process). In a fire, the organic material may emit a number of hazardous substances into the air [3].

TABLE 3

Total contents of heavy metals and their corresponding TCLP leachate concentrations for printed circuit boards tested

Item	Sample No.						
	PCB-NL		PCB-SY		PCB-SP		
	A	B	A	B	A	B[a]	B[b]
Ni	85	0.60	95	0.60	70	1.4	1
Cu	142,695	<0.10	180,144	<0.10	112,500	1.2	<0.05
Cr	216.5	<0.20	6.6	<0.20	50	0.1	0.1
Cd	494.8	12.43	71.4	4.67	30	0.37	0.08
Pb	13,476.7	187.80	51,839.7	58.70	4,200	56	3.6
Zn	28,704.6	30.00	42,831.7	76.30	33,000	280	240
Initial pH	—	7.35	—	6.70	—	7.31	7.31
Final pH	—	4.88	—	4.80	—	5.30	5.30

Notes: 1. Column A denotes the total content of each heavy metal.
2. Column B denotes the TCLP leachate concentration of each heavy metal.
3. All figures are in mg/L units except pH.
[a] Denotes particle sizes in the range of 4–9.5 mm; [b] Denotes particle sizes <4 mm.

The result of atomic emission spectrophotometry showed that the specimen obtained from the 12" B/W TV set contained Fe, Cu, Sn, Si, Al, Ca, Mn, Ag, Ba, Cr, Ni, Zn and Pb. This is in good agreement with another study conducted by X-ray fluorescence [4]. It is believed that Fe and Ni are major compositions for IC components; Cu for conducting loop; Sn and Pb for solders; Ag for electronic contacts; Si for fiber glass; and Ca as an additive for epoxy resin.

The pH, heavy metal content, and TCLP leachate concentrations, for all specimens are shown in Table 3. From this table, it is evident that printed circuit boards in color TV sets contain high levels of Pb, Zn, Cu and Cd. A similar observation was found for the specimen from the B/W TV set except a lower content of cadmium. The results of the TCLP test also suggest that printed circuit boards are all hazardous. For specimens from color TV sets, the leachate concentration for Cd, Pb and Zn were much greater than the present R.O.C. regulatory thresholds. The leachate concentrations of Pb and Zn for specimen from the B/W TV set were also found to be not in compliance with the regulatory standards.

4. Conclusions

The TCLP test has showed that picture tubes for color and B/W TV sets and many display tubes for personal computers are hazardous. Color picture tubes are hazardous due to their Zn and Pb concentrations and the amber picture

tube because of the Cd concentration. On the other hand, green, white and paper-white picture tubes would be considered nonhazardous according to present R.O.C. regulatory standards. The color ones are hazardous because of the compositions of their blue and green phosphors and frit seal. Cd in the phosphor is the reason for the amber picture tube being hazardous.

Printed circuit boards from color and B/W TV sets are considered hazardous as well. The reason is that the TCLP leachate concentrations of Cd, Pb and Zn are not in compliance with regulatory thresholds.

Due to the potential threats posed on the environment by the hazardous picture tubes and printed circuit boards, these wastes should be managed properly. Disposal of such wastes or anything containing these wastes in an uncontrolled manner is likely to cause soil and groundwater pollution due to the leaching of heavy metals associated with these wastes.

Recommendations

To control and mitigate the pollution from the discarded picture tubes and printed circuit boards, proper waste management is indeed necessary. To this end, several treatment methods and regulatory measures are suggested:

1. Use finely ground picture tube powders as a supplementary raw material for ceramic products such as floor tiles and the like. In so doing, heavy metals associated with the picture tubes would be very difficult to leach out under natural conditions.

2. Use phosphors containing no heavy metals as a replacement for heavy-metal-containing phosphors currently used for color emission of picture tubes. For instance, using $(Ba, Mg)AlO_3 : Eu$ to substitute $ZnS : Ag$ (blue) and $(Ce, Mg)AlO_3 : Tb$ to replace $ZnS : Cu, Al$ (green); or even $Y_2O_3 : Eu$ (red) to substitute $Cd_5Cl(PO_4)_3 : Mn$ (orange or amber).

3. Separate, recover and recycle various metals and the base materials of printed circuit boards. This is technically feasible in the laboratory as has been done by another researcher [4].

4. Employ technologies of solidification/stabilization, incineration, or pyrolysis as alternative disposal methods for the wastes studied, particularly printed circuit boards. Further studies should be conducted in this regard to evaluate the process.

Acknowledgements

References

1 Energy & Resources Laboratories, ITRI, Investigation of Metal Scraps Produced in Taiwan, ERL-79-R121, Hsinchu, Taiwan, June 1990 (in Chinese).
2 U.S. Federal Register, 51(216) (1986) 40643–40652.
3 Philips Components, Philips Components Products in Environment, Eindhoven, The Netherlands, 1990, p. 9.
4 N.H. Yang, A Study on Separation and Recovery of Values from Scrap IC Boards, M.S. Thesis, National Cheng-Kung University, Kaohsiung, Taiwan, R.O.C., July 1990 (in Chinese).

Destruction of cresols by chemical oxidation

Y. Zheng, D.O. Hill and C.H. Kuo*

Department of Chemical Engineering, Mississippi State University, Mississippi State, MS 39762 (USA)

Abstract

   This work investigates the reaction rates and kinetics of the oxidative destruction of cresol isomers in water by ozone and hydrogen peroxide. Cresols are oxidized slowly by hydrogen peroxide though the reaction rates are enhanced in the presence of Fenton's reagent and other catalysts. Rapid oxidation takes place between ozone and a cresol isomer for complete conversion to intermediates in less than 0.1 second. Further reactions or decomposition of the intermediates result in rupture of the aromatic ring and production of carbon oxide, acetic and other acids. Three moles of ozone are required for the destruction of a cresol isomer, and the overall kinetics is first order with respect to the concentrations of ozone and cresol isomer. At 25 C. the reaction rate constants are 32 240, 60 870 and 45 460 $M^{-1}s^{-1}$ respectively, for the ozonation of o-, m- and p-cresol. In the temperature range of 10 to 40 °C, m-cresol is the most reactive species of the three isomers with ozone in the aqueous phase.

1. Introduction

   The present work concerns the reaction of three cresol isomers with hydrogen peroxide and ozone in water at various temperatures. Cresols, also known as methylphenols or hydroxytoluenes, are toxic compounds used in the manufacture of wood preservation agents, pesticides, phenolic resins and other industrial compounds. Like many phenolic compounds, these chemicals are found in drinking water and industrial waste streams, and treatment for removal or destruction of these compounds is required. Cresols also are present in the atmosphere, and according to a recent NATICH report [1], the total emission rate in the United States is about 75 tons/year. These compounds are classified as hazardous air pollutants in Title III of the 1990 Clean Air Act Amendments; and the US Environmental Protection Agency is required to promulgate emission limitations for these compounds based on maximum achievable control technology. The present research, therefore, was undertaken to study the reactivity and kinetics of the chemical oxidation of the

---

*To whom correspondence should be addressed.

cresol isomers in water. Results obtained from this investigation might be useful to both air and water pollution abatement.

There is little information in the literature regarding the oxidation of cresols by hydrogen peroxide. None the less, the favorable treatment of water containing o- and m-cresols by ozone was reported as early as 1953 by Niegowski [2]. The rupture of the aromatic rings of o- and p-cresols following ozone treatment was reported by Dore et al. [3], and products of the ozonation were identified by Bauch et al. [4]. Hoigne [5] indicated that the ozonation rate of cresols is very fast with large rate constants. The reaction of ozone with cresols in gas–liquid contactors was investigated by Gould [6], Gurol and Nekouinaini [7], Beltran et al. [8], and others. Although some phenolic compounds are not amendable to biological treatment, Wang [9] reported that anaerobic biological treatment of o-cresol and other compounds is attainable if sufficient oxidation is induced by ozone.

In the gas–liquid systems used by earlier investigators to study the ozonation of cresols, the mass transfer rates were controlled by both diffusion of the ozone in the liquids as well as chemical reactions. Thus, reliable data may not be available for accurate assessment of the reaction kinetics of the oxidation process. In this work, the stopped-flow technique was applied to study the ozonation reactions in a homogeneous, liquid phase reactor. Absorbance data were obtained and analyzed to determine reaction rates and orders of the oxidation reactions. In addition, an agitated reactor was used to study some slow reactions between cresols and hydrogen peroxide with or without catalysts.

2. Experimental details

Ozone gas was produced from a Welsbach Model T-408 ozonator using pure, extra dry oxygen. The ozone gas was then bubbled into distilled water for 10 to 30 minutes depending upon the desired concentrations. The initial concentrations of the dissolved ozone were determined by both iodiometric titration and spectrophotometric technique, as discussed in some earlier publications [10, 11]. An aqueous solution of hydrogen peroxide was prepared by dilution of the concentrated solution (30 wt%, ACS reagent).

The ozone gas also was introduced into distilled water to oxidize any contaminants before the water was used to prepare the reactant solution of a cresol isomer. All cresol isomers were ACS grade reagents purchased from the Aldrich Chemical Company.

A stopped-flow spectrophotometer system (High-Tech Scientific Model SF-51) was used to conduct the kinetic experiments. Prior to an experimental run, two reactant solutions (dissolved ozone or hydrogen peroxide in one and cresol isomer in another) were kept in two driving syringes at a specified temperature maintained through a thermostat flow circuit around a spectrometer unit in the system. By actuating a pneumatic flow circuit, the two

solutions were mixed rapidly in a mixing jet and allowed to flow into an observation cell (0.04 cm^3 in volume) where the mixed solution was stopped abruptly. Simultaneously, a monochromatic light was allowed to pass through the solution during the reaction in the mixing cell, and its resultant intensity was projected on to a photomultiplier tube. This output, proportional to the light intensity transmitted by the reacting solution, was processed and stored in an automatic data acquisition system for further analysis. The stopped-flow apparatus is advantageous in allowing complete mixing of the two reactants in less than one millisecond, and therefore, the absorbance changes in the mixed solution during a rapid reaction can be traced. The system is designed for continuous measurement of the transmittance or absorbance of the solution at a fixed wavelength between 200 to 800 nm.

A gas chromatograph (Hewlett-Packard Model 5840A) was utilized to measure concentrations of cresols in some reactions. It was also applied to determine the stoichiometry and products of the ozonation reactions using several packed columns.

3. Analysis of kinetic data

The oxidation reactions studied in this work are irreversible, and the kinetic data can be analyzed by assuming an overall reaction of the following type:

$$aA + bB \rightarrow pP + qQ + \cdots \tag{1}$$

According to the above reaction, the rate of depletion of the reactants, A and B, can be written as,

$$\frac{1}{a}\frac{dC_A}{dt} = \frac{1}{b}\frac{dC_B}{dt} = -kC_A^m C_B^n \tag{2}$$

If A is a limiting reactant by conducting an experiment with B in large excess, then eq. (2) can be simplified to:

$$\frac{dC_A}{dt} = -k'C_A^m \tag{3}$$

where,

$$k' = akC_B(t)^n \approx akC_B(0)^n \tag{4}$$

By assuming a reaction order, m, with respect to the concentration of A, eq. (3) can be integrated to yield:

$$\frac{C_A(t)}{C_A(0)} = \exp(-k't) \quad \text{for} \quad m=1 \tag{5}$$

and,

$$\left\{\frac{C_A(t)}{C_A(0)}\right\}^{1-m} = 1 + (m-1)C_A(0)^{m-1}k't \qquad \text{for} \quad m \neq 1 \tag{6}$$

In the stopped-flow reactor, the total absorbance of a reacting solution is measured continuously as a function of the reaction time. Preliminary tests showed that in dilute solutions, the absorbance of an individual component increases linearly with its concentration, as dictated by Beer's law. Under this condition, the following relationship between the absorbance and the concentration of the limiting reactant A can be derived [11]:

$$\frac{C_A(t)}{C_A(0)} = \frac{S(t) - S(\infty)}{S(0) - S(\infty)} \tag{7}$$

where $S(0)$ represents the initial absorbance of the mixed solution and $S(\infty)$ is the asymptotic absorbance measured at the end of a reaction period.

Equations (5), (6) and (7) imply that the concentration or absorbance data obtained in an experiment can be plotted against the reaction time, t, in a certain manner to verify the reaction order (m) assumed. If the reaction is first order with respect to A, then a linear plot can be obtained on a semi-logarithmic scale for the dimensionless concentration or absorbance versus time. For other values of m, a plot of the dimensionless concentration or absorbance of exponent $(1-m)$ versus time yields a straight line. The apparent rate constant, k', can be calculated from the slope of the straight line. According to eq. (4), a straight line can be drawn from a logarithmic plot of k' versus $C_B(0)$ for various experiments conducted at the same condition of temperature and acidity. Therefore, the reaction order (n) with respect to B and the overall rate constant, k, can be determined from such a plot.

4. Mechanism and stoichiometry of ozonation

As mentioned earlier, the ozonation products were identified by Bauch et al. [4]. They reported that the decomposition of 80% for cresols was achieved with 2 moles of ozone per mole of the cresol isomer, and that at least 3 moles of ozone were required for complete destruction. According to these investigators, the methyl group of each cresol is oxidized to the corresponding carboxylic acid in the initial ozonation. Continued ozonation results in rupture of the aromatic ring and produces maleic acid which is oxidized further to mesotartaric acid. Several acids including propionic, acetic, glycolic, glyoxylic and oxalic acids, and carbon dioxide are also formed. For example, the ozonation of o-cresol produces salicylic acid initially, and the other acids as the final products:

$$HOCC-CH=CH-COOH \rightarrow HOOC-CH(OH) \ CH(OH)-COOH$$

$$CH_3CH_2COOH + CH_3COOH + HOCH_2COOH + OHC \ COOH + HOOC \ COOH + CO_2$$

(8)
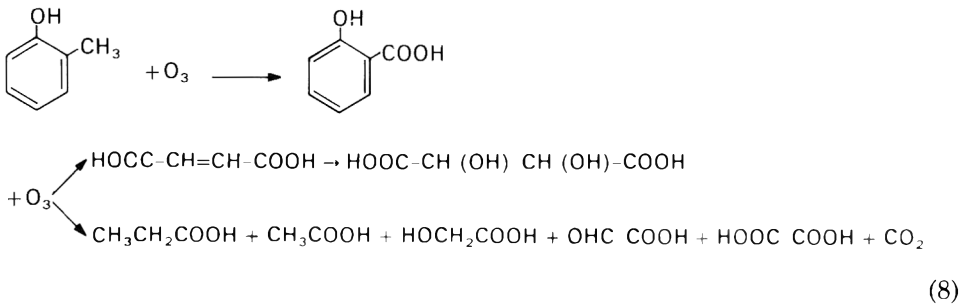
Several of the above acids are also produced in the ozonation of phenol [11, 12].

Beltran et al. [8] reported that two moles of ozone were consumed per mole of o-cresol in the gas–liquid system. This is in agreement with the two strongest nucleophilic positions in the o-cresol to activate the *ortho* and *para* positions of the hydroxyl group, as suggested by the authors. Similar to the earlier conclusion of Dore et al. [3], the authors suggested that methylcatechol is produced in the attack of the first ozone molecule, and the 1,3-dipolar addition of the second ozone molecule breaks the aromatic ring as follows:

(9)
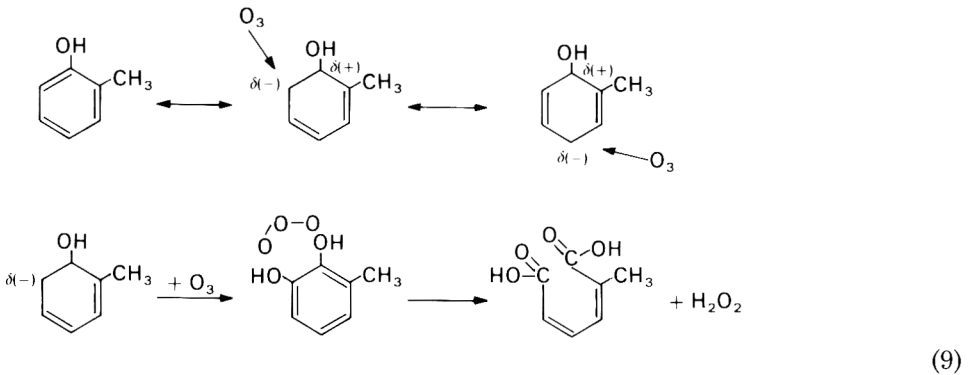
It is likely that the dicarboxylic acid can be oxidized further, though no identification of the final products was reported by Beltran et al. [8].

Another possible mechanism can be postulated on the basis of the hexagon formula of Kekule (proposed in 1865), as discussed by Haijman and Wibaut [13]. From the result of the ozonation of benzene to form a triozonide, it was confirmed that benzene behaves as a compound with three double bonds and that the six carbon–carbon bonds in the benzene nucleus are equivalent. In the ozonation of o-xylene and 1,2,4-trimethyl benzene to form aldehydes and ketones, the ozone addition was not affected by steric hindrance of the methyl groups as concluded by Haijman and Wibaut [13]. If this same conclusion holds for the methyl and hydroxyl groups of cresols, then three ozone molecules would be required to attack one molecule of a cresol isomer to form a triozonide in the initial step. Further decomposition and reaction of the triozonide may produce the acids identified by Bauch et al. [12].

   The stoichiometries of the ozonation of the three cresol isomers were deter-
mined in this work. In each experiment, two reactant solutions with different
concentrations of the cresol isomer and dissolved ozone were mixed, and two
solution samples withdrawn at 5 or 20 minutes. One sample was utilized to
determine the residual amount of the cresol by the chromatographic method
using a carbowax 20M column. Another sample was titrated to determine the
concentration of residual ozone in the solution. The ratio of moles of ozone
consumed per mole of cresol reacted is calculated to be about three for all
measurements. Results of the various measurements are plotted in Fig. 1 indi-
cating that the cresol was consumed completely if the initial ratio was 3 moles
of ozone or more per mole of cresol. If the initial ratio was less than three, then
the dissolved ozone was completely consumed but a fraction of the cresol was
not reacted. Some tests were also performed in the stopped-flow system by
continued measurement of the absorbance of a mixed solution. The total
absorbance increased very rapidly and then declined indicating the formation
and further decomposition of products of high absorbance. If the dissolved
ozone was in large excess in an experiment, then the rate of decrease of the
absorbance was very slow after a short period (less than one second). By
assuming that the slow rate of the absorbance decrease was due to self-
decomposition of the excessive ozone, the amount of ozone consumed was
again estimated to be about 3 moles per mole of cresol. Thus both the chromato-
graphic and spectrophotometric methods confirmed that three moles of ozone
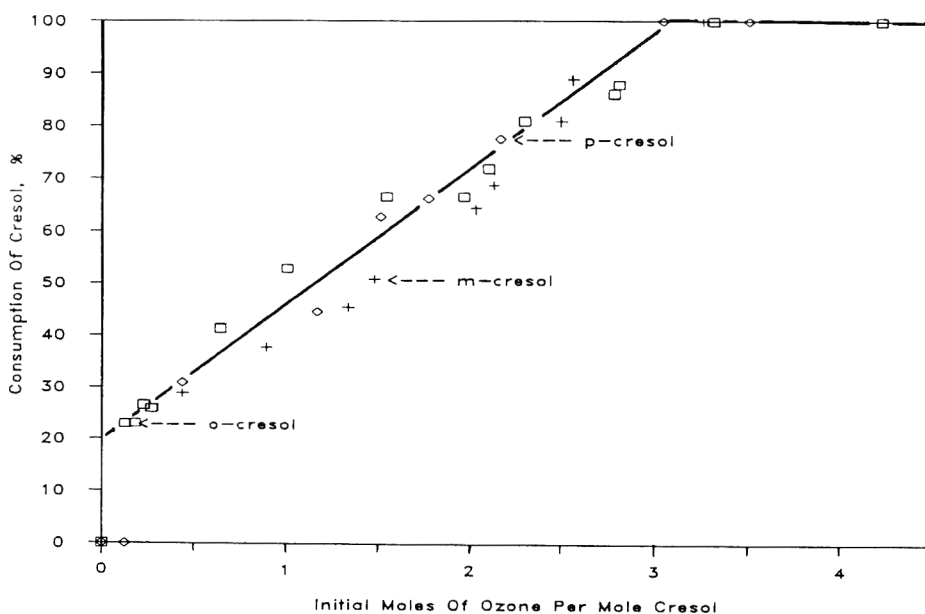
Fig. 1. Cresol–ozone reaction in water. Effect of initial mole ratio.

are needed for complete conversion of each mole of cresol in the ozonation reaction. This result is in general agreement with that concluded by Bauch et al. [4].

Attempts were made to identify the final products of the ozonation. In such a test, ozone gas was introduced continuously into an aqueous solution containing the cresols, and a small sample withdrawn and injected into the gas chromatograph every 20 min for a total of 2 h. Acetic acid was detected but several other peaks in the chromatograms could not be identified. In each experiment, the concentration of the acetic acid increased as the concentration of the cresol decreased with time, suggesting that the acetic acid is a stable product in the ozonation.

From the foregoing discussion, it can be concluded that 3 moles of ozone are required for complete consumption of each mole of cresol. This result does not agree well with the stoichiometric ratio of two determined in some gas–liquid contactors [8]. It should be cautioned that for complete destruction to carbon dioxide and water, 5.67 moles of ozone per mole of cresol are required from the stoichiometric calculation. In actual applications of the ozonation process, the ratio could be higher than 5.67 because of possible side reactions [4]. Several mechanisms of the ozone attack might be possible as discussed earlier. However, it is not known which path is predominant in the ozonation of cresols.

5. Kinetics of ozonation of cresols

Preliminary tests were conducted to determine the absorbance behavior of cresols and ozone in aqueous solutions in the wavelength range of 200–300 nm. For all cresol isomers, the absorbance of a solution increases to a maximum at about 220 nm and then declines to a minimum at 250 nm before approaching another maximum value at 280 nm. For a solution with dissolved ozone, the absorbance increases gradually to a maximum value at 254 nm and then declines, as discussed in some earlier papers [10, 11]. Since the solubilities of cresols are much higher than that of ozone, it is desirable to carry out a kinetic experiment with cresols in large excess. Based on this consideration, the absorbances were measured at the fixed wavelength of 250 nm in the kinetic runs to minimize the contribution of the excessive reactants (cresols). This allows significant variation in the absorbance during a reaction to reflect the concentration change of the limiting reactant, ozone, in the solution. This, in turn, enhances the accuracy of results obtained in analyses of the kinetic data.

The kinetic experiments were carried out in distilled water at temperatures ranging from 10 to 40 °C. The initial pH value of a mixed solution was about 5.2 but varied slightly depending upon the initial concentrations of the reactants. The pH value decreased slightly during reaction, and could be as much as 0.5 less than the initial value at the end of the experiment. The initial concentration of dissolved ozone in the solutions varied from 0.000 025 to 0.0004 M. For

the cresol isomers, the initial concentration ranged from 0.000 25 to 0.0125 M in the experiments.

As indicated earlier, the absorbance of a mixed solution increases rapidly to a maximum (within 0.1 s for all cases) in the early period and then declines in the latter life of the reaction. This phenomenon is demonstrated in Fig. 2 for several runs with different initial concentrations of o-cresol and dissolved ozone in water. For analyses of the kinetic data, it is only necessary to utilize the absorbance data obtained during the early period, as discussed by Li et al. [11].

Regression analyses were performed on the absorbance data by assuming different values for m, the order of reaction with respect to the concentration of ozone. The absorbance data from the three experimental runs given in Fig. 2 are utilized in Fig. 3. As shown in this figure, straight lines can be drawn for these runs by plotting the dimensionless concentration or absorbance against the reaction time on a semi-logarithmic scale. As dictated by eqs. (5) and (7), these results illustrate that the kinetic data can be best fitted by assuming first order with respect to the concentration of ozone. The result of the regression analyses confirmed this finding. The apparent rate constants then can be calculated from the slopes of the straight lines (or from the regression analyses).

The apparent rate constant can be plotted against the initial concentration of cresol on a logarithmic scale to determine the order with respect to o-cresol,
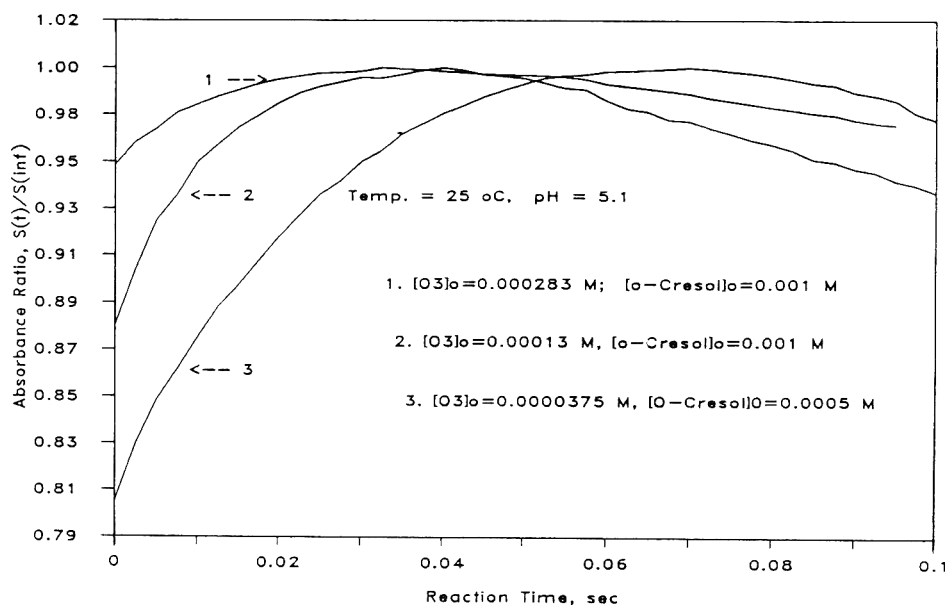
Fig. 2. Absorbance during reaction. Ozonation of o-cresol in water at 25 °C.
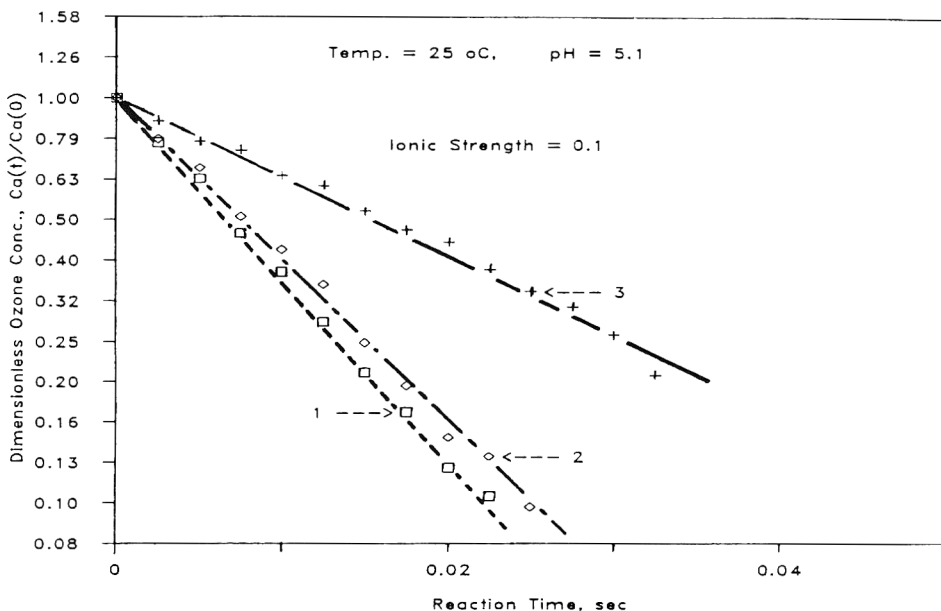
Fig. 3. Ozone concentration in reactions. Ozonation of o-cresol in water at 25 C.

n, as indicated by eq. (4). Figure 4 shows the apparent rate constants obtained for all experiments conducted at three different temperatures for the ozonation of o-cresol in water. The apparent rate constants obtained for the ozonation of m- and p-cresol are given in Figs. 5 and 6. As illustrated in these figures, the slopes are nearly unity for all systems though best correlations are drawn from the experiments conducted at 10 °C. At higher temperatures, appreciable fractions of the reactants were consumed before complete mixing (in one millisecond or less) causing large errors in the data analyses. The slope of unity in these figures indicates that the ozonation reaction can be treated as first order with respect to the concentration of a cresol. Using the stoichiometry of 3 moles of ozone to react with each mole of cresol ($a = 3$, $b = 1$) determined in this work, the overall rate constant, k, for each experimental run can be calculated from eq. (4) by substituting $n = 1$. The average rate constants for the overall reactions at different temperatures and the standard deviations are tabulated in Table 1.

The average second order rate constants for the ozonation of o-cresol are 13 460, 32 240 and 58 600 $1/M$s at 10, 25 and 40 °C respectively. For the ozonation of m-cresol, the overall rate constants are 25 990, 60 870 and 120 870 $1/M$s respectively, at 10, 25 and 40 °C. The rate constants are 20 900, 45 460 and 96 640 $1/M$s at the three respective temperatures for the p-cresol–ozone reaction. The standard deviations vary from 8 to 30% for the three isomers at different temperatures. For the total of 58 experiments conducted in this research, the
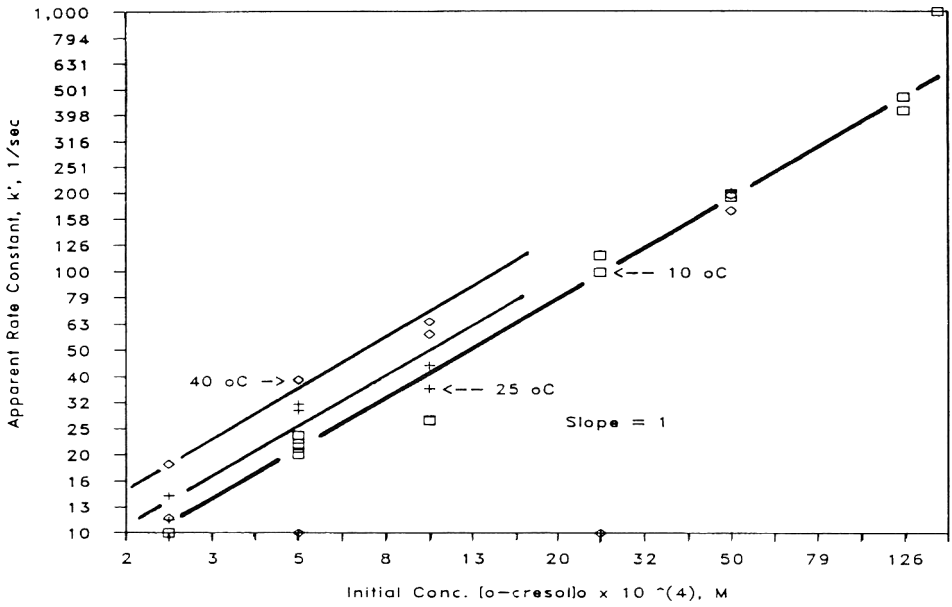
Fig. 4. Apparent rate constant. Ozonation of o-cresol in water.
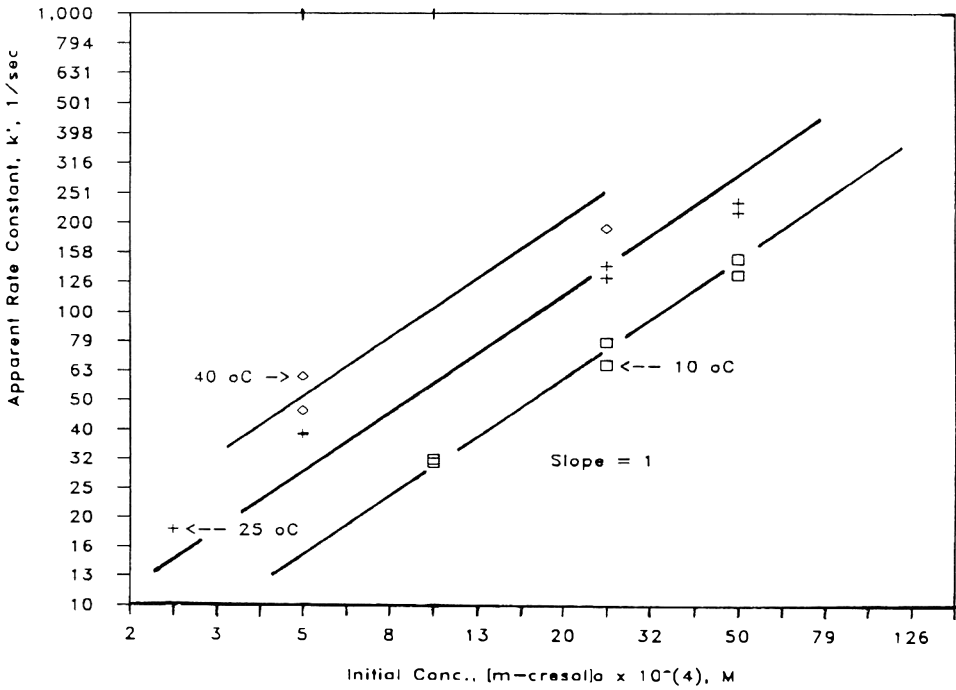
Fig. 5. Apparent rate constant. Ozonation of m-cresol in water.
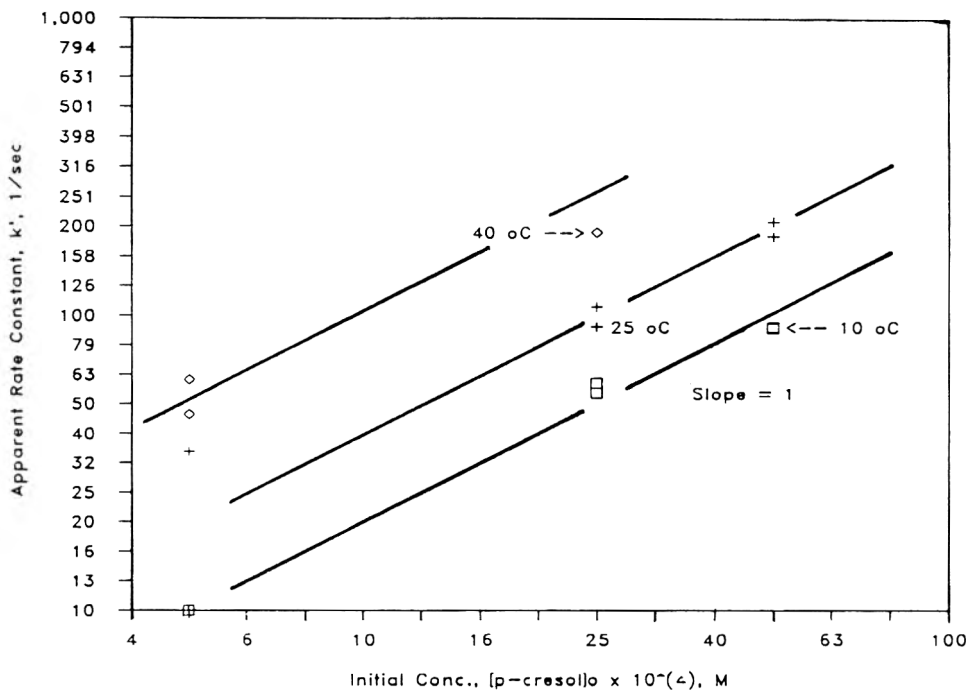
Fig. 6. Apparent rate constant. Ozonation of p-cresol in water.

TABLE 1

Overall rate constants for ozonation of cresols in water

Pollutant	Temperature ($°C$)	Average rate constant ($1/Ms$)	Standard deviation ($1/Ms$)	Deviation (%)
o-Cresol	10	13 460	2 965	22.0
	25	32 240	5 582	17.3
	40	58 600	17 300	29.5
m-Cresol	10	25 990	4 603	17.7
	25	60 870	14 204	24.1
	40	120 870	10 204	8.4
p-Cresol	10	20 900	2 408	11.5
	25	45 460	13 505	29.7
	40	96 640	22 666	23.5

individual rate constants deviated less than 30% frcm the average values except for two runs. The deviations were 41 and 52% for these two runs, probably due to the depletion of large fractions of the reactants prior to the dead time, yielding large errors in the absorbance measurements. The average
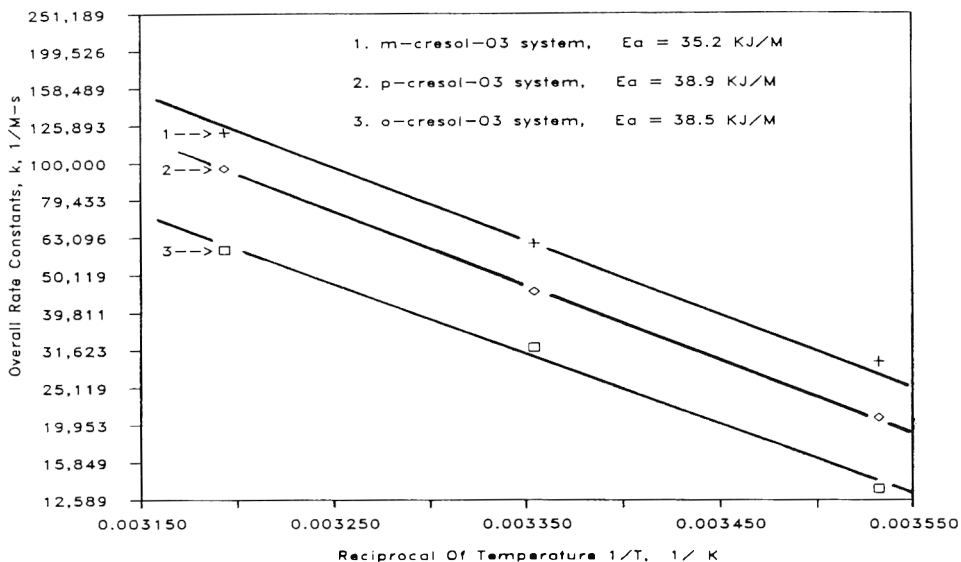
Fig. 7. Overall rate constant. Ozonation of cresols at 10 to 40 C.

rate constants are plotted in Fig. 7 in accordance with the Arrhenius equation to observe the temperature effect. The calculated activation energies are 38.5, 35.2 and 38.9 kJ/M respectively, for the ozonation of o-, m- and p-cresol. The differences in the activation energies are small though the reaction rates are different; the ozonation rate of o-cresol is the slowest and that of m-cresol, the fastest, at a fixed temperature.

6. Oxidation with hydrogen peroxide

Preliminary tests indicated the rates of oxidation between the cresols and hydrogen peroxide are very slow with or without the presence of a catalyst. The absorbance of a mixed solution changed little in the stopped-flow reactor even after several hours of reaction. Since analysis of the absorbance data may not yield accurate results under this circumstance, there are no advantages in using the stopped-flow system. Therefore, the kinetic experiments were conduced in the agitated reactor with hydrogen peroxide in large excess to observe the reactivity of cresols. For each experiment, samples were drawn every hour for about 10 h, and the cresol concentrations determined by the gas chromatographic method using a carbowax 20M column.

The concentration profiles of o-cresol are illustrated in Fig. 8 for two experimental runs with or without a catalyst (Fe_2O_3, 0.5 wt%). Although the oxidation speed was enhanced in the presence of Fenton's reagent, the reaction was
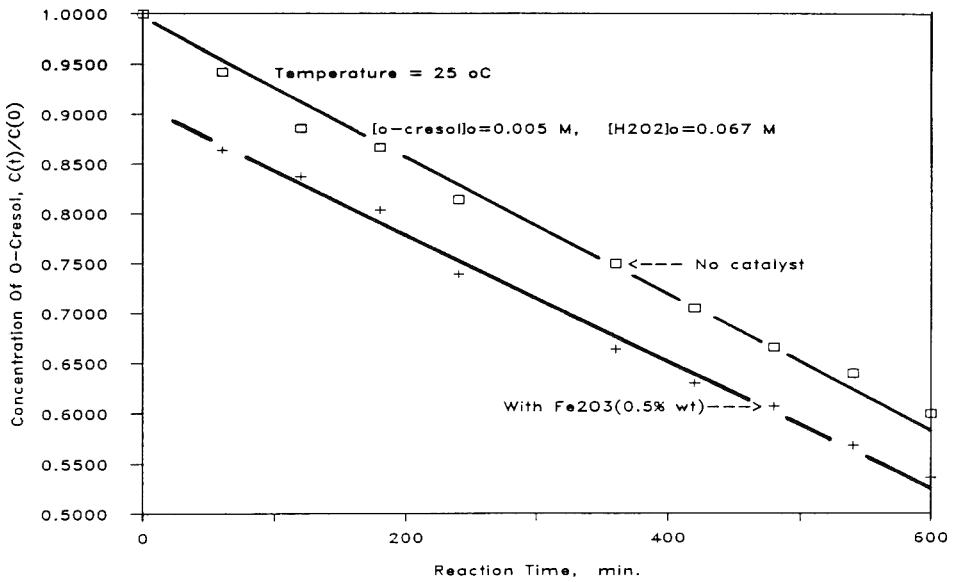
Fig. 8. Hydrogen peroxide–cresol system. Oxidation in water at 25°C.

very slow at 25 °C. As can be seen from the figure, less than 50% of the o-cresol was consumed after the reaction time of 10 h.

Regression analyses of the kinetic data were performed. For the hydrogen peroxide–cresol experiments, the cresol is the limiting reactant with hydrogen peroxide in large excess. With this exception, the concentration data can be analyzed in the same manner as those for the ozonation reactions. The reaction is found to be first order with respect to the concentration of o-cresol, and one-half order with respect to the concentration of hydrogen peroxide. The overall reaction between the cresol and hydrogen peroxide is one and one-half order for the reactions of all cresol isomers.

The overall rate constants are 0.000 055 and 0.000 069 $M^{-0.5}s^{-1}$ for the reaction between o-cresol and hydrogen peroxide with and without Fenton's reagent at 25 °C, respectively. The rate constants for m- and p-cresol oxidation are slightly lower, though the reactions were enhanced in the presence of ferric oxide.

7. Discussion

The experimental results indicate that the cresols are not very reactive with hydrogen peroxide. In addition to the data reported, several other catalysts (both soluble and insoluble) were tested in this work yielding similar results. However, this does not rule out the oxidation potential of hydrogen peroxide

under other circumstances (for example, enhancement by ultraviolet light irradiation). Hydrogen peroxide of high concentration (50% or more) is available for commercial applications, and it may be suitable for treatment of some liquid wastes containing cresols.

In the ozonation of the cresols, the absorbance of a mixed solution increased very rapidly to a maximum value in less than 0.1 s and then declined, as demonstrated in Fig. 2. This absorbance behavior suggests the possible formation of ozonides with high absorptivity in the early period, and further reaction or decomposition of the ozonides in the latter life of a reaction. None the less, the reaction mechanism is not determined in this work, though there are several possible reaction paths, as discussed in an earlier section. The only conclusion arrived at in this research is that 3 moles of ozone are required to react with each mole of a cresol isomer to produce acetic acid and other products.

The overall kinetics of the ozonation of cresols is second order with first order in each reactant. The reaction is very rapid with the second order rate constants of 32 240, 60 870 and 45 460 $1/M$ s at 25 °C for the ozonation of o-, m- and p-cresol respectively. This implies that m-cresol is the most reactive species of the three isomers at room temperatures. These phenolic compounds are more reactive than simple phenol with ozone. The ozonation of phenol was studied previously in this laboratory [11]; the overall reaction is also second order with the rate constant of 29 520 $1/M$ s in distilled water at 25 °C. Thus, the ozonation rates of o-, m- and p-cresol respectively, are 1.1, 2.1 and 1.5 times faster than that of phenol. These rate ratios are different from those reported by other investigators [7], but the discrepancy is not unexpected. Many heterogeneous systems such as gas–liquid contactors are designed for mass transfer studies [14]. Because of complex influences of chemical reactions on mass transfer rate, these reactors might not be suitable for obtaining kinetic information for homogeneous, liquid phase reactions. The stopped-flow spectrophotometer system used in this work is advantageous in enabling measurements of rapid changes in absorbance for a reaction with half-life of as short as a few milliseconds. The absorbance data obtained in the very short period can then be analyzed to yield accurate results on the kinetics of the reaction.

The influence of temperature on the ozonation rates is similar for the three cresol isomers. As the temperature increases four times from 10 to 40 °C; the rate constant increases 4.1 to 4.6 times for each species. As indicated in the Arrhenius plot in Fig. 7, the three lines for the three isomers are nearly parallel. The calculated activation energies are 38.5, 35.2 and 38.9 kJ/M, respectively, for o-, m- and p-cresol. The small differences in the activation energies might suggest that the mechanism governing ozonation is the same for the three isomers.

Though the initial pH value of the reactants in the distilled water was about 5.2, it dropped to as low as 4.7 at the end of some reactions. The increase in the acidity of the reacting solution might be indicative of the formation of acetic and other acids identified in this and other reports [4]. To apply the ozonation

process to oxidize soils or water contaminated by cresols, further treatment for acid removal might be required.

The information obtained in this research might be useful to air pollution control as indicated earlier. Due to the high reactivities of cresols, any cresols emitted into the atmosphere might be converted in a short period to the acids as secondary pollutants in the presence of ozone and moisture.

8. Conclusions

This research studied the oxidation rates of *o*-, *m*- and *p*-cresol by hydrogen peroxide and ozone in water at a temperature range from 10 to 40 °C. Hydrogen peroxide is not very reactive with cresols, even in the presence of Fenton's reagent. The overall kinetics is first order with respect to the concentration of the cresol isomer and one-half order with respect to the concentration of hydrogen peroxide. The overall rate constants are 0.000 055 and 0.000 069 $M^{-0.5}s^{-1}$ for the oxidation in the absence and presence of Fenton's reagent. The oxidation rates of *m*- and *p*-cresol are also slow though the reactions are catalyzed by metal oxides.

Three moles of ozone are required to react with each mole of cresol. The ozonation of cresols in water is very rapid though the reaction rates are different for the three isomers. The half-life of a reaction is only a few milliseconds for most cases. The overall kinetics of the ozonation of a cresol is second order with first order in each reactant. The reaction rate increases with temperature in the range 10–40 °C investigated in this work. For the ozonation of *o*-cresol, the overall rate constants are 13 460, 32 240 and 58 600 $1/M$ s, respectively, at 10, 25 and 40 °C. The ozonation rate of *m*-cresol is the fastest; the rate constant increases from 25 990 to 120 870 $1/M$ s in the temperature range of 10–40 °C. For the ozonation of *p*-cresol, the rate constant varies from 20 900 to 96 640 $1/M$ s as the temperature increases from 10 to 40 °C.

The ozonation rate of cresols is faster than that of simple phenol. Of the three cresol isomers investigated, *m*-cresol is the most reactive species. On the other hand, the reaction rate between o-cresol and ozone is slower than those of the other isomers in the temperature range of 10–40 °C. The activation energies are nearly the same for the three isomers at about 39 kJ/M.

Acknowledgments

Nomenclature

a	Stoichiometric ratio for reactant A
b	Stoichiometric ratio for reactant B
C_A	Concentration of a limiting reactant
C_B	Concentration of an excessive reactant
k'	Apparent rate constant
k	Overall reaction rate constant
m	Reaction order with respect to a limiting reactant
n	Reaction order with respect to an excessive reactant
S	Absorbance of a reacting solution
t	Reaction time

References

1   NATICH Data Base Report on State, Local and EPA Air Toxics Activities, EPA 450/3-90-012, prepared by Radian Corporation, OAQPS, U.S. Environmental Protection Agency, Research Triangle Park, NC, 1990.
2   S.J. Niegowski, Destruction of phenols by oxidation with ozone, Ind. Eng. Chem., 45 (1953) 632
3   M. Dore, B. Langlais and B. Legube, Mechanism of the reaction of ozone with soluble aromatic pollutants, Ozone Sci. Eng., 2 (1980) 39.
4   H. Bauch, H. Burchard and H.H. Arsovic, Ozone as an oxidative disintegrant for phenols in aqueous solutions, Gesundheits-Ingenieur, 91(9) (1970) 258.
5   J. Hoigne, Mechanisms, rates and selectivities of oxidations of organic compounds initiated by ozonation of water, In: R.G. Rice and A. Netzer (Eds.), Handbook of Ozone Technology and Applications, Vol. 1, Ann Arbor Science, Ann Arbor, MI, 1982, pp. 341–379.
6   J.F. Gould, Correlation between chemical structure and ozonation kinetics: Preliminary observations, Ozone Sci. Eng., 9 (1987) 207.
7   M.D. Gurol and S. Nekouinaini, Kinetic behavior of ozone in aqueous solutions of substituted phenols, Ind. Eng. Chem. Fundam., 23 (1984) 54.
8   F.J. Beltran, J.M. Encinar and J.F. Garcia-Araya, Ozonation of o-cresol in aqueous solutions, Water Res., 24 (1990) 1309.
9   Y.T. Wang, Methanogenic degradation of ozonation products of biorefractory or toxic aromatic compounds, Water Res., 24 (1990) 185.
10 C.H. Kuo, K.Y. Li, C.P. Wen and J.L. Weeks, Absorption and decomposition of ozone in aqueous solutions, AIChE Symp. Ser., 73(166) (1977) 230.
11 K.Y. Li, C.H. Kuo and J.L. Weeks, A kinetic study of ozone–phenol reaction in aqueous solutions, AIChE J., 25 (1979) 583.
12 H. Bauch and H. Burchard, Investigations concerning the influence of ozone on water with few impurities, Wasser, Luft u. Betrieb, 14(7) (1970) 270.
13 P.W. Haijman and J.P. Wibaut, Quantitative investigation of the ozonization of ortho-xylene and 1,2,4-trimethyl benzene, Rec. Trav. Chim. Pays-Bas, 61 (1942) 842.
14 K.Y. Li and C.H. Kuo, Absorption and reactions of ozone in phenolic solutions, AIChE Symp. Ser., 76(197) (1980) 161.

Book Reviews

Siting Low-Level Radioactive Waste Disposal Facilities, by Mary R. English,
   Auburn House, Greenwood Publishing Group Inc., Westport, CT, 1992, ISBN
   No. 0-89930-560-1, pp. 304, US $49.95.

Siting dilemmas, like other public policy dilemmas, are permeated with
questions of values. Drawing upon a large body of material collected over
several years of formal and informal research, Mary R. English explores how
values on issues concerning authority, trust, risk, and justice have affected
implementation of the 1980 Low-Level Radioactive Waste Policy Act
(LLWPA). According to the LLWPA and the 1985 Low-Level Radio-
active Waste Policy Amendment Act (LLWPAA) in January 1993, Nevada,
Washington, and South Carolina will no longer be the primary waste disposal
sites for the U.S. The acts encourage states to unite regionally, to form
compacts, and to select states to host new, permanent disposal facilities. Mary
R. English discusses conflicts and questions surrounding three commonly used
siting approaches: (1) the "best site" approach; (2) the "fair play" approach;
and (3) the "volunteerism/incentives" approach.

By examining the central issues underlying the dilemma of siting low-level
radioactive waste (LLW) disposal facilities, reviewing current decision-
making methodologies, and citing examples of recent siting efforts,
Mary R. English vividly illustrates the problems and possibilities individual
states face in choosing disposal sites for their LLW. Her questions range from
very broad philosophical, political, and sociological issues related to *fairness*,
and the *quest for legitimacy*, to specific community concerns, including respons-
ibility, health risks, and socioeconomic and environmental impacts of LLW
disposal. In fact, the most crucial challenge in the siting dilemma (the primary
focus of this volume), is establishing community confidence in authority to
secure appropriate sites for permanent facilities. Ultimately, risk management
is the focus of this challenge. Community inquiry may become public opposi-
tion unless qualitative measures are taken in the initial stages of the siting
process to (1) promote effective *risk communication*; (2) to minimize the *need*
for trust; and (3) to determine and strengthen authority. If these measures fail,
justice, as a viable route to the durable legitimacy of a public policy, becomes
the obvious recourse for achieving long-term mission success. While Mary R.
English cannot specifically define *justice*, she suggests that regardless of the
siting approach used, the claims of society as a whole are often incompatible,
and one interest [authority/individual] may be satisfied at the expense of
another.

Mary R. English's intent is not to offer a solution to the siting dilemma, but rather to provide background information; to determine when siting *becomes* a dilemma; to arouse awareness of the siting issues; and to suggest conflict resolution tools. She magnanimously advocates scientific literacy in the public sector, and more effective communication efforts from the scientific community as priority goals in the LLW disposal facility siting dilemma. In addition, appendices include the complete LLWPA and the LLWPAA, and actual state siting programs.

<div align="center">LISA D. NANSTAD and CURTIS C. TRAVIS</div>

Hazardous Waste: Identification and Classification Manual, by T.P. Wagner, Van Nostrand Reinhold, New York, NY, 1990, ISBN: 0-442-00399-4, 239 pp., $39.95.

The Resource Conservation and Recovery Act (RCRA) and its amendments, have spawned the largest and most comprehensive (and sometimes incomprehensible) set of regulations of any U.S. environmental law. The book was written to assist environmental specialists in identifying and classifying hazardous materials in accordance with the stringent provisions of RCRA and the Hazardous Materials Transportation Act (HMTA). Indeed, a useful book it is for clearly waste classification is the first step in the disposal process. To err is dangerous, for if the waste escapes the hazardous materials stream, one risks U.S. EPA prosecution; alternately, if one disposes nonhazardous waste, as a hazardous waste, one is wasting money — much money.

Chapter 1 (Introduction), discusses the historical background of waste generation. It includes a brief discussion of RCRA, HMTA and the emerging area of medical wastes.

The book's agenda really begins with a short (actually all chapters are quite short) Chapter 2 (Hazardous Waste Identification/Classification Process). Next comes a discussion of the definition of solid waste (Chapter 3), which may be a liquid under RCRA's provisions.

However, there are exceptions that allow waste to escape from the system. Chapter 4 discusses exemptions or exclusions including domestic sewage, industrial points source discharges, irrigation return flows, radioactive wastes, in-situ mining wastes, pulping liquors, spent sulfuric acid, secondary material returned to original process, household waste, agricultural waste, mining overburden, discarded wood products, chromium waste, underground storage tanks cleanup waste (petroleum-contaminates), etc. Also discussed are special categories of waste the Congress told the U.S. EPA to study, i.e. cement kiln dust and utility waste. Finally eight special categories of hazardous waste (such as treatability samples) are discussed.

Chapter 5 discusses those wastes the U.S. EPA has specifically listed as hazardous. If "listed", a waste is designated as "hazardous" regardless

of its actual chemical composition. Delisting is possible and is also discussed.

The characteristics of hazardous waste are discussed in Chapter 6. These characteristics that make a waste hazardous, according to the law, are: ignitability, corrosiveness, reactivity and toxicity.

Recycling is discussed in Chapter 7. Included is a discussion of recycled materials that are regulated under U.S. EPA regulations (i.e., sludge) and those that are not (i.e., scrap metal). Burning and blending of waste fuels is also discussed in this chapter.

The most interesting chapter for me was Chapter 8, entitled Waste Identification Case Studies since they illustrated the application of RCRA's regulation; over 30 different cases are illustrated. Finally, Wagner discusses the HMTA, in Chapter 9, entitled appropriately, "Classification of Hazardous Waste for Transportation".

One of the aspects that makes the book useful is the inclusion of numerous flow charts and sample exercises that assist in making the written material as understandable as possible.

One aspect of books that I find disconcerting is an overly long appendices section; and this book has a very long set of appendices that comprise almost one-half of the book. These appendices are:

- Guide to waste identification and classification
- Synonyms of hazardous wastes
- EPA's regulations for identifying and classifying hazardous waste: Title 40 CFR Parts 261 and 266
- Glossary

GARY F. BENNETT

Drinking Water Health Advisory: Volatile Organic Compounds, U.S. Environmental Protection Agency, Office of Drinking Water Health Advisories, Lewis Publishers, Chelsea, MI, 1991, ISBN: 0-87371-436-9, 250 pp., $59.95.

Health advisories are prepared for the U.S. EPA by the Criteria and Standards Division, Office of Drinking Water. Their advice provides technical guidelines to public health officials on health effects, analytical methodologies, and treatment technologies associated with drinking water contamination.

The book contains health advisories for the 15 organic chemicals listed below:

1,1,2-Trichloroethane . . . .
Trichlorofluoromethane . . . .
o-Chlorotoluene . . . .
Hexachlorobutadiene . . . .
1,1,1,2-Tetrachloroethane . . . .

Chloromethane ....

Bromochloromethane ....

1,3,5-Trichlorobenzene ....

1,2,4-Trichlorobenzene ....

Bis-(2-chloroisopropyl)ether ....

p-Chlorotoluene ....

1,2,3-Trichloropropane ....

Bromomethane ....

Dichlorodifluoromethane ....

Naphthalene ....

Each health advisory summarizes available data concerning the occurrence, environmental factors, pharmacokinetics (adsorption, distribution, metabolism and excretion), and health effects (both human and animal) of a specific contaminant (mixture as well as analytical methods and treatment technologies for the contaminant). The health effect data are used to estimate concentration of the contaminant in drinking water that are not expected to escape any adverse noncarcinogenic health effect over specific exposure duration.

As with all U.S. EPA work produced, the material is very well written and well referenced.

GARY F. BENNETT

The Fate and Effects of Oil in Freshwater, edited by J.W. Green and S.W. Trett, Elsevier Applied Science Publishers Ltd. /The British Petroleum Company p.l.c., London, 1989, ISBN 1-85166-318-5, xii + 338 pp., £56.00.

Catastrophic supertanker accidents, pipeline breaks and leaking underground storage tanks: All of these emission sources threaten a fragile aquatic environment. The book does not discuss pollution of the ocean, but rather focusses on the fate and effects of oil in freshwater. The editors' objectives in writing the book were to provide a comprehensive compilation, summary and critical evaluation of the available scientific literature on the impact of petroleum on freshwater organisms; to review procedures for the cleanup of petroleum from freshwater habitats and to examine restoration and recovery rates; to provide background information on the chemistry and fate of petroleum in freshwater; and to identify gaps in the information on the effect of petroleum-related contamination of freshwater.

I believe these goals were reached. The book is well written and certainly comprehensive being comprised of nine chapters written by UK university, industrial and research center scientists.

By title the chapters are:

1. Introduction
2. Composition, sources and source identification of petroleum hydrocarbons and their residues

3. Input, behaviour and fates of petroleum hydrocarbons
4. Biological and ecological effects of oils
5. Biological and ecological effects of dispersants
6. Biodegradation of oil in freshwaters
7. Clean-up technology
8. Restoration and recovery
9. Summary on conduction

There are over 600 references cited; a glossary is given and in addition a standard index, the authors have compiled a systematic (biological species) index.

GARY F. BENNETT

Heavy Metals in the Environment (Trace Metals in the Environment Vol.1), edited by J.-P. Vernet, Elsevier, Amsterdam, 1991, ISBN 0-444-89064-5, xviii + 406 pp., Dfl. 270.00.

Studies released recently in the United States have revealed that lead is a far more toxic pollutant than previously thought. And more steps are being taken to limit human exposure through air (lead from gasoline), water (lead in soldered joints), and solid phase (lead in paint and soil) pathways. Concern for lead and other metals is not solely a U.S. problem; it is global; hence the series of books, *Trace Metals in the Environment*, is well conceived. The goal is to provide a forum for transdisciplinary studies on heavy metal pollutant fate, transport, effects and abatement.

The continuing worldwide interest in the role of heavy metals in the environment has led to seven international conferences, the first in 1975 in Toronto, the seventh in 1989 in Geneva. This volume, the first in a new series, contains 22 papers selected from the many presented at the last conference (at the time of printing Vol. 2 in the series has appeared).

The coverage is very broad as the title of the various chapters listed below (and the number of papers in each chapter) indicate:

- Atmospheric transport: Large scale transport, modes (1)
- Acid deposition and soil acidification (2)
- Soil interaction (2)
- Regional studies: Freshwater and marine environment (3)
- Bio-accumulation (2)
- Microbial adaptation and microbial interaction (1)
- Health effects of metals (1)
- Radionuclides as chronometers and tracers (4)
- Wastewater (4)
- Analytical and general methods (2)

GARY F. BENNETT

Gas, Dust and Hybrid Explosions (Fundamental Studies in Engineering Vol. 5), by W.E. Baker and M.J. Tang, Elsevier, Amsterdam, 1991, ISBN 0-444-88150-6, xx + 256 pp., Dfl. 185.00.

The first author of the text, W.E. Baker, was a distinguished scholar in the area of the science of explosions and a member of the editoral advisory board. Unfortunately, he passed away as this book was being published. His demise was a great loss to this *Journal*, as well as to the field of explosion science.

The authors' goal in writing the book was an attempt to gather and present the available material for explosions in air of the "non-ideal" explosion sources most often encountered in industrial accidents. With this purpose they discussed both theoretical and experimental approaches to these classes of explosions with rather complete descriptions of the physical processes known or believed to occur. Types of explosion sources discussed include: Dust explosions, (including grain elevator explosions), reactor gas explosions (including unconfined vapor cloud explosions), hybrid explosions (such as may occur when combustible dusts and gases are mixed with air in strong, vented or unvented enclosures and then are ignited), non-reactive gas and flash evaporating fluid explosions (often referred to as a single pressure burst), and finally liquid propellant explosion.

Each chapter follows the general form when the authors discuss fundamentals (theory) scaling (or scale-up), testing methods, and control methods.

This reviewer is clearly not an expert in the field of explosion science. But Baker was and this most excellent book is a testimony to his expertise.

GARY F. BENNETT

Surface Impoundments: Design, Construction and Operation, by R.P. Hartley, Noyes Data Corp., Park Ridge, NJ, 1992, ISBN 0-8155-1302-X, 183 pp., $45.00.

This book was produced by the author, a member of the consulting firm of P.E.I. Associates, for the U.S. Environmental Protection Agency. The goal of the book is to provide "up-to-date" information on the design, construction, and operation of surface impoundments used for the treatment, storage, or disposal of hazardous and non-hazardous wastes.

The topic is an important one as in a 1983 study; the U.S. EPA identifies over 180,000 surface impoundments. The concern of course is their potential impact on groundwater quality if they leak. Leak prevention is the key to their safe operation and that is accomplished by preservation of the integrity of their hydraulic barriers: Polymeric membranes and low permeability soil. To this end, the Resource Conservation and Recovery Act's "minimum technology requirements" specify double-lined structures with a leak collection and removal layer.

To assist engineers in complying with these requirements, the book has the following chapters:
- Pre-design requirements
- Design requirements
- Construction requirements
- Operation, maintenance, and monitoring
- Contingency planning
- Closure and post-closure care

An excellent (extensive) bibliography is provided.

GARY F. BENNETT

Organization for Hazardous Materials Emergencies: (1) Hazard Analysis, (2) The Emergency Plan, and (3) Exercises, Three videotapes: 28, 22 and 29 minutes long, respectively; Emergency Film Group, Plymouth, MA, 1992, VHS; $265/tape; $645/set of three tapes.

Title III of SARA (the Superfund Amendments and Reauthorization Act) passed by the U.S. Congress in 1986 requires planning and training for hazardous materials emergencies. Guided by a State Emergency Response Committee, planning is undertaken at the local level by Local Emergency Planning Committees (LEPC). In the state of Ohio, this local planning occurs at the County level — and this reviewer co-chairs his county LEPC. This excellent set of videotapes, *Organization for Hazardous Materials Emergencies*, is designed to assist the LEPCs and the chemical plants in their communities in meeting the requests of SARA. My impression is that the tapes do that very well, although they describe, in my opinion, a somewhat idealistic process, beginning with the first tape, *Hazard Analysis*. In this tape, the commentator explains what Hazard Analysis is and how to conduct one. The commentator uses case studies to teach hazard identification vulnerability analysis and probability analysis, stressing the difference between hazard and risk. As reading (supplemental) material the tape is accompanied by FEMA/DOT/U.S. EPA's book, *Handbook of Chemical Analyses Procedures*. The goal is for community planners to identify the hazard potential of chemical/industries.

Part two, *The Emergency Plan*, outlines the responsibility of companies, response personnel, and community groups within the framework of the emergency plan. This videotape outlines five steps: (1) reviewing existing plans, (2) conducting hazards analysis, (3) assessing response capabilities, (4) developing the plan, and (5) testing, revising, and monitoring the plan. The tape is accompanied by the National Response Team's *Hazardous Materials Emergency Plan Guide*.

The final (and for me the most useful tape, probably because I am so devoid of experience in that area) is entitled *Exercises*. It is designed to help communities and industries carry out comprehensive exercise programs to test and evaluate

the plan. To me, this is the key to the whole emergency planning process. How to design tabletop, functional and field exercises is discussed. Covered too, are the tasks of writing the emergency test scenario. The control plan, dealing with the media and the neighborhood, assessing the effectiveness of the team, finding support from governments and private agencies and followup activities are all thoroughly discussed. The tape is accompanied by two federally written publications:

- *Developing a Hazardous Materials Exercise Program*, put out by the Material Response Team
- *Hazardous Material Exercise Evaluation Methodology Manual*, put out by FEMA.

I strongly recommend the tape to all those involved in community emergency planning. One may not (probably will not) follow all their suggestions, but one cannot avoid being helped by them. They neatly review the process of emergency planning and gives many helpful tips to accomplish it.

GARY F. BENNETT

Mobility and Degradation of Organic Contaminants in Subsurface Environments, by Warren J. Lyman, Patrick J. Reidy, and Benjamin Levy, C.K. Smoley, Inc., Lewis Publishers, 121 South Main Street, Chelsea, MI 48118, 1992, ISBN 0-87371-800-3, 367 pp., plus index, $59.95.

This book provides a relatively complete summary of the current understanding of how organic contaminants move and transform in the environment. The book is an outgrowth of work by Camp Dresser & McKee, Inc. performed under a U.S. Environmental Protection Agency contract focussed on control of leakage from underground storage tanks (USTs). As such, it focusses on petroleum products with data and examples restricted to gasoline and constituent chemicals found in gasoline. However, the phenomena described and the equations provided for calculating fate and transport can be applied to most low density organic contaminants given the required input data. The book begins with a description of the thirteen different locations or states in which a low density organic contaminant can be found in the subsurface environment: (1) vapor within unsaturated zone soil gas; (2) liquid film on "water-dry" soil particles; (3) dissolved chemical in the water film around soil particles in the unsaturated zone; (4) chemical sorbed onto "water-wet" solids (saturated or unsaturated zone); (5) liquid between particles in the saturated zone; (6) liquid between particles in the unsaturated zone; (7) liquid floating on the water table; (8) dissolved chemical in saturated zone ground-water; (9) chemical adsorbed onto colloidal particles in soil water (saturated and unsaturated zone); (10) chemical diffused into solid particles (either zone); (11) chemical sorbed onto microbiota (either zone); (12) dissolved chemical in

mobile pore water in the unsaturated zone; and (13) liquid in rock fractures (either zone).

The remainder of the book consists of a chapter addressing each of the thirteen locations/states. The chapters are developed around a set format beginning with a description of the subject locations/state and a discussion of the fate and transport phenomena that will determine the effectiveness of remediation. Equations are provided to numerically describe phase transfer and transformation processes. Tables are included providing the input data for gasoline chemical constituents to be used in the equations. Means of estimating the average and maximum storage capacity in the location are presented along with example calculations. The chapters conclude with a summary of the relative importance of the location/state to overall remediation. In addition to being a good text on fate and transport mechanisms, the book is an excellent reference on the properties of common gasoline constituents. I recommend the book to anyone who deals with the fate, transport and/or remediation of gasoline releases.

GAYNOR DAWSON

Bioremediation of Hazardous Wastes, by Office of Research and Development, U.S. Environmental Protection Agency, Washington, D.C., Report No. EPA/600R-92/126, August 1992, 119 pp. (No price/no ISBN.)

This short book contains synopses of papers presented at the U.S. EPA's Fifth Annual Symposium on Bioremediation of Hazardous Wastes. The symposium was held in Chicago, Illinois in May 1992. Presented were 28 papers and 9 poster exhibitions, reporting on recent U.S. EPA bioremediation research program achievements and results of research projects aimed at bringing bioremediation into widespread use.

The proceedings are comprised of an executive summary, an introduction and then brief summaries of the papers and poster presentation categories as follows:
1. Site Characterization (4 entries): The four papers discuss research on petroleum spill cleanup, the efficiency of *Pseudomonas* bacteria to remediate chemical contamination, and on constraints to the proposed use of methane-oxidizing bacteria for a TCE plume.
2. Bioremediation Field Introduction (10 entries): The eight papers and two poster exhibits covered the field evaluations underway at sites utilizing bioventing, biochemical techniques, and bioremediation under a variety of aerobic and anaerobic conditions.
3. Performance Evaluation (4 articles): The topic deals with the development of bioremediation approaches that protect public health. The four papers presented discuss the risks related to bioremediation and potential genotoxicity.

4. Research; including laboratory, pilot-scale, and field research (16 articles): The eleven papers and five poster presentations are in a topic area that focuses on identifying microorganisms that can degrade contaminants as well as developing new biosystems for treatment of pollutants in surface waters, sediments, soils, and subsurface material.
5. Modeling (3 articles): Two presentations concern the mechanisms by which granulated microbial activated carbon systems degrade hazardous wastes; third presentation deals with biodegradation kinetics.

<div align="right">GARY F. BENNETT</div>

SUBMISSION OF PAPERS

Submission of a manuscript implies that it is not under consideration for publication elsewhere and further that, with the exception of review papers, original work not previously published is being presented.

Papers should be submitted to Dr. G.F. Bennett, Department of Chemical Engineering, University of Toledo, 2801 W. Bancroft Street, Toledo, OH 43606, U.S.A. or Dr. R.E. Britter, Department of Engineering, University of Cambridge, Cambridge CB2 1PZ, Great Britain. Authors in the Far East should submit papers to Dr. T. Yoshida, Chemical Engineering Laboratory, Department of Mechanical Engineering, Faculty of Engineering, Hosei University, 7-2 Kajino-cho 3-chome, Koganei-shi, Tokyo 184, Japan.

MANUSCRIPT PREPARATION

Three copies of the manuscript should be submitted in double-spaced typing on pages of uniform size with a wide margin on the left. The top copy should bear the name and the full postal address of the person to whom the proofs are to be sent. An abstract of 100–200 words is required.

References should be numbered consecutively throughout the text and collected together in a reference list at the end of the paper. Journal titles should be abbreviated. The abbreviated title should be followed by the volume number, year (in parentheses), and page number.

ILLUSTRATIONS

Line drawings should be in a form suitable for reproduction, drawn in Indian ink on drawing paper. They should preferably all require the same degree of reduction, and should be submitted on paper of the same size as, or smaller than, the main text, to prevent damage in transit. Photographs should be submitted as clear black-and-white prints on glossy paper. Each illustration must be clearly numbered. Colour illustrations can be reproduced at the author's expense.

Legends to the illustrations must be submitted in a separate list.

All tables and illustrations should be numbered consecutively and separately throughout the paper.

LANGUAGE

The principal language of the journal is English, but papers in French and German will be published.

PROOFS

Authors will receive page proofs, which they are requested to correct and return as soon as possible. No new material may be inserted in the text at the time of proofreading.

REPRINTS

A total of 50 reprints of each paper will be supplied free of charge to the principal author. Additional copies can be ordered at prices shown on the reprint order form which accompanies the proofs.

> A pamphlet containing detailed instructions on the preparation of manuscripts for JOURNAL OF HAZARDOUS MATERIALS may be obtained from the publishers.

JOURNAL OF HAZARDOUS MATERIALS

CONTENTS